2014-06-23

Designing Proton Conductivity in a Metal-Organic Framework from a Molecular Scale

Kim, SiRim

UNIVERSITY OF CALGARY

Designing Proton Conductivity in a Metal-Organic Framework from a Molecular Scale

by

SiRim Kim

A THESIS

SUBMITTED TO THE FACULTY OF GRADUATE STUDIES

IN PARTIAL FULFILMENT OF THE REQUIREMENTS FOR THE

DEGREE OF DEGREE OF MASTER OF SCIENCE

DEPARTMENT OF CHEMISTRY

CALGARY, ALBERTA

JUNE, 2014

Abstract

Two design strategies were investigated to enhance proton conductivity of a proton conducting MOF named β-PCMOF2. First design strategy was isomorphous ligand replacement where an entire C_3-symmetric trisulfonate ligand was substituted with a C_3-symmetric tris(hydrogen phosphonate) ligand to yield PCMOF2½, which had its proton conductivity raised 1.5 orders of magnitude, to 2.1×10^{-2} S cm^{-1} at 85 °C and 90% relative humidity compared to the parent material, while maintaining the parent MOF structure. To further enhance the proton conductivity of PCMOF2½, isomorphous ligand replacement was paired with heterocycle doping. Seven new PCMOFs were synthesized and investigated. One resulting material, PCMOF2½(Pyrazole), had its proton conductivity raised 1.9 orders of magnitude compared to the parent material, to 1.1×10^{-1} S cm^{-1} at 85 °C and 90% relative humidity, while maintaining the parent MOF structure. In addition, the exact mechanism of isomorphous ligand replacement synthesis was elucidated to be a thermodynamically driven solid state reaction.

Acknowledgements

Foremost, I would like to thank my supervisor Dr. George K. H. Shimizu for his continuous support and understanding starting from my undergraduate work-experience via the Inorganic Exchange Program in 2010 to my final year of graduate studies in 2014. Under Dr. Shimizu's guidance and mentorship, I became more mature and cognizant with respect to the scientific inquires and became skilled in academic administration.

Following, I would like to thank my committee members, Dr. Venkataraman Thangadurai, Dr. Robert Marriott, Dr. Milana Trifkovic, Dr. Belinda Heyne for taking time to review my work. In addition, I would like to thank Dr. Roland Rosler and Dr. Christopher Clarkson for taking part in my candidacy examination.

I would also like to thank the departmental staffs who have provided technical and administrative assistance with my projects: Wade White, Dorothy Fox, Johnson Li, Quio Wu, Dr. Michelle Forgeron, Late Ms Bonnie King, and Janice Crawford. I would like to thank Dr. Karl Dawson for scientific and editorial assistance for the PCMOF2½ project, as well as synthetic assistance for the PCMOF2½(Pyrazole) project. I would like to thank Benjamin Gelfand for running SEM/EDX experiments as well as his synthetic assistance.

Finally, I would like to thank my family and friends who has given me support and encouragement throughout my university career.

Table of Contents

List of Tables

List of Figures and Illustrations

List of Symbols, Abbreviations and Nomenclature

1-D .....One dimensional

2-D .....Two dimensional

3-D .....Three dimensional

A.....Area, measured in cm^2

AC.....Alternating current

Bdc.....1,4-Benzenedicarboxylate

DC.....Direct current

DSC.....Differential scanning calorimetry

EA .....Elemental analysis

E_a.....Activation energy, measured in electron volts (eV)

EDX .....Energy dispersive X-ray spectroscopy

f .....Frequency, measured in Hz

h.....Height, measured in cm

i .....Current, measured in A

K_a .....Acid dissociation constant

Na_3L1 .....trisodium 2,4,6-trihydroxy-1,3,5-trisulfonate benzene

Na_3H_3L2.....trisodium 1,3,5-benzenetriphosphonic acid

M.....mol/L

MIL .....Materials of Institute Lavoisier

MIL-101.....$(M^{3+})_3(F_x(OH)_{(1-x)}Bdc(H_2O)_2$; $M^{3+} = Cr^{3+}$ or Fe^{3+}, $x \leq 1$

MOF.....Metal-Organic Framework

MTV.....Multivariate

NMR .....Nuclear magnetic resonance

PCMOF.....Proton Conducting Metal-Organic Framework

α-PCMOF2.....Na_3L1, low temperature phase

β-PCMOF2.....Na_3L1, high temperature phase

PCMOF2½.....$(Na_3L1)_{0.66}(Na_3H_3L2)_{0.34}(H_2O)1.2$

PCMOF3.....$Zn_3(L2)(H_2O)_2$

PCP .....Porous coordination polymer

pK_a .....Negative logarithm of the acid dissociation constant

PXRD.....Powder X-ray diffraction

q.....Charge, measured in coulombs.

R.....Resistance, measured in Ω

RH.....Relative humidity (P/P_o of water vapour, times 100)

RO.....Reverse osmosis

S cm^{-1} .....Siemens per centimetre

SEM .....Scanning electron microscopy

T.....Temperature, measured in K

t .....Time, measured in s

t .....Thickness, measured in cm

Z.....impedance, measured in Ω

Z'.....Real phase of Z, measured in Ω

Z" .....Imaginary phase of Z, measured in Ω

ΔS.....Entropy, measured in J/K

n.....Number of mobile charge carriers per unit volume, measured in m^{-3}

μ.....Ion mobility, measured in cm^2 Hz/V

σ.....Ion conductivity, measured in S cm^{-1}

Chapter One: **INTRODUCTION**

1.1 Scope of the Thesis

This manuscript based thesis will feature two first author manuscripts, each as a separate chapter. The focus of my graduate research was to investigate proton conduction in a class of material called Metal-Organic Frameworks (MOFs). The investigation successfully yielded one first author publication (communication) in the Journal of the American Chemical Society,[1] one first author manuscript (full article) submitted to the Journal of the American Chemical Society, and a co-authored perspective article in Science.[2] This introductory chapter will present a concise description of Metal-Organic Frameworks and proton conduction, followed by a brief overview of each chapter and a statement of contribution describing the co-authors' contributions to the respective manuscripts.

1.2 General theme of the research – proton conduction in metal-organic frameworks

Metal-Organic Frameworks (MOFs) are crystalline porous solids composed of organic linkers connected by metal centers. MOFs are modular in nature where the bulk material's physical and chemical properties can be imparted and/or tuned by rational design of its building blocks (unit cells). This ability to envisage a material from its molecular scale forms the central dogma of MOF chemistry. By using X-ray crystallography, a chemist can visualize the exact molecular structure of a MOF. Furthermore, by systematically studying the chemical and physical properties of a MOF, precise structure-property relationships can be determined. MOFs have seen an enormous growth in interest owing to their versatility and modular nature – in fact, they are under

intense research as potential porous sorbents for gas capture and separation,[3] catalysts,[4] molecular sensors,[5] and solid state proton conductors.[6]

Proton conduction in a solid state material takes place via two mechanisms: vehicular transport and the proton hopping (Grotthuss). For the case of vehicular transport, protons migrate through a channel as protonated ions, such as H_3O^+. With respect to the Grotthuss mechanism, protons hop from one site or carrier to one another through a hydrogen bond network. Correspondingly, the facile movement of charges through the material requires an unobstructed proton conduction pathway that is lined with acidic moieties with similar pK_as, separated by small energy barriers.[7]

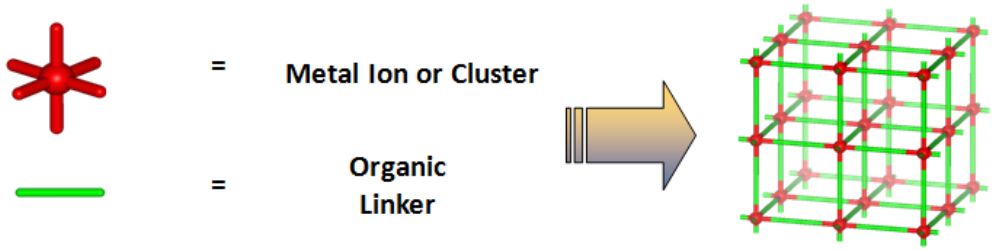

Figure 1.1 Basic structure of a Metal-Organic Framework

In investigating MOFs' application as solid state proton conductors, the Arrhenius equation, which is derived from the Nernst-Einstein relation, provides the fundamental guideline in designing an efficient and improved proton conducting MOFs (PCMOFs).[6]

$$\sigma = \frac{ne^2 D_o \exp\left(\frac{\Delta S_m}{k}\right)}{kT} \exp\left(\frac{-E_a}{kT}\right) \rightarrow \sigma = \frac{\sigma_o}{T} \exp\left(\frac{-E_a}{kT}\right)$$

σ = Ionic conductivity
n = Number of charge carriers (temperature independent mobile site occupancy)
e = Charge of the mobile ion
D_o = Constant which is related to the mechanism of ionic conductivity
k = Boltzmann constant
T = Temperature
ΔS_m = Motional entropy

E_a – Motional enthalpy (activation energy for ion transport)

Equation 1.1 Arrhenius equation

According to the Arrhenius equation, improving conductivity can be achieved via four different methods: 1) by increasing the number of charge carriers, 2) by increasing the motional entropy, 3) by decreasing the activation energy of proton transfer, and 4) by increasing the operational temperature. Increasing the number of charge carriers can be achieved by introducing highly acidic moieties such as H_2SO_4, RSO_3H, H_3PO_4, water/H_3O^+, RCO_2H, or protonated N-heterocycles functional group into the inherent framework and/or as impregnated guest species in the proton conduction channels. Also, it is important that only about 50% of the charge carriers are ionized and they are distributed in a homogeneous manner; protons hop from one site to another and it is just as important to provide unprotonated sites that can act as facile proton acceptors in addition to maximizing the number of proton donors. Lastly, how the proton carriers interact with each other as well as the magnitude of host-guest interactions significantly affect the resultant proton conductivity. For instance, a proton carrier such as protonated N-heterocycle may need to reorient itself following a proton transfer. The proton carrier would re-align its proton donor/acceptor site to minimize the proton hopping distance and the activation barrier for receiving the next proton for transport. This is closely related to the structure of the PCMOF and the degrees of freedom its proton carriers experience, and it is represented by the following three variables in the Arrhenius equation: D_o, ΔS_m, and E_a.

Ultimately, the best PCMOF would have a 3-dimensional pore structure with large number of available protons and proton carriers that have many rotational degrees

of freedom. Proton carriers would interact weakly with the framework and they should be close enough to each other for proton hopping (within the H-bonding distance). Yet, the proton carriers should not be too close to each other to hinder reorientation following proton transfer.

Building from this knowledge, two design strategies were investigated to enhance proton conductivity of a proton conducting MOF named β-PCMOF2. β-PCMOF2, which stands for the β-phase of the proton conducting metal organic framework #2, was originally reported by Hurd *et al*.[8] β-PCMOF2 consists of 2-D sheets of 2,4,6-trihydroxy-1,3,5-benzene trisulfonate ligand in a honeycomb-like structure, that are cross linked in the third dimension with sodium counter cations (Figure 1.2). β-PCMOF2 contains 1-dimensional pores lined with sulfonate oxygen atoms, that are 5.6 Å in diameter. The 1-dimensional pores are hydrophilic in nature, and form pathways for proton conduction (as indicated by the blue arrow in Figure 1.2). The proton conductivity of β-PCMOF2 was found to be 1.3×10^{-3} S cm^{-1} at 90% relative humidity and 85 °C, and 1×10^{-9} S cm^{-1} under anhydrous conditions and at 100 °C. First design strategy investigated was isomorphous ligand replacement where an entire C_3-symmetric trisulfonate ligand, the building block of β-PCMOF2, was substituted with a C_3-symmetric tris(hydrogen phosphonate) ligand to yield PCMOF2½ (Chapter 2).[1] Subsequently, isomorphous ligand replacement was combined with the second design strategy, heterocycle doping (previously studied by Hurd *et al*), to further enhance the proton conductivity of PCMOF2½ (Chapter 3).

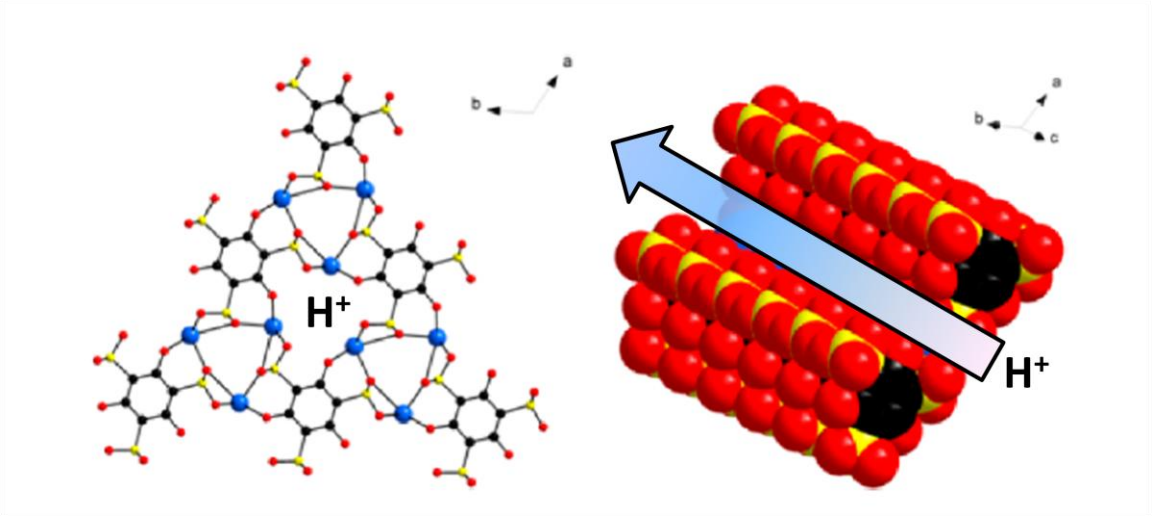

Figure 1.2 Structure of β-PCMOF2 showing a single pore (left) and space-filling cross section of a pore (right). Sodium, oxygen, sulfur and carbon are blue, red, yellow, and black respectively.

1.3 Overview of Chapter 2: Enhancing Proton Conduction in a Metal-Organic Framework by Isomorhpous Ligand Replacement

Chapter 2 presents my first-author publication in the Journal of the American Chemical Society.[1] The communication is titled *Enhancing Proton Conduction in a Metal-Organic Framework by Isomorphous Ligand Replacement*. This work, combined with another JACS communication by Dr. Jared M. Taylor,[9] led to an invited Perspective article in Science (2013, co-authored) that highlighted my work as a significant achievement in the field.[2] Lastly, this work, paired with Dr. Taylor's publication, was featured in the chemical news section of Canadian Chemical News - March/April 2013: *Metal-organic frameworks advance fuel cell technology*.[10]

Herein, a rational design strategy called *isomorphous ligand replacement* was utilized to increase the proton conductivity of a proton conducting metal organic framework (PCMOF) named β-PCMOF2. The concept of isomorphous replacement was applied to entire ligands where an entire C_3-symmetric trisulfonate ligand was substituted

with a C_3-symmetric tris(hydrogen phosphonate) ligand, while maintaining the parent MOF structure. The resultant material, PCMOF2½, had its proton conductivity raised 1.5 orders of magnitude compared to the parent material, to 2.1×10^{-2} S cm^{-1} at 90% relative humidity and 85 °C.

1.4 Overview of Chapter 3: Synergistic Merging of Two Design Strategies in a Proton Conducting Metal-Organic Framework

Following the publication featured chapter 2, I decided to investigate merging of the two design strategies – isomorphous replacement and guest-loading (small amphiprotic molecules are inserted into the structure to aid proton conduction) – to further enhance the proton conduction of PCMOF2½. Chapter 3 features my second, first-author manuscript submitted to the Journal of the American Chemical Society titled *Synergistic Merging of Two Design Strategies in a Proton Conducting Metal-Organic Framework*. It is a full article that features 7 new PCMOFs and a comprehensive study of synergistically merging the two design strategies. One resulting material, PCMOF2½(Pyrazole), had its proton conduction raised 1.9 orders of magnitude compared to the parent material, to 1.1×10^{-1} S cm^{-1} at 90% relative humidity and 85 °C, while maintaining the parent β-PCMOF2 structure. In addition, the exact mechanism of isomorphous ligand replacement synthesis was elucidated to be a thermodynamically driven solid state reaction.

1.5 Statement of contribution

1.5.1 *Enhancing Proton Conduction in a Metal-Organic Framework by Isomorhpous Ligand Replacement*

Author list: SiRim Kim, Karl W. Dawson, Benjamin S. Gelfand, Jared M. Taylor, and George K.H. Shimizu*

S.R.K synthesized and fully characterized PCMOF2½ S.R.K prepared the manuscript. S.R.K conducted detailed analyses on the mechanism of isomorphous ligand replacement via powder XRD, elemental analysis, and SEM/EDX that were instrumental for addressing reviewers' comments for the manuscript revision. B.S.G provided valuable assistance in completing the SEM/EDX measurements. K.W.D provided assistance in characterizing and analyzing the conductivity data for PCMOF2½, and also performed edits on the manuscript. K.W.D and S.R.K prepared the supporting information. J.M.T conducted water sorption isotherm measurements on PCMOF2½; the isotherm measurements were completed, but were not included in the manuscript. G.K.H conceived the isomorphous ligand replacement strategy and supervised the project. G.K.S performed the final edits on the manuscript prior to publication.

1.5.2 Synergistic Merging of Two Design Strategies in a Proton Conducting Metal-Organic Framework

Author list: SiRim Kim, Jeff A. Hurd, Karl W. Dawson, Benjamin S. Gelfand, Norman E. Wong, and George K.H. Shimizu*

S.R.K synthesized and fully characterized 7 out of 10 PCMOFs featured in this manuscript, which included the three key PCMOFs of the study: PCMOF2½(Pyrazole), PCMOF2½(Triazole), and PCMOF2½ *Melamine*. S.R.K prepared the manuscript and the supporting information. S.R.K conceived the synergistic merging of the two design strategies and successfully executed the experiments. J.A.H synthesized and characterized 2 out of 10 PCMOFs that were featured in the work for which N.E.W. performed conductivity measurements for the 2 PCMOFs under anhydrous conditions. J.A.H conceived the heterocycle doping strategy as well the synthesis and

characterization of β-PCMOF2. K.W.D re-synthesized 3 out of 10 PCMOFs originally studied by Jeff A. Hurd. S.R.K characterized these 3 PCMOFs. B.S.G. conducted SEM/EDX measurements, synthesized H_6L2, and provided assistance in Powder XRD analysis and d-spacing calculations. G.K.H supervised the project and provided the final edits on the manuscript.

Chapter Two: **ENHANCING PROTON CONDUCTION IN A METAL-ORGANIC FRAMEWORK BY ISOMORPHOUS LIGAND REPLACEMENT**

2.1 Introduction

Metal-organic frameworks (MOFs) are versatile crystalline solids that are currently being investigated for various applications.[1] The predominant interest in MOFs is as sorbents for gas capture and separation which stems from their potential to show high porosity and guest selectivity.[2] Emerging applications for MOFs include catalysts,[3] molecular sensors,[4] and drug delivery.[5] Properties of MOFs that distinguish them from many other classes of materials are their highly ordered structures and modular nature. The ability to determine the exact structure of the solid using X-ray crystallography provides valuable insight into structure-property relationships. Combined, these two features allow for customization of the material to yield desired physical and chemical properties using rational design.

With regards to the design of a better proton conducting material, MOFs have shown themselves to be advantageous in a number of respects, and this area has seen tremendous growth in the recent past.[6-11] The regular structure of MOFs can serve as a scaffold to anchor acidic groups and form efficient proton transfer pathways.[7,8] The crystalline nature of MOFs can allow for direct visualization of the proton conduction pathway and offer firm handholds for modeling. The regular porous structure of MOFs can be loaded with less volatile, amphiprotic guests to enable proton conduction over 100 °C.[9-11] In this latter theme, we have previously reported β-PCMOF2, a trisodium 2,4,6-trihydroxy-1,3,5-trisulfonate benzene (Na_3L1) complex containing pores lined with sulfonate oxygen atoms (Figure 1.2).[10] The pores in this MOF were 5.6 Å in diameter and

were able to be loaded into with 1,2,4-triazole. β-PCMOF2 itself, with nonloaded pores, conducted on the order of 10^{-9} S cm^{-1} at 100 °C under anhydrous conditions. With a loading of 0.3 triazole molecules per formula unit, a jump in conductivity of 5 orders of magnitude was observed reaching 2×10^{-4} S cm^{-1} at 150 °C under anhydrous conditions. While lower loadings of triazole did not augment conductivity, higher loadings (up to 0.6 triazole) only resulted in modest changes (up to 5×10^{-4} S cm^{-1}).[10]

Conductivity is a product of the magnitude of the charge, the number of charge carriers, and mobility of the charges. Given the rather narrow range of conduction observed with substantive variation in the carrier molecule, it was hypothesized that, in the β-PCMOF2 system, the limiting factor for proton conduction was the availability of acidic protons. With the pore lined with exclusively sulfonate groups, other than replacing Na ions with protons (which to any extent would likely compromise the structure) there was no option for directly modifying the system to increase acidity. The ligand 1,3,5-benzenetriphosphonic acid, H_6L2, has been previously reported[12] including as the Zn^{2+} complex in PCMOF3.[8] Both L1 and L2 are ligands containing a single aromatic core, possessing C_3 symmetry, and having a hydrophilic periphery (Figure 2.1). We had noted a general structural trend, as observed in β-PCMOF2, of forming structures with one-dimensional columns where hydrophobic interactions between arene cores and hydrogen bonding about the periphery were maximized. It seemed that if trianionic molecules of L1 in β-PCMOF2 could be replaced by trianionic, but triprotic, H_3L2 molecules, the pores would be partially lined with hydrogen phosphate groups rather than exclusively nonprotonated sulfonate groups which should augment proton conduction.

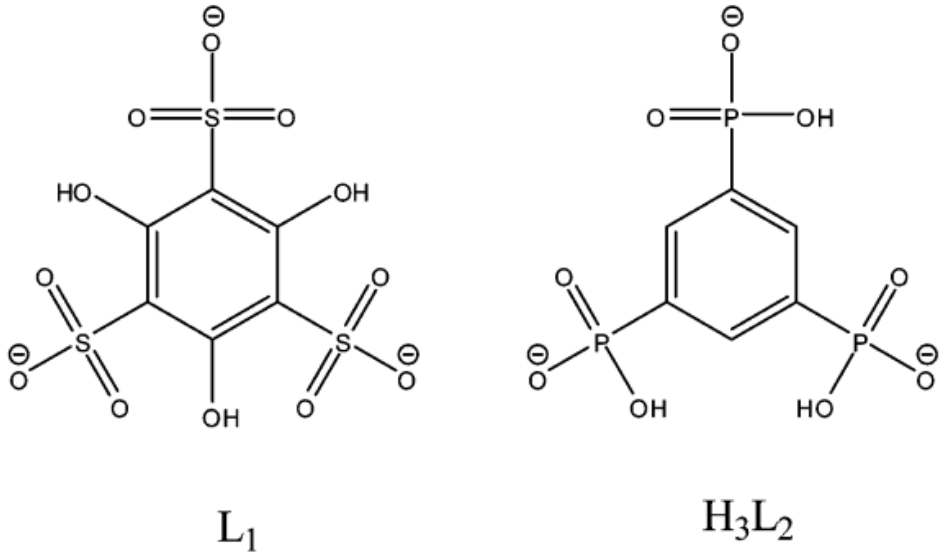

Figure 2.1 Molecular structures of L1 and H_3L2

2.2 Results

Herein, we report the isomorphous replacement of L1 molecules in the β-PCMOF2 structure with H_3L2 molecules. We call the mixed ligand system PCMOF2½ to convey both the hybrid nature (components of both PCMOF2 and PCMOF3) and the fact the resulting structure is related to β-PCMOF2. The impact on conductivity is profound, as the proton conductivity increases 1.5 orders of magnitude. At 90% relative humidity and 85 °C, the proton conductivity reaches 2.1×10^{-2} S cm^{-1}, the best proton conduction value reported in any proton conducting coordination material to date (January 2013; also see Tables 2.2 and 2.3 shown at the end of the chapter).

β-PCMOF2 was prepared as previously reported.[10] PCMOF2 has a lower temperature α-phase and a higher temperature β-phase; all preparations initially yield the α-phase which must be converted hydrothermally to the β-phase. In the PCMOF2½ synthesis, a prevailing question is whether the two ligands are intimately combined at the nanoscale or whether they are merely intermingled at the microscale. Initially, parallel

preparations were carried out on a hydrothermally prepared sample of α-PCMOF2, H_6L2, and Na_2CO_3 (see section 2.3 Experimental analysis) and on a mechanically mixed sample of α-PCMOF2 and Na_3H_3L2. Hydrothermal conditions were not sufficient to afford a pure phase material; however, the molecular formula of the product was calculated to be $[Na_3L1]_{(0.66)}[Na_3H_3L2]_{(0.34)}(H_2O)1.2$ merging elemental analysis and thermogravimetric analysis. During the course of impedance analysis on this hydrothermal product (at up to 90% relative humidity and up to 85 °C), a phase transformation was observed to afford PCMOF2½. Subsequently, pelletization (a mild version of which is employed in the conductivity analysis) was determined as a key variable for preparation of PCMOF2½ (*vide infra)*. Given that neither humidity dependent proton conductivity measurements nor isomorphous ligand replacement in MOFs is truly commonplace, we feel there is merit to presenting these results in a chronological manner. Figure 2.2 summarizes the parallel between the mechanical mixture preparation and the hydrothermal preparation; the two preparations ultimately yield the mixture of Na_3L1 (β-PCMOF2) and Na_3H_3L2, which converts to PCMOF2½ when placed under the impedance analysis conditions.

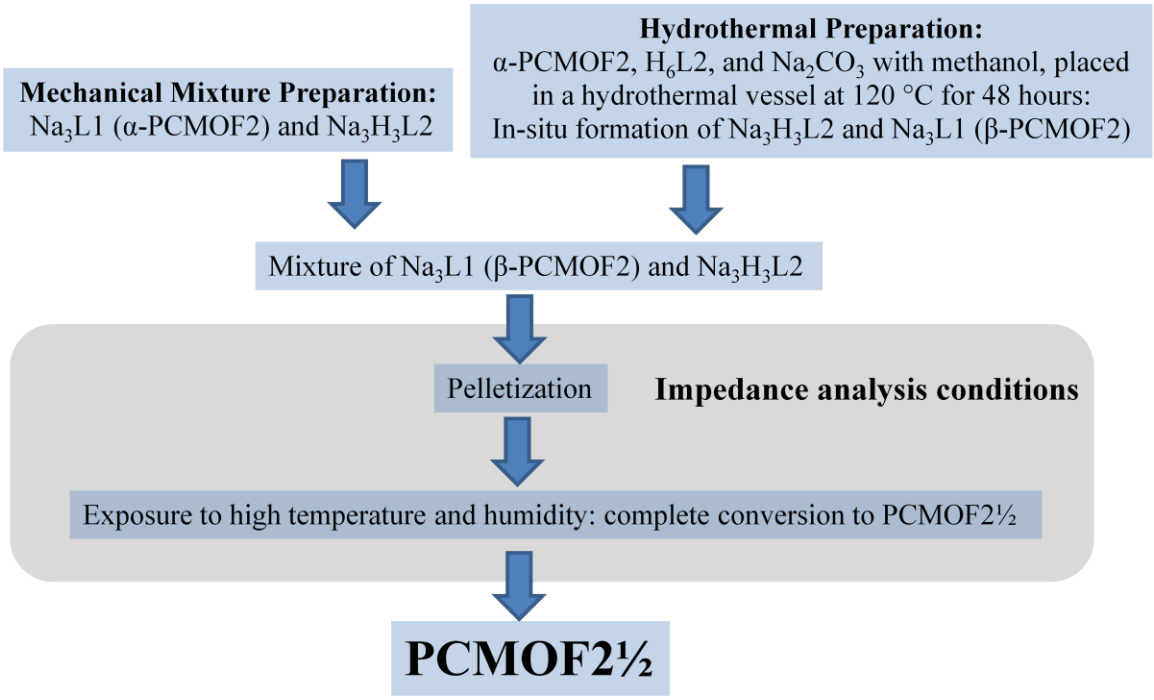

Figure 2.2 A schematic diagram of the two parallel preparations of PCMOF2½: the mechanical mixture preparation and the hydrothermal preparation. Both preparation ultimately yields the mixture of Na_3L1 (β-PCMOF2) and Na_3H_3L2, which converts to PCMOF2½ when placed under impedance analysis conditions.

2.3 Experimental analysis

Two-probe AC impedance analyses were performed on a Princeton Applied Research VersaSTAT potentiostat/galvanostat from 10^6 to 1 Hz. Pristine powder samples were placed in a ceramic cell and manually compressed between two titanium electrodes. The sample cells were placed inside a temperature and humidity controlled chambers. Proton conductivity was measured from 20 to 85 °C for two complete heating and cooling cycles. Samples were equilibrated for at least 8 h after each step in temperature and 48 h after each step in humidity. These conditions have been employed on numerous samples in our group with reliable results. On the first heating cycle, incongruous data were obtained (Figure 2.3). This was initially attributed to nonequilibrium with respect to humidity. The second cycle showed more consistent data as the cooling run retraced the

heating cycle and data could be fit to an Arrhenius relationship (Figure 2.3). Further testing showed that equilibration times for temperature (Figure 2.4) and humidity (Figure 2.5) were sufficient.

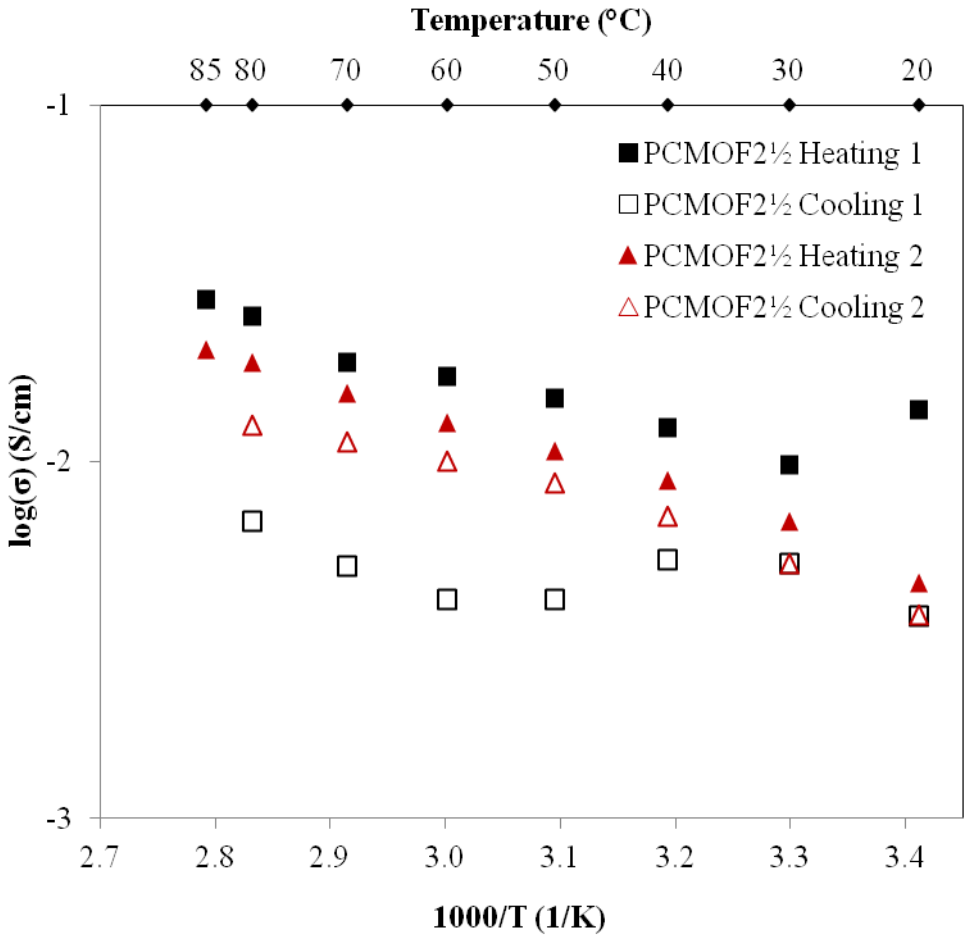

Figure 2.3 Log conductivity versus 1/temperature plot of the multiple heating and cooling cycles required for the equilibration of PCMOF2½.

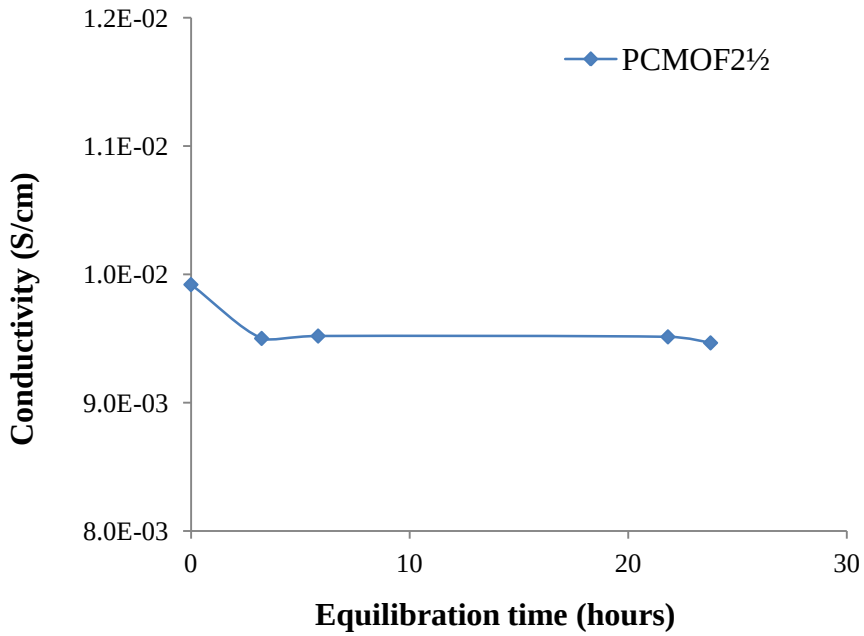

Figure 2.4 Conductivity versus equilibration time plot of PCMOF2½ at 30 °C and 90% relative humidity. Temperature has been increased from 20 °C to 30 °C at the zero hour mark.

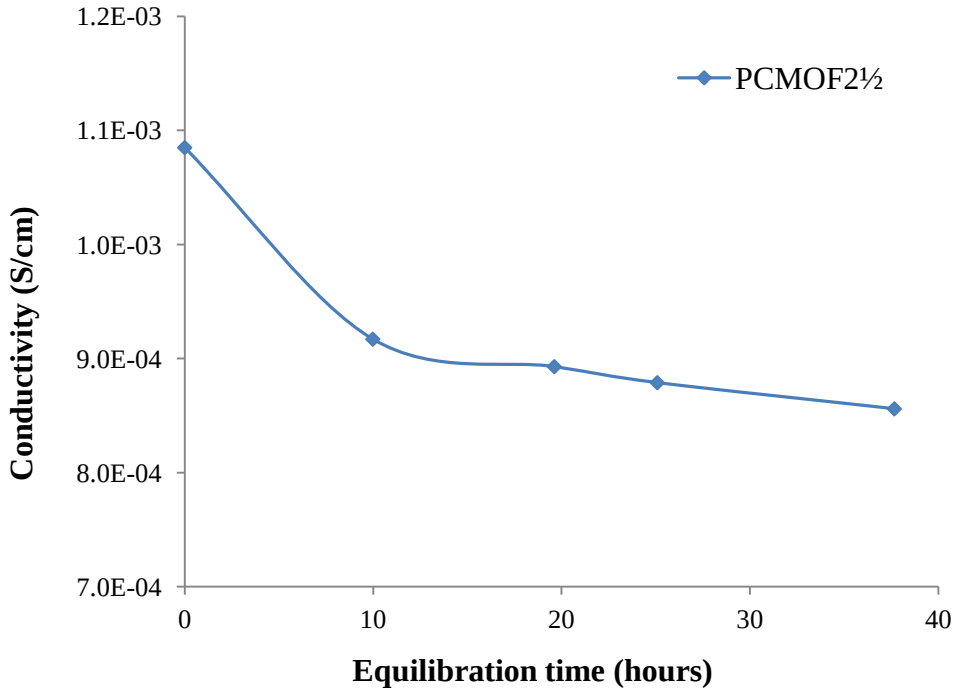

Figure 2.5 Conductivity versus equilibration time plot of PCMOF2½ at 20°C and 70% relative humidity. Humidity has been decreased from 90% to 70% at the zero hour mark.

As a routine, we perform chemical analyses on samples after impedance and the PXRD pattern of the postimpedance hydrothermal sample appeared very similar to pure β-PCMOF2 as well the simulated powder XRD of β-PCMOF2 obtained from its single crystal structure (Figure 2.6 B-C, a small peak at 23.5° 2θ, possibly Na_3H_3L2 are visible). The presence of L2 in the pre- and postimpedance samples were confirmed through ^{1}H and ^{31}P NMR analysis. Thermogravimetric and elemental analysis confirmed $[Na_3L1]_{(0.66)}[Na_3H_3L2]_{(0.34)}(H_2O)0.75$ as a postimpedance composition (the same 2:1 ratio of L1:L2 as has been initially prepared). Henceforth, the PCMOF2½ descriptor will refer to this phase. All conductivity data reported here are based solely on the equilibrated second heating/cooling cycles. A mechanical mixture prepared by minimal mixing of α-PCMOF2 and Na_3H_3L2 (Figure 2.6 G-I) was also examined by impedance analysis for comparison of its proton conductivity. This sample also showed an erratic first heating cycle but ultimately gave PXRD and proton conductivity (1.9×10^{-2} S cm^{-1}, Figure 2.7 and 2.8) comparable to PCMOF2½. This sample, although related (Figure 2.2), did not possess an identical ratio of L1:L2 and will not be discussed as PCMOF2½ (see section 2.4.7).

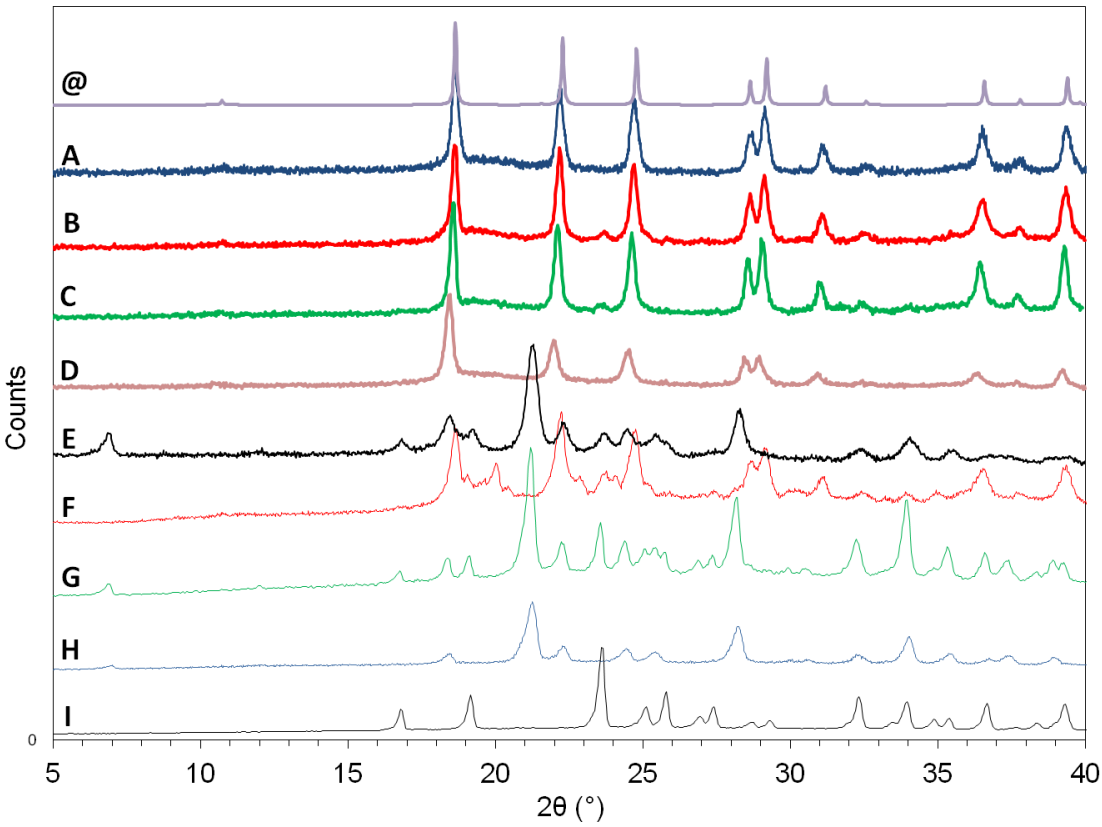

Figure 2.6 [@] Simulated powder XRD pattern of β-PCMOF2 from its single crystal structure; powder XRD patterns of [A] β-PCMOF2 post-impedance; [B] PCMOF2½ prepared hydrothermally, post-impedance; [C] PCMOF2½ prepared mechanically, post-impedance; [D] PCMOF2½ prepared by pelletization, pre-impedance; [E] Intermediate PCMOF2½, prepared by pelletization; [F] Intermediate PCMOF2½ prepared hydrothermally; [G] Mechanical mixture of Na_3L1 and Na_3H_3L2 ; [H] α-PCMOF2 (Na_3L1); [I] Na_3H_3L2.

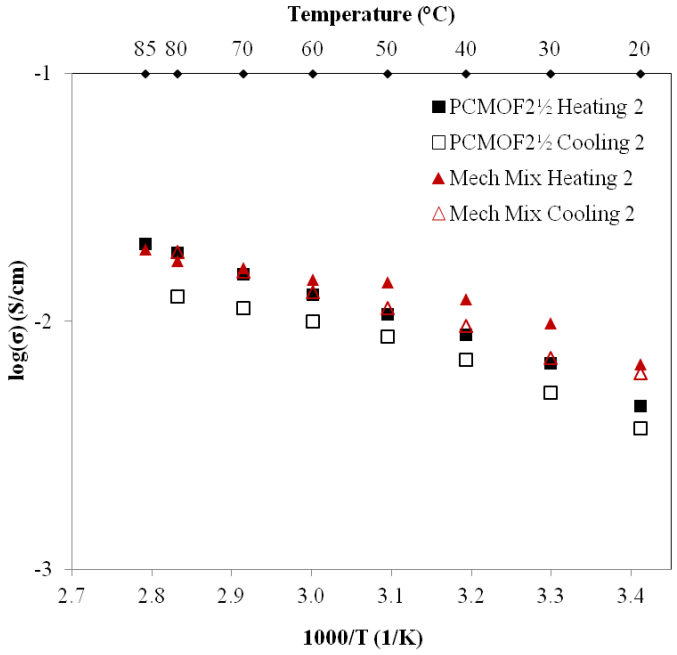

Figure 2.7 Log conductivity versus 1/temperature plot of the mechanical mixture and PCMOF2½'s second heating and cooling cycles.

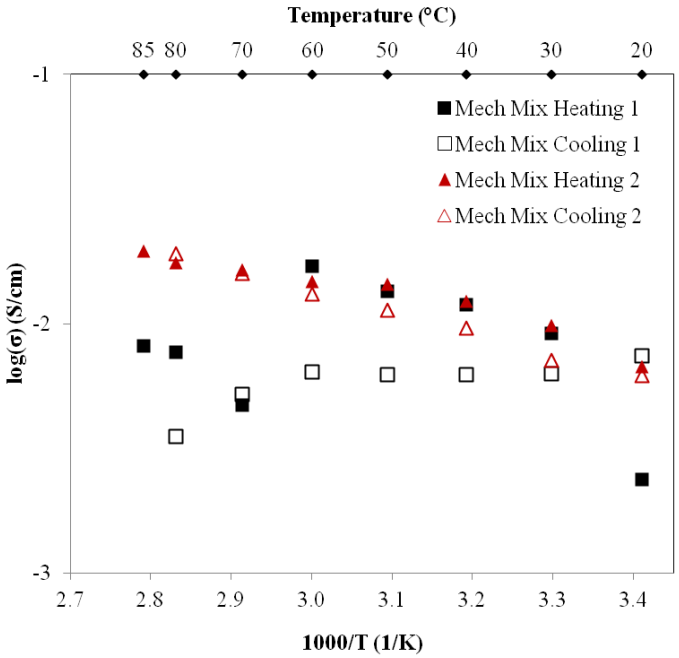

Figure 2.8 Log conductivity versus 1/temperature plot of the multiple heating and cooling cycles required for the equilibration of the mechanical mixture of α-PCMOF2 and Na_3H_3L2.

2.4 Synthesis and analytical methods

2.4.1 Synthesis and analytical procedures

All starting materials were obtained from commercial suppliers (Alfa Aesar, Sigma Aldrich) and were used without further purification. ^{1}H and ^{31}P NMR spectra were collected on a Bruker Advance II 400 MHz NMR spectrometer. Thermogravimetric analysis was performed on a Netzsch STA 409 PC TGA/DCS analyzer in aluminum pans under 60 mL/min flow of N_2 at a heating rate of 2 °C/min from room temperature to 450°C. Elemental analyses were performed using a Perkin Elmer Model 2400 series II. Powder X-ray diffraction data was collected on a Rigaku Miniflex II Desktop X-Ray Diffractometer (Cu K_α X-ray source) using an automated six sample changer.

2.4.2 Synthesis of β-PCMOF2

Anhydrous phloroglucinol (8.05 g, 63.9 mmol) was dissolved in dry dimethyl carbonate (200 mL) and the resulting yellow solution cooled to 0 °C under Ar. Chlorosulfonic acid (12.4 mL, 187 mmol, 2.93 equiv.) was added dropwise over the course of 2 minutes with vigorous stirring, resulting in an orange colored solution. The reaction was warmed to ambient temperature and allowed to proceed for 1.5 h under a steady flow of Ar before the system was sealed and stirred for an additional 22.5 h. The solvent was then removed via rotary evaporation and the resulting viscous, brown oil dissolved in 150 mL of water. Sodium bicarbonate was added to the solution until it reached a pH of 2.0. Addition of the aqueous solution to 4 L of acetone resulted in the formation of a thick white precipitate, which was isolated via vacuum filtration. Yield: 22.6 g, 84%. This phase (α) was then converted to the β-phase via heating in a bomb apparatus. As synthesized α-PCMOF2 (0.50 g, 1.2 mmol) was placed into a 23 mL

Teflon autoclave. To this a mixture of water (5 mL), methanol (1.5 mL) and acetone (1.5 mL) was added. The Teflon autoclave was then sealed in a hydrothermal bomb. The bomb was heated at 100 °C for 24 h and then cooled back to room temperature over a period of 12 hours. The resulting white precipitate was isolated via vacuum filtration. Yield: 0.49 g, 98%.

2.4.3 Synthesis of hexaethyl 1,3,5-benzenetriphosphonate (Et_6L2)

Hexaethy-1,3,5-benzenetriphosphonate was synthesized by literature methods using the nickel catalyzed Michaelis-Arbuzov reaction.[30] 1,3,5-Tribromobenzene (9.203 g, 29.23 mmol) and nickel (II) bromide (1.50 g, 6.86 mmol) were mixed in 1,3-diisopropylbenzene (20.0 mL) in a 3-neck round bottom flask with a water cooled condenser and a needle valve addition funnel. Triethyl phosphite (33.0 mL, 205 mmol) was dissolved in 1,3-diisopropylbenzene (20.0 mL) in the addition funnel. The setup was placed under an inert atmosphere of dried argon, and the round bottom flask was heated to reflux. Once refluxing, the triethyl phosphite solution was added dropwise as slowly as possible. The mixture was refluxed for one day, then cooled to room temperature and filtered to remove the insoluble nickel compounds. Excess phosphite and solvent were removed by room temperature vacuum distillation, resulting in viscous black oil. The oil was dissolved in dichloromethane (~ 200 mL) and filtered through a silica gel plug (230 to 400 mesh) to remove the soluble nickel compounds, and washed with acetone to ensure complete removal of the product from the silica. The organics were combined, and the solvents were removed by rotary evaporation, resulting in yellow oil. Any remaining phosphate and phosphite impurities were then removed by heating to 150°C under vacuum for 4 to 6 hours, resulting in yellow oil. ^{1}H NMR (400 MHz, $CDCl_3$): δ = 8.38

(m, 3H, aromatic H), δ = 4.15 (m, 12H, CH_2), δ 1.33 (t, 18H, CH_3); ^{31}P {^1H} NMR (162 MHz, $CDCl_3$, trimethyl phosphate internal reference standard): δ = 15.39.

2.4.4 Synthesis of 1,3,5-benzenetriphosphonic acid (H_6L2)

H_6L2 was synthesized by literature methods using acid hydrolysis.[30] Hexaethyl-1,3,5-benzenetriphosphonate (0.874 g, 1.80 mmol) was dissolved in a mixture of RO water (25 mL) and concentrated hydrochloric acid (25 mL). The solution was refluxed for 8 hours, then cooled to room temperature to give a dark yellow solution. The hydrochloric acid was removed by rotary evaporation to give dark yellow oil. The oil was dissolved in RO water (50 mL) and decolourized by stirring with charcoal (Norit A). The mixture was filtered to remove the charcoal to yield a clear colourless solution. Water was removed by rotary evaporation to yield a white crystalline powder which was dried under high vacuum for 6 hours (0.440 g, 1.38 mmol, 76.8% yield). Elemental analysis calculated (%): C=22.66, H=2.85; Found: C=22.38, H=2.81. ^1H NMR (400 MHz, DMSO-d_6): δ = 8.11 (m, 3H, aromatic H); ^{31}P {^1H} NMR (162 MHz, DMSO-d_6, trimethyl phosphate internal reference standard) δ = 12.13.

2.4.5 Synthesis of $Na_3H_3L2 \cdot 2.75H_2O$

H_6L2 (67.9 mg, 0.213 mmol) and Na_2CO_3 (34.0 mg, 0.321 mmol) were placed in a vial with methanol (1 mL) and RO water (1 mL). The mixture was heated with a heat gun to help dissolve the solids. A small amount of the solids remained insoluble, so the clear supernatant liquid was decanted into a new vial, to which methanol (20 mL) was added and stirred to precipitate the product which was filtered to give a white, crystalline powder (40.9 mg, 0.0943 mmol, 44.3% yield). Elemental analysis calculated (%):

C=16.62, H=2.67; Found: C=16.82, H=2.52. TGA: 21 – 200 °C: -11.46% observed, -11.43% calculated for loss of 2.75 waters; 200 – 450 °C: -6.57% observed.

2.4.6 Synthesis of PCMOF2½; $[Na_3L1]_{0.66}[Na_3H_3L2]_{0.34}\cdot 1.20H_2O$

α-$Na_3L1\cdot 2.75H_2O$ (α-PCMOF2, 70.0 mg, 0.145 mmol), H_6L2 (25.9 mg, 0.0814 mmol) and Na_2CO_3 (8.4 mg, 0.0793 mmol) were placed in a 23 mL Teflon autoclave with methanol (2 mL). This mixture was stirred for 15 minutes, and then the Teflon autoclave was sealed in a stainless steel jacket and heated to 120°C over two hours, held at 120°C for 48 hours, and then cooled back to room temperature over 12 hours. The product was filtered and rinsed with methanol (10 mL) and was dried with flowing air on the filter paper. A white, crystalline powder was obtained (62.8 mg, 0.141 mmol, 60.% yield). Elemental analysis for $[Na_3L1]_{0.66}[Na_3H_3L2]_{0.34}\cdot 1.20H_2O$ Calculated (%): C=16.47, H=1.48; Found: C=16.87, H=1.41. ^{1}H NMR (400 MHz, D_2O): δ = 8.24 (m, L_2 aromatic H); ^{31}P {^{1}H} NMR (162 MHz, D_2O, unreferenced): δ = 13.63. TGA: 21 – 200 °C: -4.99% observed, -4.94% calculated for loss of 1.20 waters; 200 – 325 °C: -2.61% observed, partial framework decomposition; 325 – 450 °C: -30.17% observed, major framework decomposition; 450 – 800 °C, final framework decomposition and carbonization (Figure 2.9 and 2.10). Post impedance composition: Elemental analysis for $[Na_3L1]_{0.66}[Na_3H_3L2]_{0.34}\cdot 0.75H_2O$ calculated (%): C=16.78, H=1.30; Found: C=16.74%, H=1.14%. ^{1}H NMR (400 MHz, D_2O): δ = 8.25 (m, L_2 aromatic H); ^{31}P {^{1}H} (162 MHz, D_2O, unreferenced): δ = 13.74.

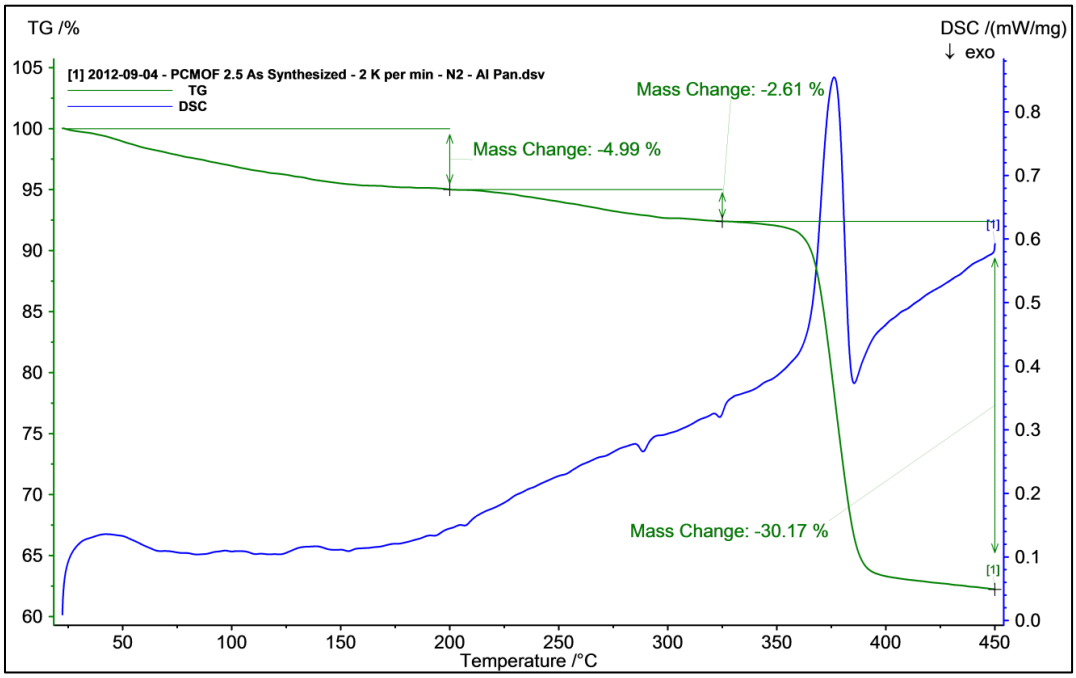

Figure 2.9 Combined TGA (in green)/DSC (in blue) of PCMOF2½ pre-impedance with the calculated mass losses. Measured at 2K per minute under N_2 atmosphere.

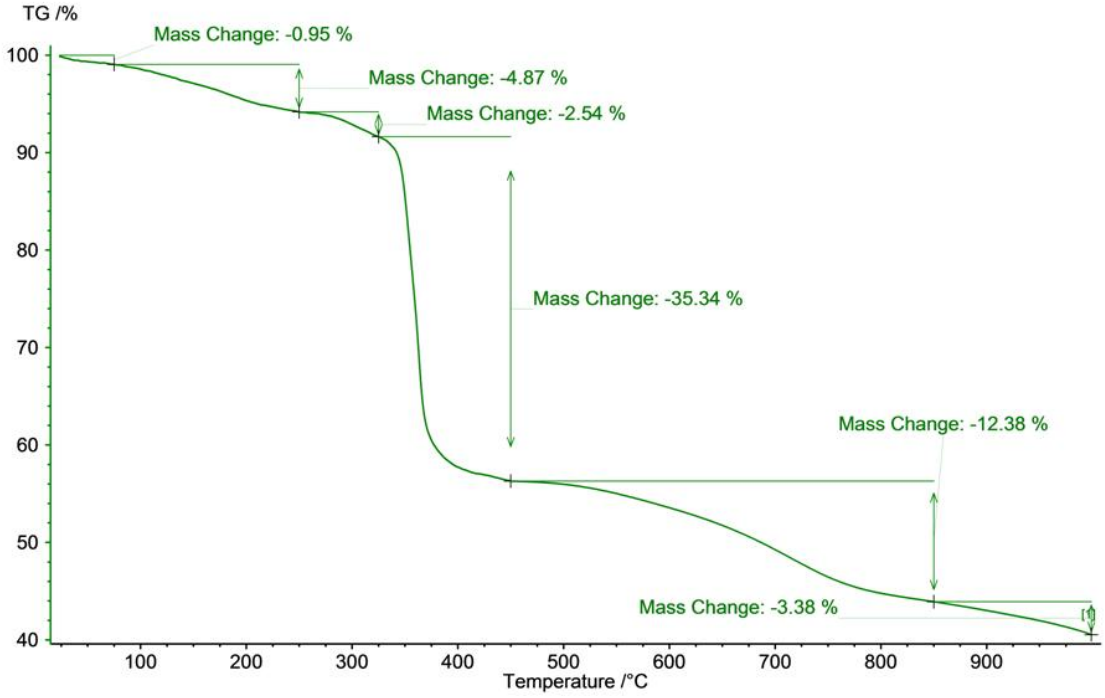

Figure 2.10 TGA (in green) of PCMOF2½ pre-impedance with the calculated mass losses. Measured at 0.5K per minute to 450K, then at 10K per minute up to 1000K. The low temperature mass loss up to 350K is still broad at the slower ramp rate.

2.4.7 Mechanical mixture of α-PCMOF2 and Na_3H_3L2

α-PCMOF2 and Na_3L2 were individually ground into fine powders using a mortar and pestle. Ground α-$Na_3L1{\cdot}2.75H_2O$ (50.1 mg, 0.104 mmol) and ground $Na_3H_3L2{\cdot}2.75H_2O$ (24.9 mg, 0.0574 mmol) were placed in a vial and mechanically shaken to produce a mechanical mixture. Elemental analysis for $[Na_3L1{\cdot}2.75H_2O]_{0.65}[Na_3H_3L2{\cdot}2.75H_2O]_{0.35}$ Calculated (%): C=15.51, H=2.07; Found: C=15.23, H=1.66. Post impedance composition: Elemental analysis for $[Na_3L1]_{0.79}$ $[Na_3H_3L2]_{0.21}{\cdot}0.48H_2O$ Calculated (%): C=16.73, H=1.07; Found: C=16.34, H=0.68.*

* Of the components β-PCMOF2, Na_3H_3L2, and PCMOF2½, Na_3H_3L2 has by far the greatest water solubility. The mechanical mixture discussed here is formed by minimal manual combination of the phases (no grinding or heating) and it is expected that some of the Na_3H_3L2 was dissolved. When a sample is prepared hydrothermally or by pelletization, the Na_3H_3L2 is readily incorporated into *and retained* in the β-PCMOF2 structure as confirmed by elemental analysis & the SEM-EDX analysis (please see section 2.5 Formation and confirmation of PCMOF2½).

2.4.8 AC impedance analysis

Powdered samples (20 – 40 mg each) were placed in a porous zirconium pyrophosphate ceramic cell and were compressed between 2 solid titanium electrodes (0.3175 cm diameter). The sample length was measured by the difference between the empty cell and the filled cell, and was typically 1 to 2 mm. The sample cells were places inside a temperature and humidity controlled chamber (Espec BTL-433) and connected to a Princeton Applied Research VersaSTAT 3 impedance analyzer using a 2 probe setup. AC impedance data was collected by cycling between 10^6 and 10^0 Hz with 200 mV of

applied potential using VersaStudio software. Samples were equilibrated for at least 8 hours after each step in temperature or 48 hours for each step in relative humidity.

2.4.9 Environmental controls

Exposure of the sample to humid environments was performed for conditions at and below 90% relative humidity using an Espec BTL-433 humidity control oven. Temperature was monitored using thermocouples place next to the samples as well as the instrumental readings of the humidity control oven.

2.4.10 Powder XRD of PCMOFs

Powder XRD was used to validate the structures of the synthesized PCMOFs. Data was collected on a Rigaku Multiflex "theta-theta' X-ray diffractometer equipped with a PSPC scintillation counter using Cu K_α tube (λ = 0.15418 nm) operated at 40 kV and 40 mA. Samples for analysis were ground into fine powders using a mortar and pestle. They were then mounted onto a zero background sample holders and the surface of the powders leveled using a glass slide. A scan range of 2-theta = 3° to 60°, with a scan speed of 0.2 deg/min and a sample width equal to 0.02° were employed. Following collection, the data was processed using winJADE software.

2.4.11 Scanning electron microscopy imaging & energy dispersion X-ray spectroscopy (SEM/EDX)

SEM/EDX was used to determine the incorporation of Na_3H_3L2 into the β-PCMOF2 structure by measuring the 2-dimensional elemental distribution of phosphorous and sulfur of PCMOF2½ and comparing this to SEM images. Samples were prepared for analysis by attaching a piece of carbon tape onto a flat aluminum sample holders and then putting the various materials on the tape. N_2 flow was gently blown over

the sample holder to remove the excess material. Samples were analyzed on a Zeiss ΣIGMA VP instrument using the backscattered electron detector, a chamber pressure of 1 × 10^{-7} bar, and an accelerating voltage of 20 keV from the thermal field emission source. EDX was collected on an Oxford Instruments x-act system using a 10 mm^2 silicon drift detector and processed with INCA analysis software.

2.5 Formation and confirmation of PCMOF2½

In considering the in situ formation of PCMOF2½ during impedance analysis (when hydrothermal conditions were not successful), it was hypothesized that a key variable could be the compaction of the sample. Samples of α-PCMOF2 and Na_3H_3L2 in a 2:1 molar ratio were ground by mortar and pestle, thoroughly mixed, and then pressed into a pellet with 10,000 pounds/$inch^2$ of pressure. This pellet was then placed in a 23 mL autoclave with a vial containing water (1.7 mL). Heating at 80 °C for 48 h gave complete conversion to PCMOF2½, as shown by PXRD (Figure 2.11), with the expected ligand ratio as confirmed by elemental analysis and SEM-EDX (Figure 2.13). This conversion was monitored by performing PXRD at 0, 6, and 24 h intervals (Figure 2.11), and the fully converted PXRD was compared with that of post-impedance samples of PCMOF2½ and β-PCMOF2 (Figure 2.12). The SEM-EDX (Figure 2.13 and 2.14) show initial aggregates of P which over time converts to samples that give an even distribution of P and S throughout the material. While the PXRD patterns in Figure 2.6 A-D and @ appear similar, they are not identical. Based on the peak picking and the d-spacing analysis using NaCl as a standard, the pattern for PCMOF2½ is slightly shifted and gives differences of 0.093 Å and 0.041 Å in *d*-spacing for the 011 place (in the place of the ligand arene rings) and the 001 plane (perpendicular to the ligands) respectively (Figure 2.15 and

Table 2.1). While these changes are small, they are consistent and affirm the pattern is not that of pure β-PCMOF2.

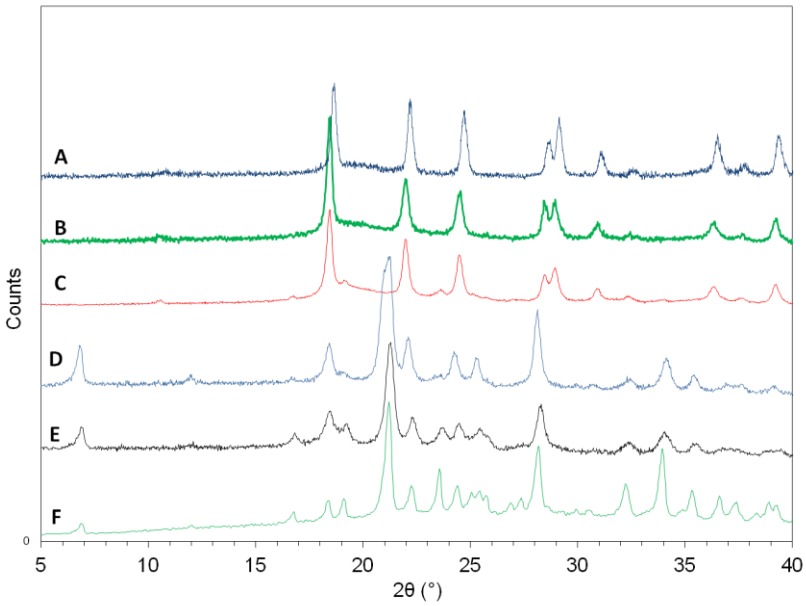

Figure 2.11 Powder XRD patterns of: [A] β-PCMOF2, post-impedance; [B] PCMOF2½, 48 hour hold time (fully converted); [C] PCMOF2½, 24 hour hold time, [D] PCMOF2½, 6 hour hold time; [E] PCMOF2½, 0 hour hold time; [F] mechanical mixture of *:* α-PCMOF-2 and Na_3H_3L2.

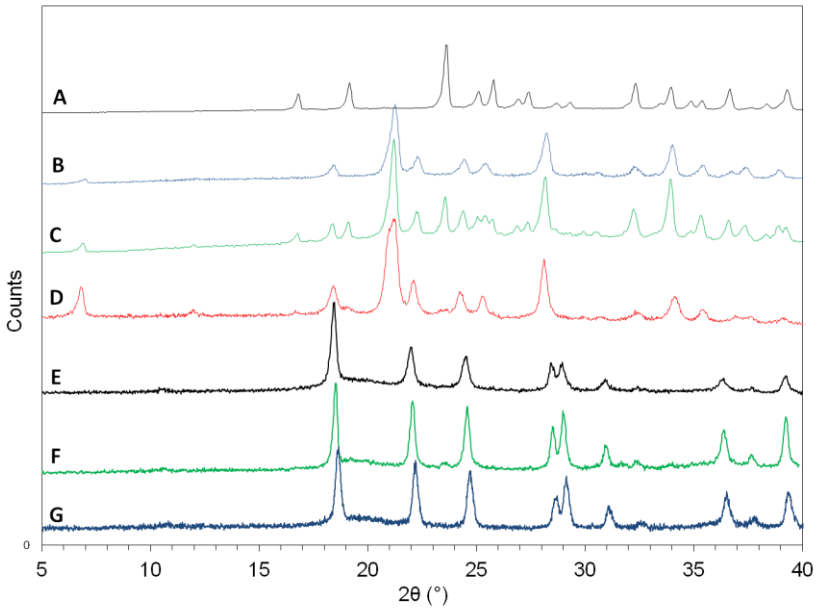

Figure 2.12 Powder XRD pattern of: [A] Na_3H_3L2; [B] α-PCMOF2; [C] mechanical mixture, pre-impedance (resembles A + B); [D] PCMOF2½, 6 hour hold time; [E] PCMOF2½, 48 hour hold time (complete conversion); [F] PCMOF2½, post-impedance; [G] β-PCMOF2, post-impedance.

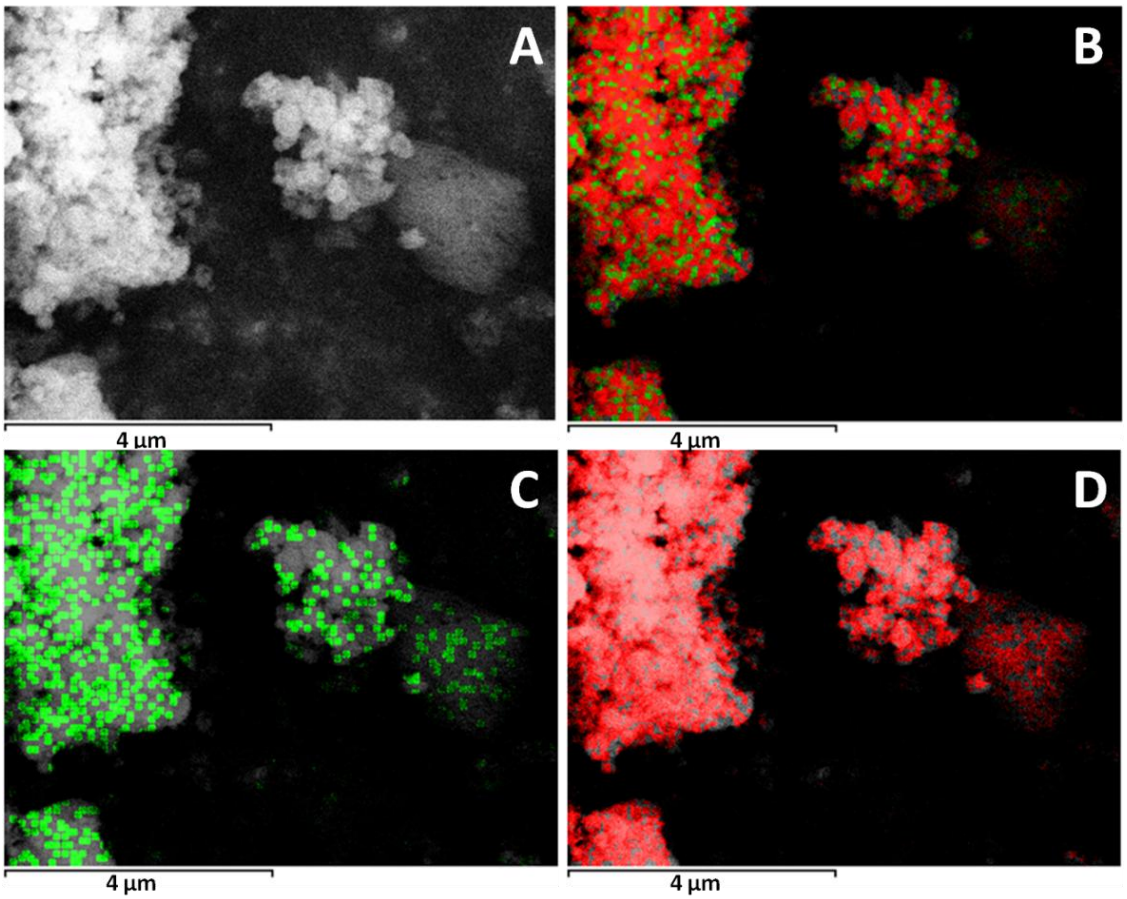

Figure 2.13 SEM/EDX analysis of PCMOF2½ (fully converted from the mechanical mixture); [A] SEM image of PCMOF2½; [B] overlaid elemental distribution of phosphorous (green) and sulfur (red); [C] overlaid elemental distribution of phosphorous (green); [D] overlaid elemental distribution of sulfur (red).

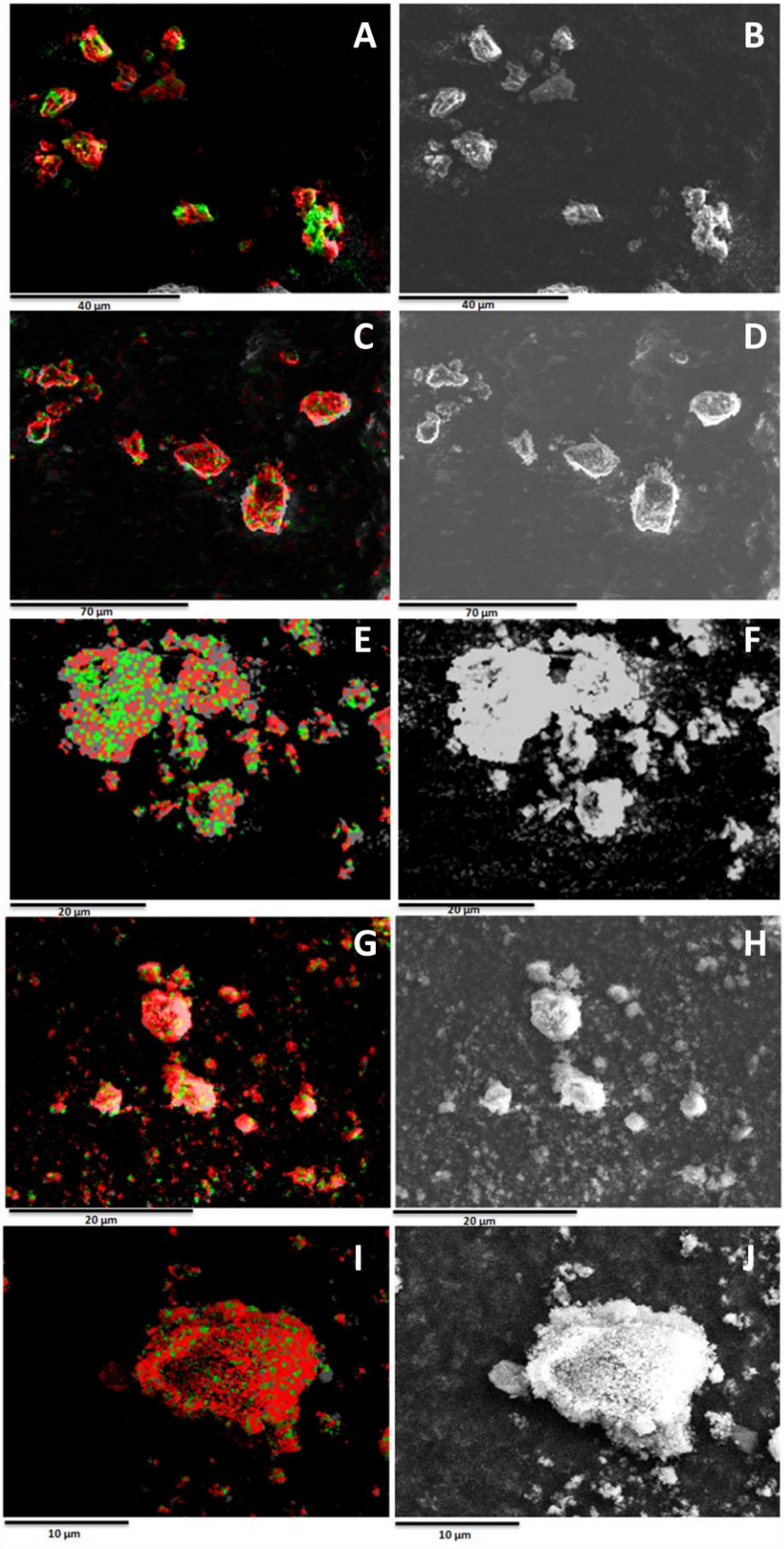
A
B
40 µm
40 µm
C
D
70 µm
70 µm
E
F
20 µm
20 µm
G
H
20 µm
20 µm
I
J
10 µm
10 µm

Figure 2.14 SEM/EDX analysis of PCMOF2½ conversion from the pelletized mechanical mixture; images on the left column [A, C, E, G, I] are overlaid elemental distributions of phosphorous (green) and sulfur (red); images on the right column [B, D, F, H, J] are the corresponding SEM images. [A & B] = Mechanical mixture of Na_3L1 and Na_3H_3L2. Note the phosphorous (Na_3H_3L2) aggregates on the lower right corner. [C & D] = Intermediate PCMOF2½, 0 hour hold time. [E & F] = Intermediate PCMOF2½, 6 hour hold time. The diffusion of sulfur into the central phosphorous cluster is under way. [G & H] = PCMOF2½, 24 hour hold time. [I & J] = PCMOF2½, 48 hour hold time. Even distribution of phosphorous and sulfur is observed throughout the sample. The scale here is 10 µm.

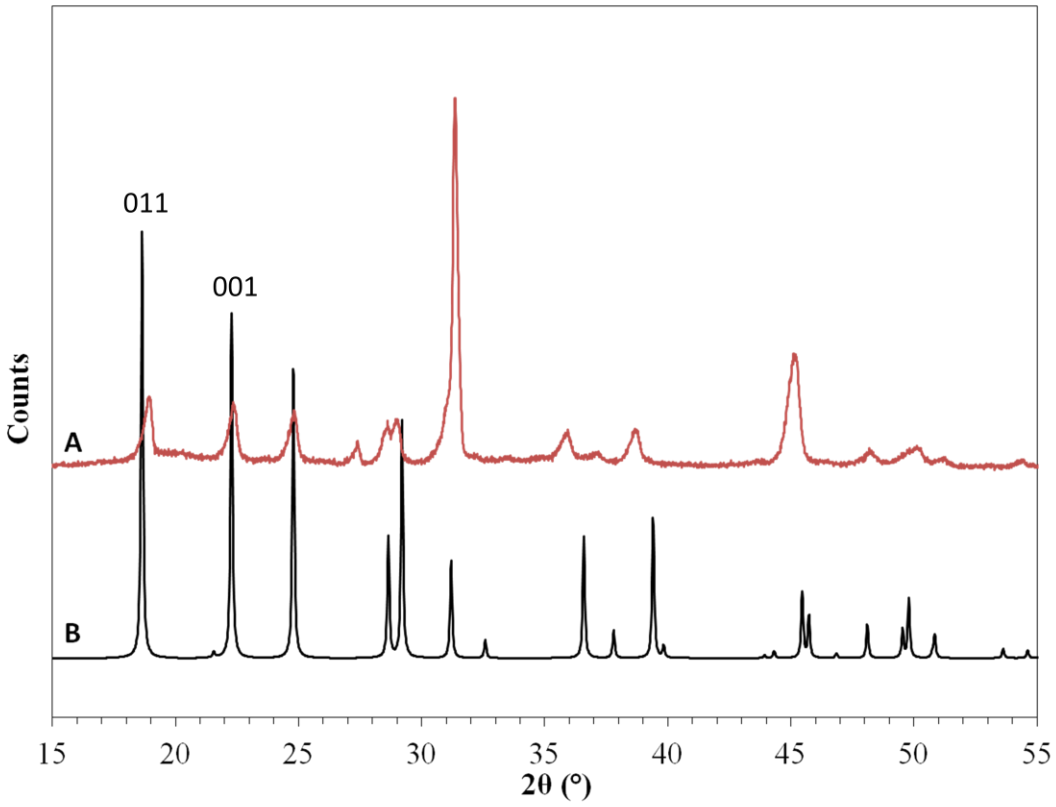

Figure 2.15 Powder XRD patterns of [A] PCMOF2½ with NaCl standard; [B] β-PCMOF2, simulated patern from the single crystal structure. Peaks at 18.56 and 22.12 2θ are indexed to be 011 and 001 hkl values respectively based on the single crystal structure of β-PCMOF2.

	hkl index	2θ (degrees)	d-spacing (Å)	Δd from β-PCMOF2 (Å)
β-PCMOF2	011	18.56	4.780	0
PCMOF2½	011	18.93	4.688	-0.093
β-PCMOF2	001	22.12	4.019	0
PCMOF2½	001	22.35	3.978	-0.041

Table 2.1 Experimental PXRD d-spacing differences between the PCMOFs featured in this study. The c-axis is perpendicular to the ligand/MOF layers in the β-PCMOF2 structure. NaCl was used as an internal standard with the following reference peaks: 2θ = 27.36, 31.70, 35.44, 53.86 and 56.46 degrees. Powder XRDs used for the d-space calculation were collected with sample width of 0.01° and scan speed of 1°/minute, using Cu K_α X-ray source (λ = 0.15418 nm).

As hydrothermal means could not yield PCMOF2½ and pelletization clearly favored conversion, a dissolution mechanism seemed improbable. However, for confirmation, an experiment was performed by making a pellet of pure α-PCMOF2, pressing onto it a pellet of Na_3H_3L2, and applying proper temperature and humidity conditions to affect conversion. SEM-EDX mapping of this solid (Figures 2.16 – 2.18) showed higher concentrations of P atoms in the α-PCMOF2 sample near the interface and lower amounts progressively farther away. A dissolution mechanism would result in growth of a homogenous sample. The general scope of isomorphous ligand replacement is under study in our group. Beyond the structural conversion, the results of the impedance analysis provided a validation of the isomorphous ligand replacement approach.

2.5.1 Two-tiered pelletization experimental details

Two-tiered pellet (Figure 2.16) was formed by pressing two pellets each composed of the pure α-PCMOF2 and Na_3H_3L2 respectively. SEM/EDX analysis was performed at site 1 and 3 before the two-tiered pellet was placed under the humidity

treatment. The pellet was placed into a 23 mL Teflon autoclave, along with a vial containing 1.7 mL of water. The Teflon autoclave was then sealed in a stainless steel jacket and heated to 80°C over two hours, held at 80°C for 24 hours, and then cooled back to room temperature over 12 hours. The pellet was placed in a desiccator for 12 hours to remove excess moisture. The pellet was then carefully separated into three sections (section 1, 2, 3 in Figure 2.16 below), ground into a fine powder using mortar and pestle, and placed for SEM/EDX, and elemental analysis (Figure 2.17 and Figure 2.18). Post humidity treatment elemental analysis of the two-tiered pellet: Elemental analysis for site 1: $[Na_3L1]_{0.63}[Na_3H_3L2]_{0.37}\cdot 0.99H_2O$ Calculated (%): C=16.68, H=1.42; Found: C=16.28, H=1.17. Elemental analysis for site 2: $[Na_3L1]_{0.72}[Na_3H_3L2]_{0.28}\cdot 1.03H_2O$ Calculated (%): C=16.68, H=1.24; Found: C=16.51, H=0.97. Elemental analysis for site 3: $[Na_3L1]_{0.93}[Na_3H_3L2]_{0.07}\cdot 1.37H_2O$ Calculated (%): C=15.96, H=1.29; Found: C=16.08, H=0.94.

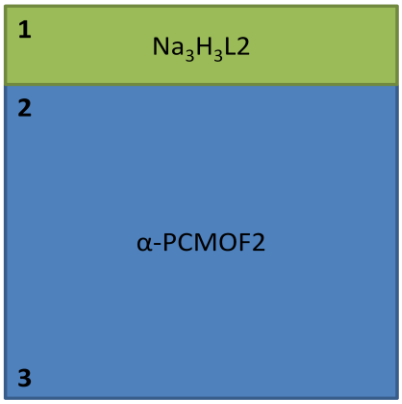

Figure 2.16 Schematic diagram of the two-tiered pellet. The three sites of interest are indicated by #1, 2 and 3. Site #2 represents the interface region between Na_3H_3L2 and α-PCMOF2.

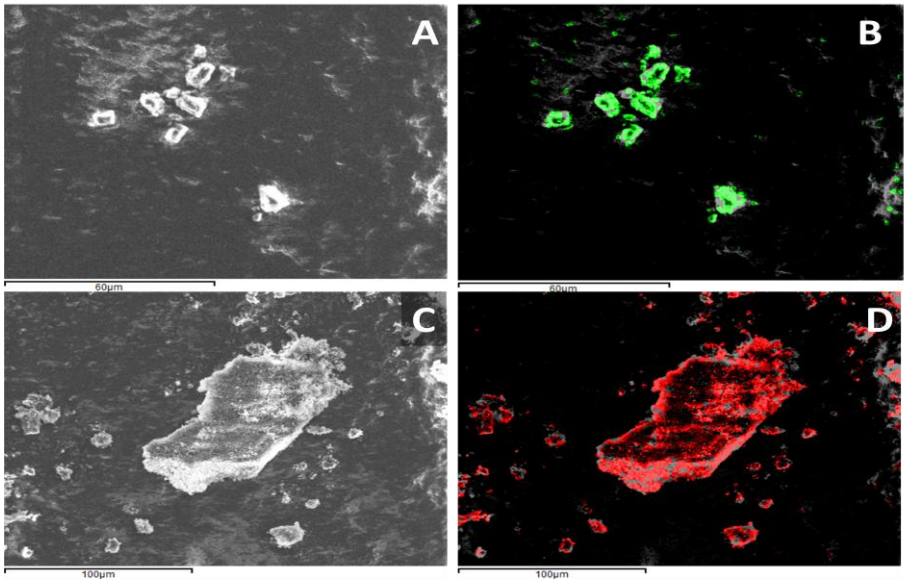

Figure 2.17 SEM/EDX analysis of pure α-PCMOF2 and Na_3H_3L2 at site 1 and 3 before the two-tiered pellet was placed under humidity treatment; [A] SEM image of Na_3H_3L2 at site 1; [B] overlaid elemental distribution of phosphorous (green) [C] SEM image of α-PCMOF2 at site 3; [D] overlaid elemental distribution of sulfur (red).

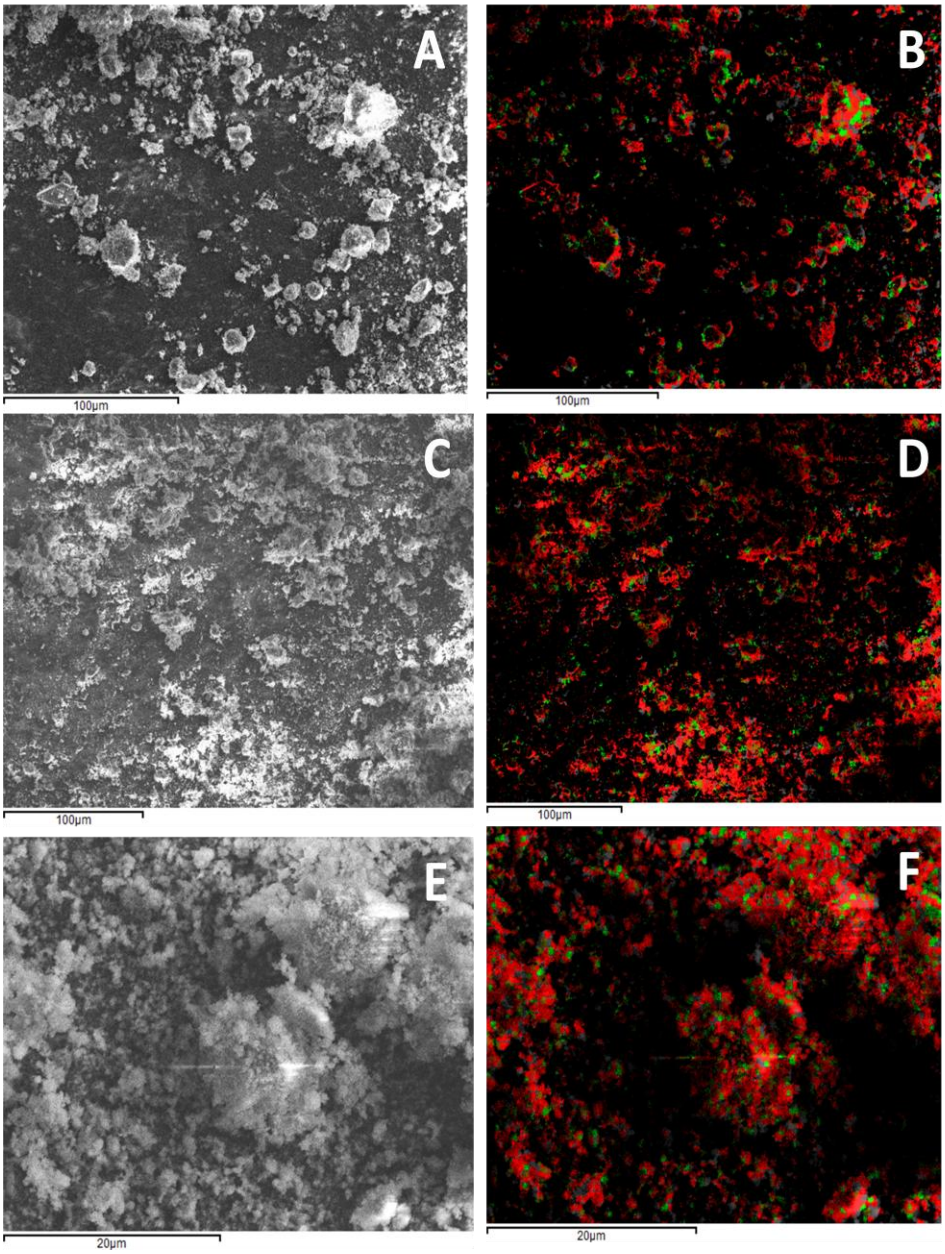

Figure 2.18 SEM/EDX analysis of the two-tiered pellet after a 24 hour humidity treatment at site 1, 2, and 3; [A] SEM image of site 1; [B] overlaid elemental distribution of phosphorous (green) and sulfur (red) of site 1; [C] SEM image of site 2; [D] overlaid elemental distribution of site 2; [E] SEM image of site 3; [F] overlaid elemental distribution of site 3. The sulfur to phosphorous ratio was calculated through the EDX quantification. The quantity of sodium ion was used as the sum of the phosphorous and sulfur ions. This effectively subtracted the background phosphorous and sulfur signals. Sulfur to phosphorous ratio of site 1 was 3.78, site 2 was 6.41, and site 3 was 8.36. An increasing gradient of sulfur to phosphorous ratio was observed as expected; this was also confirmed by the elemental analysis.

2.6 Conversion of the mechanical mixture to PCMOF2½

2.6.1 Pelletization

α-PCMOF2 and Na_3H_3L2 were individually ground into fine powders using a mortar and pestle. Ground α-$Na_3L1{\cdot}2.75H_2O$ (50.1 mg, 0.104 mmol) and ground $Na_3H_3L2{\cdot}2.75H_2O$ (24.9 mg, 0.0574 mmol) were placed in a vial and mechanically shaken to produce a mechanical mixture. Approximately 75 mg of the resulting mixture was packed into a silicon tube, sealed and pressed under a hydrostatic pressure of 10,000 pounds/inch^2 for 2 minutes. The resulting pellet was removed from the silicone tube.

2.6.2 Humidity treatment

The resulting pellet was placed into a 23 mL Teflon autoclave, along with a vial containing 1.7 mL of water. The Teflon autoclave was then sealed in a stainless steel jacket and heated to 80 °C over two hours, held at 80 °C for 48 hours, and then cooled back to room temperature over 12 hours. The pellet was placed in a desiccator for 12 hours to remove excess moisture, and ground into a fine powder using a mortar and pestle. A pale yellow, crystalline powder was obtained at a quantitative yield.

2.6.3 Monitoring the conversion via powder XRD

A series of identical pellets of the mechanical mixture were made and placed under the humidity treatment (as described above) for various lengths. Three pellets were prepared and placed separately in 23 mL Teflon autoclaves. The autoclaves were sealed in stainless steel jackets and heated to 80 °C over two hours, held at 80 °C for 0, 6, and 24 hours respectively, and then cooled back to room temperature over 12 hours. The pellets were placed in a desiccator for 12 hours to remove excess moisture, ground into a fine powder using mortar and pestle. Powder XRD was measured for each sample.

Elemental analysis, ^{1}H and ^{31}P $\{^{1}H\}$ NMR, and SEM/EDX analysis were performed for these samples as well to confirm the presence of the H_3Na_3L2.

Elemental analysis for PCMOF2½, 48 hour hold time (fully converted)

$[Na_3L1]_{0.67}$ $[Na_3H_3L2]_{0.33}\cdot 1.88H_2O$ Calculated (%): C=16.42, H=1.50; Found: C=16.15, H=1.26.

Elemental analysis for PCMOF2½, 24 hour hold time

$[Na_3L1]_{0.67}$ $[Na_3H_3L2]_{0.33}\cdot 2.09H_2O$ Calculated (%): C=16.33, H=1.55; Found: C=16.12, H=1.43.

Elemental analysis for PCMOF2½, 6 hour hold time

$[Na_3L1]_{0.76}$ $[Na_3H_3L2]_{0.24}\cdot 2.79H_2O$ Calculated (%): C=15.69, H=1.75; Found: C=15.29, H=1.35.*

Elemental analysis for PCMOF2½, 0 hour hold time

$[Na_3L1]_{0.66}$ $[Na_3H_3L2]_{0.34}\cdot 2.97H_2O$ Calculated (%): C=15.96, H=1.77; Found: C=15.97, H=1.78.

Elemental analysis for the mechanical mixture of *α-PCMOF-2 and* $Na_3H_3L_2$, before humidity treatment

$[Na_3L1\cdot 2.75H_2O]_{0.65}[Na_3H_3L2\cdot 2.75H_2O]_{0.35}$ Calculated (%): C=15.51, H=2.07; Found: C=15.23, H=1.66.

* With regards to the inconsistent composition of Na_3L1 and Na_3H_3L2 compared to the rest of the samples, the elemental analysis was performed on a small portion of the sample that is still undergoing transformation from the mechanical mixture to PCMOF2½. The powder XRD (Figure 2.11) still shows a mix of two phases.

2.7 Conductivity analysis

Previously, only anhydrous proton conduction data had been reported[10] for β-PCMOF2, so humidity dependent analysis was performed. Nyquist plots for β-PCMOF2 and PCMOF2½ are shown in Figure 2.19. β-PCMOF2 shows a distorted semicircle with a pronounced tail at low frequency attributed to blocking effects at the electrode consistent with ion migration. Conductivity was calculated from the low frequency intercept on the real axis. The high conductivity of PCMOF2½ did not allow for observation of a closed semicircle at high frequency. β-PCMOF2 showed a proton conductivity value of 1.3×10^{-3} S cm^{-1} at 90% relative humidity and 85 °C. This is in itself a very good value relative to other proton conducting coordination polymers including Nafion (Tables 2.2-2.3). Pure Na_3H_3L2 attained a value of 9.9×10^{-5} S cm^{-1} under the same conditions. Although more protic, clearly the structure of Na_3H_3L2 does not form efficient proton transfer pathways. Replacing one-third of L1 with H_3L2 in PCMOF2½ gives a conductivity value of 2.1×10^{-2} S cm^{-1} at 85 °C and 90% relative humidity (Figure 2.20). This is significantly greater than either of the starting components, 1.5 orders of magnitude greater than that of β-PCMOF2 and more than 2 orders of magnitude greater than that of Na_3H_3L2. PCMOF2½ shows the highest equilibrated MOF proton conduction to date exceeding even the value of H_2SO_4 incorporated in the pores of MIL-101.[11] The activation energy (E_a) obtained from an Arrhenius plot was 0.21 eV, indicative of a Grotthuss mechanism for proton conduction.[13] Notably, the E_a calculated for pure β-PCMOF2 at 90% relative humidity was 0.28 eV, further corroborating the effect of the ligand replacement. Conductivity was found to be highly dependent on humidity for both β-PCMOF2 and PCMOF2½. At 50%

relative humidity (Figure 2.21), the conductivity of β-PCMOF2 dropped to 1.8×10^{-6} S cm^{-1}, and that of PCMOF2½ fell to 2.4×10^{-5} S cm^{-1}.

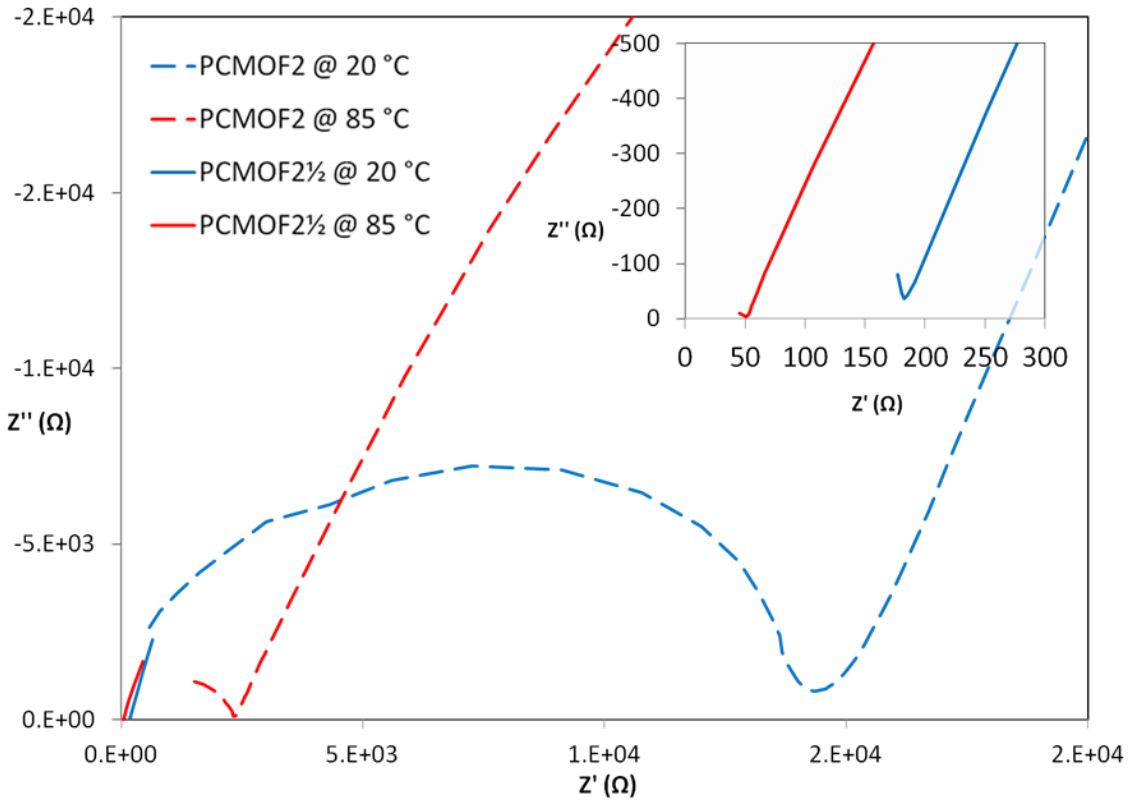

Figure 2.19 Nyquest plots for β-PCMOF2 and PCMOF2½ at 90% relative humidity. The inset shows the high frequency region for PCMOF2½.

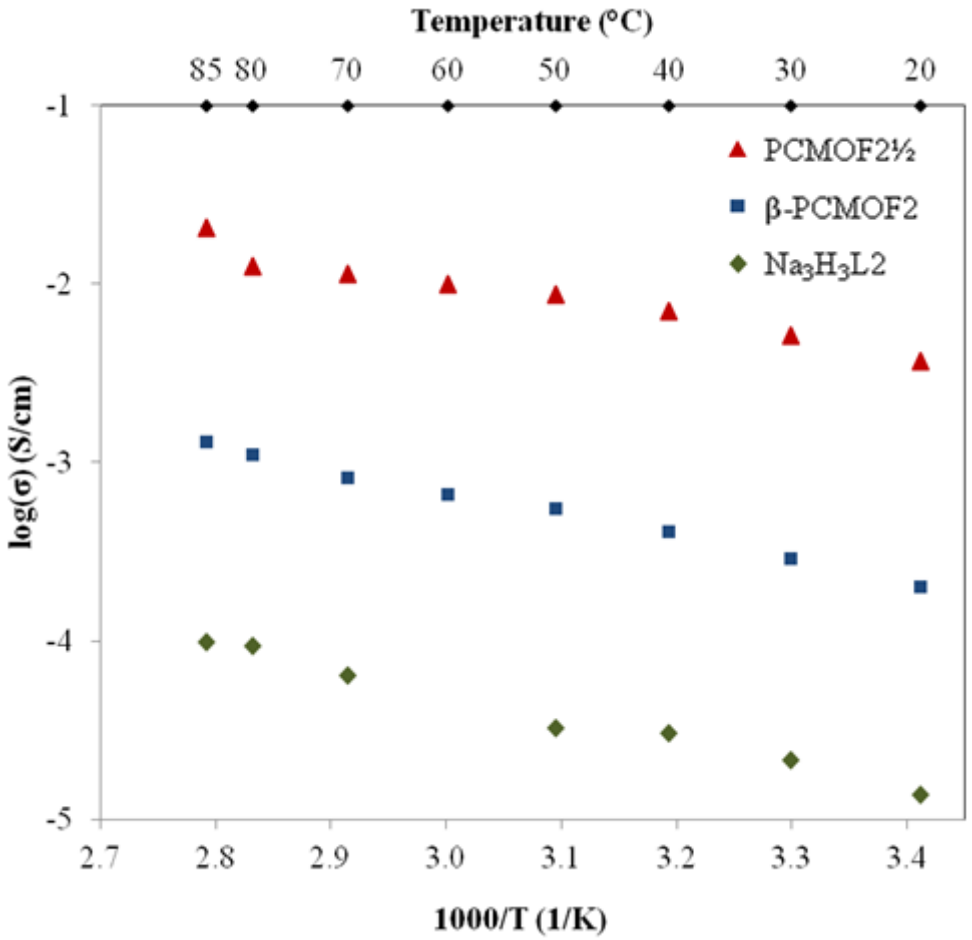

Figure 2.20 Proton conductivity data (90% relative humidity) for β-PCMOF2, Na_3H_3L2, and the isomorphous mixture, PCMOF2½. The activation energy of PCMOF2½ was found to be 0.21 eV, and the activation energy of β-PCMOF2 was found to be 0.28 eV under the measurement conditions.

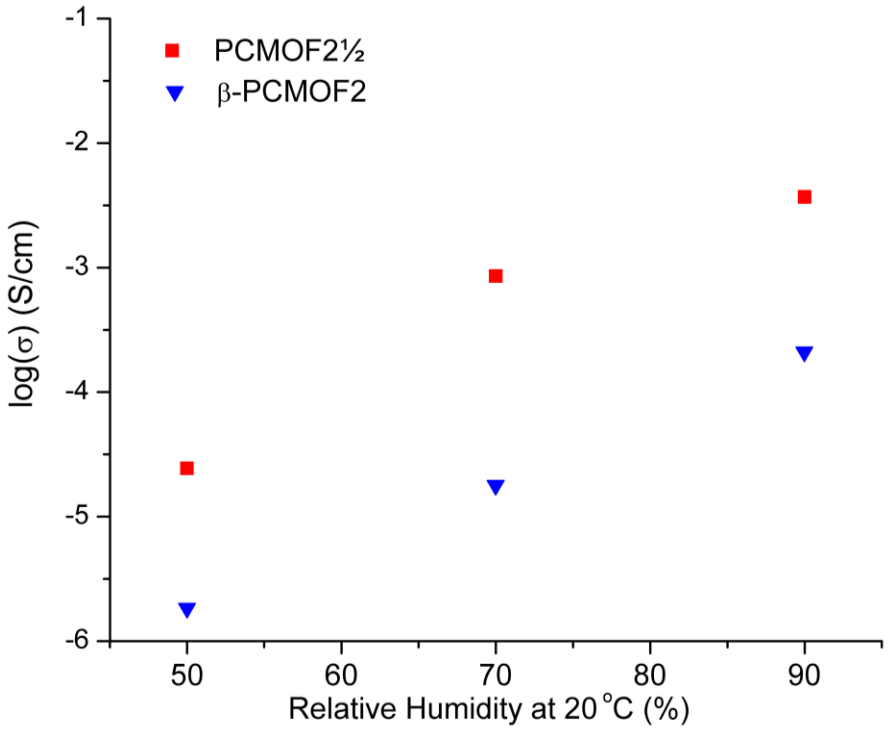

Figure 2.21 Log conductivity of PCMOF2½ and β-PCMOF2 at variable humidity conditions at 20 °C.

Regarding the stability of PCMOF2½, postimpedance analysis confirmed retention of structure. Moreover, if under the humid conditions, with dissolution occurring, it is highly unlikely that retraceable and linear conductivity behavior with temperature would be observed. Further, any substantive dissolution, which we have seen in conductivity measurements of some other MOF samples, would lead to a contraction of the sample pellet, loss of contact with the electrodes, and erratic data.

2.8 Conclusion

MOFs are heralded for their order which leads directly to the ability to view structures crystallographically. That said, it is increasingly apparent that, for some applications, the performance of MOFs with mixtures of components can exceed the sum of their parts. Deng *et al*. reported multivariate MOFs where 18 different MOF-5

derivates were prepared each with multiple different functionalities on the terephthalate linkers.[14] One of these compounds, with three different substituents on the ligand, showed greatly enhanced selectivity for CO_2 over CO. This could be viewed more as an isometric rather than an isomorphous ligand substitution, as very different functionalities are directed into the pore space off the same length linker. With the recent works demonstrating the lability of cluster bound ligands[15] and post synthetic exchange of ligands (from robust MOFs[16] and with retention of crystallinity[17]), the opportunities to make mixed ligand MOFs appear substantial. The most relevant comparison to the isomorphous replacement approach put forth here comes from Horike and Kitagawa regarding gating of gas sorption in a family of porous coordination polymers (PCPs).[18] In this work, the authors observed differences in the pressure of gating in nitro- and methoxy-isophthalate derivates of two isostructural PCPs. The gating pressure could be tuned by varying the ratios of the nitro- and methoxy derivates in a single structure in what amounts to an isomorphous replacement although not explicitly called that by the authors. From the perspective of proton conducting materials, the ability to fine-tune the acidity of structures by this approach is compelling given the pervasiveness of sulfonate and phosphonate building blocks and their isomorphous relationships.

Proton Conducting MOF Systems	Highest H^+ σ (S/cm) (Jan 2013)	E_a (eV)	T (°C)	Relative Humidity
H_2SO_4 @ MIL-101 [31]	1×10^{-2}	0.42	150	0.13%
H_3PO_4 @ MIL-101 [31]	1×10^{-2}	0.25	140	1.1%
Sulfonated MIL-53(Al) [32]	$\sim 5 \times 10^{-3}$	-	~ 65	< 10%
1,2,4-Triazole @ β-PCMOF2 [10]	5×10^{-4}	0.34	150	0%
Poly(vinylbenzyloxy-alkyl-phosphonic acid) [35]	3×10^{-4}	-	140	0%
Imidazole @ MIL-53(Al)-Ndc [34]	2.2×10^{-5}	0.6	120	0%
H_2O @ HKUST-1 [10]	1.5×10^{-5}	-	~ 21	100% MeOH
$(Me_2NH_2)[Zn(Btc)]$ [34]	5.3×10^{-6}	-	20	-
$Emim^+$ @ $Co_2NaBptc_2$ [35]	6.33×10^{-7}	0.49	170	-
Imidazole @ MIL-53(Al) [15]	1.0×10^{-7}	0.9	120	0%

Table 2.2 Highest equilibrated proton conductivities under anhydrous conditions reported in literature for MOF systems and select example systems, from highest to lowest.

Proton Conducting MOF Systems	Highest H^+ σ (S/cm) (Jan 2013)	E_a (eV)	T (°C)	Relative Humidity
Nafion 117 without heat treatment [35]	7.8×10^{-2}	0.021	25	100%
Nafion 117 – typical range [36]	1×10^{-3} to 5×10^{-2}	0.10 to 0.40	20 to 90	20 to 90
PCMOF-2½ [This Work]	2.1×10^{-2}	0.21	85	90%
LaH_5Dtmp [19]	8×10^{-3}	0.25	24	98%
$(NH_4)_2$(adipic acid)$[Zn_2(Ox)_3] \cdot 3H_2O$ [20]	8×10^{-3}	0.63	25	98%
Cd-5TIA [21]	3.61×10^{-3}	0.16	28	98%
$(NH_4)_4[MnCr_2(Ox)_6] \cdot 4H_2O$ [22]	1.7×10^{-3}	0.23	40	96%
MgH_6Odtmp [23]	1.6×10^{-3}	0.31	19	100%
β-PCMOF2 [This Work]	1.3×10^{-3}	0.28	85	90%
$Fe(Ox) \cdot 2H_2O$ [24]	1.3×10^{-3}	0.37	25	98%
In-5TIA [21]	3.85×10^{-4}	0.14	39	98%

GdHPA-II [25]	3.2×10^{-4}	0.23	25	95-98%
Ca-Btc-H_2O [26]	1.2×10^{-4}	0.18	25	98%
ZrCdtmp_lp [27]	1.0×10^{-4}	0.09	80	95%
Sr-Sbba [28]	4.4×10^{-5}	0.56	25	98%
PCMOF-3 [8]	3.5×10^{-5}	0.17	25	98%
Ca-Sbba [28]	8.58×10^{-6}	0.23	25	98%
MIL-53(Fe)-CO_2H [29]	7×10^{-6}	0.21	80	95%
ZrCdtmp_np@H [30]	6.6×10^{-6}	-	80	95%
MIL-53(Al)-OH [29]	1.9×10^{-6}	0.27	80	95%
MIL-53(Al)-H [29]	3.6×10^{-7}	0.47	80	95%
MIL-53(Al)-NH_2 [29]	4.1×10^{-8}	0.45	80	95%

Table 2.3 Highest equilibrated proton conductivities under hydrated conditions reported in literature for MOF systems, from highest to lowest. The conductivities of Nafion 117 under various conditions are included as reference comparisons.

2.9 References

(1) (a) Zhao, D.; Meek, S. T.; Greathouse, J. A.; Allendorf, M. D. *Adv. Mater*. **2011**, *23*, 249. (b) Perry, J. J.; Perman, J. A; Zaworotko, M. J. *Chem. Soc. Rev.* **2009**, *38*, 1400-1417. (c) Farha, O. K.; Hupp, J. T. *Acc. Chem. Res*. **2010**, *43*, 1166. (d) Tanabe, K. K.; Cohen, S. M. *Chem. Soc. Rev.* **2011**, *40*, 498. (e) Kuppler, R. J.;Timmons, D. J.; Fang, Q. R.; Li, J. R.; Makal, T.A.; Young, M. D.; Yuan, D. Q.; Zhao, D.; Zhuang, W. J.; Zhou, H. C. *Coord. Chem. Rev.* **2009**, *253*, 3042. (f) Czaja A. U.; Trukhan, N.; Mueller, U. *Chem. Soc. Rev.* **2009**, *38*, 1284. (g) Stock, N.; Biswas, S. *Chem. Rev.* **2012**, *112*, 933–969.

(2) (a) Férey, G.; Serre, C.; Devic, T.; Maurin, G.; Jobic, H.; Llewellyn, P. L.; De Weireld, G.; Vimont, A.; Daturi, M.; Chang, J. S. *Chem. Soc. Rev.* **2011**, *40*, 550-562. (b) Suh, M. P.; Park, H. J.; Prasad, T. K.; Lim, D.-W. *Chem. Rev.* **2012**, *112*,

782-835. (c) Li, J. R.; Sculley, J.; Zhou, H. C. *Chem. Rev.* **2012**, *112*, 869–932. (d) Mason, J. A. ; Sumida, K. ; Herm, Z. R. ; Krishna, R.; Long, J. R. *Energy Environ. Sci.*, **2011**, *4*, 3030. (e) Phan, A.; Doonan, C. J.; Uribe-Romo, F. J.; Knobler, C.B.; O'Keeffe, M.; Yaghi, O. M. *Acc. Chem. Res.* **2010**, *43*, 58.

(3) Lee, J.; Farha, O. K.; Roberts, J.; Scheidt, K. A.; Nguyen, S. T.; Hupp, J. T. *Chem. Soc. Rev.* **2009**, *38*, 1450-1459.

(4) Kreno, L. E.; Leong, K.; Farha, O. K.; Allendorf, M.; Van Duyne, R. P.; Hupp, J. T. *Chem. Rev*. **2012**, *112*, 1105-1125.

(5) Horcajada, P.; Gref, R.; Baati, T.; Allan, P. K.; Maurin, G.; Couvreur, P.; Férey, G.; Morris, R. E.; Serre, C. *Chem. Rev.* **2012**, *112*, 1232–1268

(6) (a) Nagao, Y.; Kubo, T.; Nakasujib, K.; Ikedac, R.; Kojimaa, T.; Kitagawa, H. *Synth. Met.* **2005**, *154*, 89−92. (b) Sadakiyo, M.; Yamada, T.; Kitagawa, H. *J. Am. Chem. Soc.* **2009**, *131*, 9906. (c) Yamada, T.; Sadakiyo, M.; Kitagawa, H. *J. Am. Chem. Soc.* **2009**, *131*, 3144−3145. (d) Ōkawa, H.; Shigematsu, A.; Sadakiyo, M.; Miyagawa, T.; Yoneda, K.; Ohba, M.; Kitagawa, H. *J. Am. Chem. Soc*. **2009**, *131*, 13516−13522. (e) Shigematsu, A.; Yamada, T.; Kitagawa, H. *J. Am. Chem. Soc.* **2011**, *133*, 2034. (f) Sahoo, S. C.; Kundu, T.; Banerjee, R. *J. Am. Chem. Soc.* **2011**, *133*, 17950−17958. (g) Shigematsu, A.; Yamada, T.; Kitagawa, H. *J. Am. Chem. Soc.* **2011**, *133*, 2144. (h) Pardo, E.; Train, C.; Gontard, G.; Boubekeur, K.; Fabelo, O.; Liu, H.; Dkhil, B.; Lloret, F.; Nakagawa, K.; Tokoro, H.; Ohkoshi, S.-i.; Verdaguer, M. *J. Am. Chem. Soc.* **2011**, *133*, 15328−15331. (i) Goesten, M. G.; Juan-Alcañiz, J.; Ramos-Fernandez, E. V.; Sai Sankar Gupta, K.B.; Stavitski, E.; van Bekkum, H.; Gascon, J.; Kapteijn, F. *J. Catal.* **2011**, *281*, 177. (j) Sadakiyo,

M.; Ōkawa, H.; Shigematsu, A.; Ohba, M.; Yamada, T.; Kitagawa, H. J. *Am. Chem. Soc.* **2012**, *134*, 5472−5475. (k) Horike, S.; Umeyama, D.; Inukai, M.; Itakura, T.; Kitagawa, S. *J. Am. Chem. Soc.* **2012**, *134*, 7612–7615. (l) Umeyama, D.; Horike, S.; Inukai, M.; Itakura, T.; Kitagawa, S. *J. Am. Chem. Soc.* **2012**, *134*, 12780-12785. (m) Costantino, F.; Donnadio, A.; Casciola, M. *Inorg. Chem.* **2012**, *51*, 6992.(n) Costantino, F.; Donnadio, A.; Casciola, M. *Inorg. Chem.* **2012**, *51*, 6992–7000. (o) Colodrero, R. M. P.; Olivera-Pastor, P.; Losilla, E. R.; Hernández-Alonso, D.; Aranda, M. A. G.; Leon-Reina, L.; Rius, J.; Demadis, K. D.; Moreau, B.; Villemin, D.; Palomino, M. I.; Rey, F.; Cabeza, A. *Inorg. Chem.* **2012,** *51*, 7689. (p) Colodrero, R. M. P.; Olivera-Pastor, P; Losilla, E. R.; Aranda, M. A. G.; León-Reina, L.; Papadaki, M.; McKinlay, A. C.; Morris, R. E.; Demadis, K. D.; Cabeza, A. *Dalton Trans.* **2012**, *41*, 4045. (q) Colodrero, R. M. P.; Papathanasiou, K. E.; Stavgianoudaki, N.; Olivera-Pastor, P; Losilla, E. R.; Aranda, M. A. G.; León-Reina, L.; Sanz, J.; Sobrados, I.; Choquesillo-Lazarte, D.; García-Ruiz, J. M.; Atienzar, P.; Rey, F.; Demadis, K. D.; Cabeza, A. *Chem. Mater.* **2012**, *24*, 3780−3792.

(7) Sadakiyo, M.; Yamada, T.; Kitagawa, H. *J. Am. Chem. Soc.* **2009**, *131*, 9906-9907.

(8) Taylor, J. M.; Mah, R. K.; Moudrakovski, I. L.; Ratcliffe, C. I.; Vaidhyanathan, R.; Shimizu, G. K. H. *J. Am. Chem. Soc.* **2010**, *132*, 14055–14057.

(9) (a) Bureekaew, S.; Horike, S.; Higuchi, M.; Mizuno, M.; Kawamura, T.; Tanaka, D.; Yanai, N.; Kitagawa, S. *Nat. Mater.* **2009**, *8*, 831.(b) Umeyama, D.; Horike, S.; Inukai, M.; Hijikata, Y.; Kitagawa, S. *Angew. Chem., Int. Ed.* **2011**, *50*, 11706−11709.

(10) Hurd, J. A.; Vaidhyanathan, R.; Thangadurai, V.; Ratcliffe, C. I.; Moudrakovski, I. L.; Shimizu, G. K. H. *Nat. Chem.* **2009**, *1*, 705−710.

(11) Ponomareva, V. G.; Kovalenko, K. A.; Chupakhin, A. P.; Dybtsev, D. N.; Shutova, E. S.; Fedin, V. P. *J. Am. Chem. Soc.*, **2012**, *134*, 15640–15643.

(12) Kong, D.; Clearfield, A.; Zoń, J. *Cryst. Growth Des.* **2005**,*5*, 1767.

(13) Agmon, N. *Chem. Phys. Lett.* **1995**, *244*, 456.

(14) Deng, H.; Doonan, C. J.; Furukawa, H.; Ferreira, R. B.; Towne, J.; Knobler, C. B.; Wang, B.; Yaghi, O. M. *Science*, **2010**, *327*, 846-850.

(15) Seo, J.; Bonneau, C.; Matsuda, R.; Takata, M.; Kitagawa, S. *J. Am. Chem. Soc.*, **2011**, *133*, 9005-9013.

(16) Kim, M; Cahill, J. F.; Su, Y. X.; Prather, K. A.; Cohen, S. M. *Chem. Sci.* **2012,** *3*, 126-130.

(17) Park, H. J.; Cheon, Y. E.; Suh, M. P. *Chem. Eur. J.* **2010**, *16*, 11662-11669.

(18) (a) Fukushima, T.; Horike, S.; Inubushi, Y.; Nakagawa, K.; Kubota, Y.; Takata, M.; Kitagawa, S. *Angew. Chem., Int. Ed.* **2010**, *49*, 4820-4824. (b) Horike, S.; Inubushi, Y.; Hori, T.; Fukushima, T.; Kitagawa, S. *Chem. Sci.* **2012**, *3*, 116-120.

(19) Colodrero, R. M. P.; Olivera-Pastor, P.; Losilla, E. R.; Aranda, M. a G.; Leon-Reina, L.; Papadaki, M.; McKinlay, A. C.; Morris, R. E.; Demadis, K. D.; Cabeza, A. *Dalton. Trans*. **2012**, *41*, 4045–4051.

(20) Sadakiyo, M.; Yamada, T.; Kitagawa, H. *J. Am. Chem. Soc.* **2009**, *131*, 9906-9907.

(21) Panda, T.; Kundu, T.; Banerjee, R. *Chem. Commun.* **2012**, *48*, 5464–5466.

(22) Pardo, E.; Train, C.; Gontard, G.; Boubekeur, K.; Fabelo, O.; Liu, H.; Dkhil, B.; Lloret, F.; Nakagawa, K.; Tokoro, H.; Ohkoshi, S.; Verdaguer, M. *J. Am. Chem. Soc.* **2011**, *133*, 15328–15331.

(23) Colodrero, R. M. P.; Olivera-Pastor, P.; Losilla, E. R.; Hernández-Alonso, D.; Aranda, M. a G.; Leon-Reina, L.; Rius, J.; Demadis, K. D.; Moreau, B.; Villemin, D.; Palomino, M.; Rey, F.; Cabeza, A. *Inorg. Chem.* **2012**, *51*, 7689–7698.

(24) Yamada, T.; Sadakiyo, M.; Kotagawa, H. *J Am. Chem. Soc.* **2009**, *131*, 3144-3145.

(25) Colodrero, R. M. P.; Papathanasiou, K. E.; Stavgianoudaki, N.; Olivera-Pastor, P.; Losilla, E. R.; Aranda, M. A. G.; León-Reina, L.; Sanz, J.; Sobrados, I.; Choquesillo-Lazarte, D.; García-Ruiz, J. M.; Atienzar, P.; Rey, F.; Demadis, K. D.; Cabeza, A. *Chem. Mater.* **2012**, *24*, 3780–3792.

(26) Mallick, A.; Kundu, T.; Banerjee, R. *Chem. Comm.* **2012**, 8829–8831.

(27) Costantino, F.; Donnadio, A.; Casciola, M. *Inorg. Chem.* **2012**, *51*, 6992–7000.

(28) Kundu, T.; Sahoo, S. C.; Banerjee, R. *Chem. Commun.* **2012**, 4998–5000.

(29) Shigematsu, A.; Yamada, T.; Kitagawa, H. *J. Am. Chem. Soc.* **2011**, *133*, 2034–2036.

(30) Costantino, F.; Donnadio, A.; Casciola, M. *Inorg. Chem.* **2012**, *51*, 6992–7000.

(31) Ponomareva, V. G.; Kovalenko, K. A.; Chupakhin, A. P.; Dybtsev, D. N.; Shutova, E. S.; Fedin, V. P. *J. Am. Chem. Soc.* **2012**, *134*, 15640–15643.

(32) Goesten, M. G.; Juan-Alcañiz, J.; Ramos-Fernandez, E. V.; Sai Sankar Gupta, K. B.; Stavitski, E.; Van Bekkum, H.; Gascon, J.; Kapteijn, F. *J. Catal.* **2011**, *281*, 177–187.

(33) Lee, S.; Yoon, K.; Song, M.; Peng, H.; Page, K. A.; Soles, C. L.; Yoon, D. Y. *Chem. Mater.* **2012**, *24*, 115-122.

(34) Bureekaew, S.; Horike, S.; Higuchi, M.; Mizuno, M.; Kawamura, T.; Tanaka, D.; Yanai, N.; Kitagawa, S. *Nat. Mater.* **2009**, *8*, 831–836.

(35) Sone, Y.; Ekdunge, P.; Simonsson, D. *J. Electrochem. Soc.* **1996**, *143*, 1254-1259.

(36) Marechal, M.; Souquet, J.-L.; Guindet, J.; Sanchez, J.-Y. *Electrochem. Commun.* **2007**, *9*, 1023-1028.

Chapter Three: **SYNERGISTIC MERGING OF TWO DESIGN STRATEGIES IN A PROTON CONDUCTING METAL-ORGANIC FRAMEWORK**

3.1 Transitory introduction

Following the success of the isomorphous ligand replacement strategy and the resultant PCMOF2½ presented in the previous chapter, we actively sought ways to further enhance the proton conductivity of PCMOF2½.

We have previously reported a proton conducting MOF named β-PCMOF2 under both hydrated and anhydrous conditions.[1,2] β-PCMOF2 consists of a trisodium 2,4,6-trihydroxy-1,3,5-trisulfonate benzene (Na_3L1) complex arranged in a 1D columnar structure where the pores are lined with sulfonate oxygen atoms (Figure 1.2). The pores are 5.6 Å in diameter and are hydrophilic in nature. β-PCMOF2 showed proton conductivity value of 1.3×10^{-3} S cm^{-1} at 90% relative humidity and 85 °C. Under anhydrous conditions, however, β-PCMOF2 showed very low conductivity on the order of 10^{-9} S cm^{-1} at 100 °C.

Aiming to enhance β-PCMOF2's proton conductivity under anhydrous conditions, we utilized the possibility of loading the regular pore structure of β-PCMOF2 with less volatile, amphiprotic guest molecules. Previous work by Hurd *et al.*[2] describes a β-PCMOF2(Triazole) system where the β-PCMOF2 was loaded with 0.3 equivalents of triazole molecules. The conductivity jumped 5 orders of magnitude relative to unloaded β-PCMOF2's to reach 5×10^{-4} S cm^{-1} under anhydrous conditions at 150 °C. Different loadings of triazole only resulted in a small change in the conductivity – up to 0.6 loading enabled conductivity of 5×10^{-4} S cm^{-1}. In this system, a minimum loading of heterocycle is needed to enable conduction but excess amounts bring about formation of a different

phase. The heterocycle loading is a kinetic phenomenon and controlling the amount of loading is challenging. Based on these findings, we hypothesized the variation in the number of charge carriers only impart moderate increase in the proton conductivity of β-PCMOF2. In order to further enhance the proton conductivity of β-PCMOF2, we attempted to increase the number of freely available acidic protons via a design strategy called isomorphous ligand replacement.

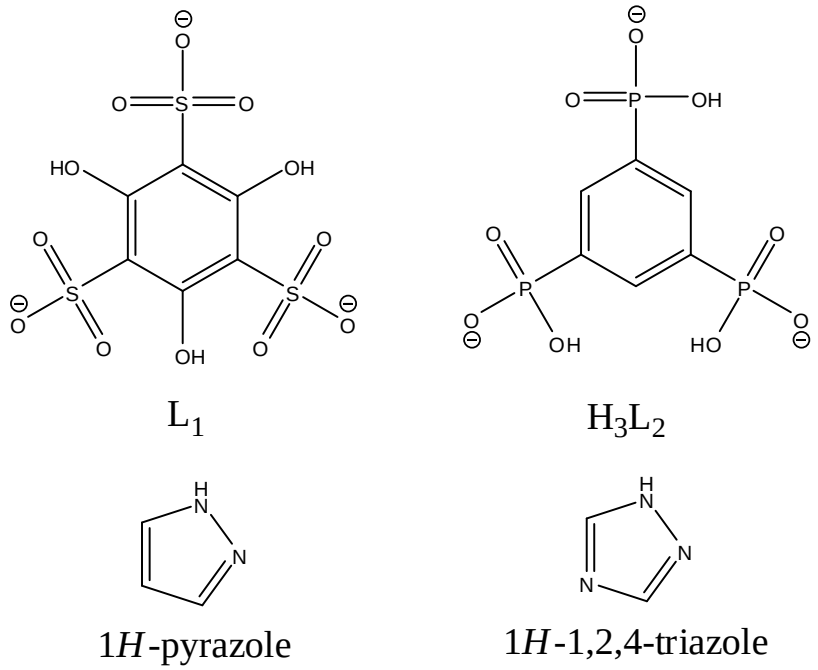

Figure 3.1 Molecular structures of L1 and H_3L2, the constituents of PCMOF2½ (top row); the molecular structures of 1*H*-pyrazole and 1*H*-1,2,4-triazole, the amphiprotic heterocycles investigated in this work (bottom row).

Since the Na_3L1 ligand that formed the backbone of β-PCMOF2 was a fully deprotonated sulfonate molecule, there was no direct way to increase the number of freely available acidic protons. Instead, we utilized a second ligand, 1,3,5-benzenetriphosphonic acid, Na_3H_3L2, which, as a trianion still possessed three acidic protons (Figure 3.1). The ligand, H_6L2, has been previously reported by Taylor *et al*. as a

Zn^{2+} complex which forms PCMOF3.[3] In the MOF framework, one third of the Na_3L1 was successfully replaced with Na_3H_3L2 without disrupting the original structure of β-PCMOF2. This was possible because L1 and H_3L2 both have an aromatic core with a C_3 symmetric polar periphery and the same overall charge. The resulting structure, PCMOF2½ -so called because it has a mixture of the linkers employed in β-PCMOF2 and PCMOF3 - had its proton conductivity raised 1.5 orders of magnitude to 2.1×10^{-2} S cm^{-1} at 90% relative humidity and 85 °C compared to the conductivity of pure β-PCMOF2 under the same condition (1.3×10^{-3} S cm^{-1}).[2] Interestingly, isomorphous ligand replacement was not attainable by any solvent-mediated synthesis. Greater insights to this phenomenon are now in place and will be discussed (section 3.5.2).

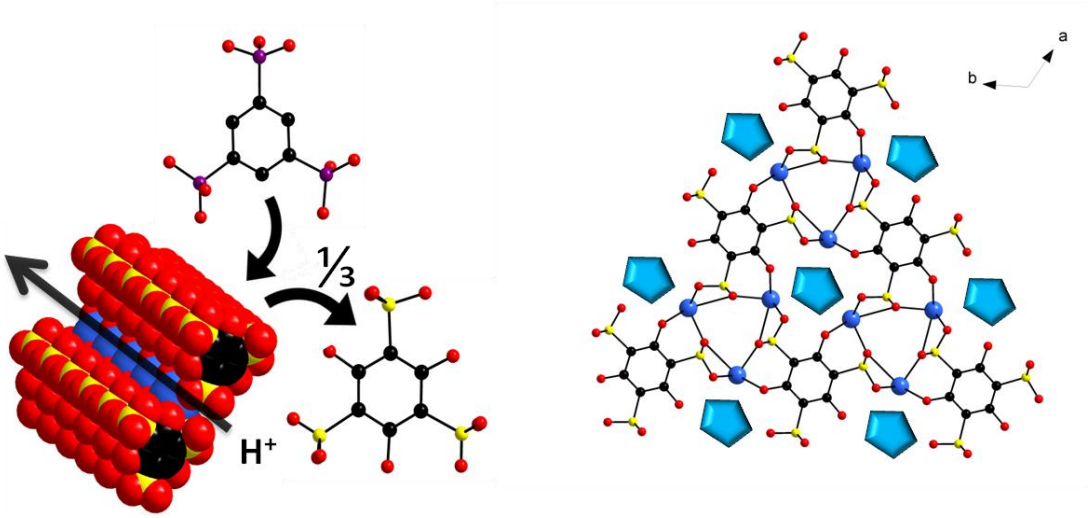

Figure 3.2 (Left) The space-filling cross section structure of β-PCMOF2 with its 1-dimensional proton conduction channel illustrated with an arrow and the schematic illustration of isomorphous replacement. (Right) A 2-dimensional crystal layout of β-PCMOF2 where the pores are impregnated with heterocycles (teal pentagons).

Given the challenges in both controlling heterocycle loading and making mixed linker PCMOFs, the question remains whether these design strategies are mutually exclusive or if they can be merged to yield greater enhancement of proton conductivity

(Figure 3.1 and 3.2). Herein, we present a simultaneous application of the two design strategies resulting in the synergistic enhancement of the β-PCMOF2's proton conductivity to yield the first MOF with proton conducting properties over 10^{-1} S cm^{-1}.

3.2 Results

Four new compounds, PCMOF2½(Pyrazole), PCMOF2½(Triazole), PCMOF2(Pyrazole) and PCMOF2½ *Melamine* were synthesized and their proton conductivities and activation energies measured under various conditions. In addition, the proton conductivity and the corresponding activation energy of PCMOF2(Triazole) was measured under hydrated conditions. The anhydrous conductivity of PCMOF2(Triazole) was previously reported by Hurd *et al.*[2]

Additionally, the following four compounds, β-PCMOF2, PCMOF2(Triazole), PCMOF2(Pyrazole), and PCMOF2½ served as control experiments in investigating the enhanced proton conductivity of PCMOF2½(Pyrazole), PCMOF2½(Triazole) and PCMOF2½ *Melamine*. Table 3.1 summarises the conductivity values and the corresponding activation energies of the various PCMOFs under their respective conditions.

Conversely, the following samples were synthesized but they were found to show extremely decreased conductivity at 85 °C and 90% relative humidity: PCMOF2½ *Melamine* (Pyrazole) and PCMOF2½ *Melamine* (Triazole), PCMOF2½ *Melamine* (Imidazole) PCMOF2½(Imidazole) and PCMOF2(Imidazole). These samples were screened for their initial conductivities at 85 °C and 90% relative humidity, and they exhibited conductivities below 10^{-6}, three orders of magnitude lower than that of β-PCMOF2. Therefore, these PCMOFs were not investigated beyond the initial

screening. Possible explanations regarding the non-conductive nature of these samples will be explored in the discussion (section 3.5.4).

Name	Conductivity ($S\ cm^{-1}$)	T (°C)	RH (%)	Ea[7] (eV)
PCMOF2½(Pyrazole)[1]	1.1×10^{-1}	85	90	0.16
PCMOF2½(Pyrazole)[1]	1.2×10^{-5}	25	30	n/a
PCMOF2½(Pyrazole)[1]	7.2×10^{-7}	150	0	0.20[8] 0.98[9]
PCMOF2½(Triazole)[1]	5.2×10^{-2}	85	90	0.19
PCMOF2½(Triazole)[1]	1.5×10^{-6}	25	40	n/a
PCMOF2(Pyrazole)[2]	4.6×10^{-2}	85	90	0.08
PCMOF2(Pyrazole)[2]	3.6×10^{-3}	25	30	n/a
PCMOF2(Pyrazole)[3]	1.3×10^{-3}	150	0	0.42[10]
PCMOF2(Triazole)[4]	1.9×10^{-2}	85	90	0.08
PCMOF2(Triazole)[4]	7.2×10^{-6}	25	30	n/a
PCMOF2(Triazole)[5]	5×10^{-4}	150	0	0.34[11]
PCMOF2½ [6]	2.1×10^{-2}	85	90	0.21
PCMOF2½ [6]	2.4×10^{-5}	20	50	n/a
β-PCMOF2 [4,6]	1.3×10^{-3}	85	90	0.28
β-PCMOF2 [4,6]	1.8×10^{-6}	20	50	n/a
β-PCMOF2 [5]	1×10^{-9}	100	0	n/a
PCMOF2½ *Melamine* [1]	2.5×10^{-2}	85	90	0.19
PCMOF2½ *Melamine* [1]	1.6×10^{-8}	25	40	n/a
PCMOF2½ *Melamine* (Pyrazole)[1]	These PCMOFs exhibited proton conductivity below 10^{-6} S cm^{-1} at 85 °C and 90% relative humidity.			
PCMOF2½ *Melamine* (Triazole)[1]				
PCMOF2½ *Melamine* (Imidazole)[1]				
PCMOF2(Imidazole)[1]				
PCMOF2½(Imidazole)[1]				

[1] New compounds and new conductivity data

[2] A compound previously synthesized by Hurd *et al*. (unpublished); its conductivity was measured under new conditions.

[3] A compound and conductivity investigated by Hurd *et al* .(unpublished).

[4] A compound previously reported by Hurd *et al*.; its conductivity was measured under new conditions.[1,2]

[5] Compound and conductivity previously reported by Hurd *et al*.[2]

[6] Compounds and conductivity previously reported by Kim *et al.* (the author).[1]

[7] Activation energy measured between the temperature of 85 °C and 25 °C.

[8] Activation energy measured between the temperature of 150 °C and 110 °C.

[9] Activation energy measured between the temperature of 110 °C and 90 °C.

[10] Activation energy measured between the temperature of 150 °C and 60 °C.

[11] Activation energy measured between the temperature of 150 °C and 90 °C.

Table 3.1 List of PCMOF samples featured in this work and their conductivity profiles.

3.3 Experimental

3.3.1 Synthesis and analytical procedures

All starting materials were obtained from commercial suppliers (Sigma Aldrich, Alfa Aesar, Acros Organics) and were used without further purification. ^{1}H and ^{31}P NMR spectra were collected on a Bruker Advanced II 400 MHz NMR spectrometer. Thermogravimetric analysis were performed on a Netzsch STA 409 TGA/DSC analyzer in aluminum oxide (Al_2O_3) crucibles under 60 mL/min flow of N_2 at a heating rate of 2 °C/min from room temperature to 1000 °C. Powder XRD was used to confirm and compare the structures of the synthesized PCMOFs to the original β-PCMOF2 sample. Data was collected on a Rigaku Multiflex "theta-theta" X-ray Diffractometer equipped with a position sensitive proportional counter (PSPC) using Cu K_α tube (λ = 0.15418 nm) operated at 40 kV and 40 mA. Samples for analysis were ground into fine powders using a mortar and pestle. Once ground, they were then mounted onto a zero background sample holder (crystalline silicon cut) and the surface of the powders leveled using a glass slide or an aluminum plate holder when sufficient sample was available to fill the plate. A scan range of 2-theta = 3° to 40°, with a scan speed of 0.2 deg/min and a sample width equal to 0.02° were used. Following collection, the data was processed using a winJADE software.

3.3.2 Synthesis of β-PCMOF2

Anhydrous phloroglucinol (8.05 g, 63.9 mmol) was dissolved in dry dimethyl carbonate (200 mL) and the resulting yellow solution cooled to 0 °C under Ar. Chlorosulfonic acid (12.4 mL, 187 mmol, 2.93 equiv.) was added dropwise over the course of 2 minutes with vigorous stirring, resulting in an orange colored solution. The reaction was warmed to ambient temperature and allowed to proceed for 1.5 h under a steady flow of Ar before the system was sealed and stirred for an additional 22.5 h. The solvent was then removed via rotary evaporation and the resulting viscous, brown oil dissolved in 150 mL of water. Sodium bicarbonate was added to the solution until it reached a pH of 2.0. Addition of the aqueous solution to 4 L of acetone resulted in the formation of a thick white precipitate, which was isolated via vacuum filtration. Yield: 22.6 g, 84%. PCMOF2 has a lower temperature α-phase and a high temperature β-phase. Preparation of PCMOF2 initially yields the α-phase, which must be converted to the thermodynamic β-phase. The conversion is achieved by placing the finely ground powder of α-PCMOF2 into a silicon tube, sealed and pressed under a hydrostatic pressure of 10,000 pounds/inch^2 for 2 minutes. This is followed placing the pellet into a 23 mL Teflon autoclave, along with a vial of water (1.7 mL), sealing the autoclave in a stainless steel jacket and heating to 80 °C over 2 hours, holding at 80 °C for 48 hours then cooling back to room temperature over 12 hours. The resulting white precipitate was isolated via vacuum filtration. Yield: 0.49 g, 98%. Complete conversion is verified by the complete change in the powder XRD pattern. In short, the α-phase is exposed to the high humidity and temperature (thermodynamic) conditions. It was found that both α-PCMOF2 and β-PCMOF2 can be used as the starting material for the isomorphous ligand replacement.

3.3.3 Synthesis of PCMOF2(Pyrazole)

An aliquot of H_3L1 solution (10 mL, 1.0 gram, 2.7 mmol) was removed and diluted to a concentration of 50 mg/mL with RO water (10 mL). 1*H*-Pyrazole (0.095 g, 1.4 mmol) was added, and the mixture was stirred for 2 minutes. Sodium carbonate (0.174 g, 1.64 mmol) was added part wise over approximately 30 seconds, and the mixture was stirred until a total of five minutes has elapsed since the start of the sodium carbonate addition. The solution was poured into acetone (200 mL) and was stirred for two minutes. The white precipitate that was formed was collected by vacuum filtration through a 350 mL fine glass frit (4.5 to 5 μm), and then washed with two 100 mL portions of acetone. The product was dried on the frit for several minutes with compressed air also being blown over the top, before being transferred to a pre-weighted 20 mL vial to finish drying in a vacuum oven at room temperature and 10 mbar vacuum. PCMOF2(Pyrazole) was obtained as a white powder (0.45 g, 61% yield). $[Na_3L1]_{1.00}[Pyrazole]_{0.49}\cdot 1.40H_2O$. Elemental analysis calculated (%) C=18.28, H=1.59, N=2.80; Found: C=18.33, H=1.88, N=3.03. TGA: 23 – 225 °C: -7.11% observed, -6.80% calculated for loss of 1.40 waters; 225 – 350 °C: -13.80% observed, -6.80% expected for loss of 0.49 Pyrazole; 350 – 450 °C: -40.32% observed, decomposition. Approximately 75 mg of the *PCMOF2(Pyrazole) as synthesized* sample was packed into a silicon tube, sealed and pressed under a hydrostatic pressure of 10,000 pounds/inch^2 for 2 minutes. The resulting pellet was removed from the silicone tube. To achieve complete conversion of α-PCMOF2 to β-PCMOF2, the resulting pellet was placed into a 23 mL Teflon autoclave, along with a vial of water (1.7 mL). The Teflon autoclave was then sealed in a stainless steel jacket and heated to 80 °C over 2 hours, held at 80 °C for 48 hours, and

then cooled back to room temperature over 12 hours. The pellet was then placed in a desiccator for minimum of 12 hours to remove excess moisture, and ground into a fine powder using a mortar and pestle. Pale pink crystalline powder of PCMOF2(Pyrazole) was obtained in quantitative yield. *$[Na_3L1]_{1.00}[Pyrazole]_{0.45}\cdot 0.40H_2O$*. Elemental analysis for $[Na_3L1]_{1.00}[Pyrazole]_{0.45}\cdot 0.40H_2O$ calculated (%) C=18.78, H=1.20, N=2.68; Found: C=18.83, H=1.60, N=3.04. Postimpedance characterization: Elemental analysis for $[Na_3L1]_{1.00}[Pyrazole]_{0.24}\cdot 1.50H_2O$ calculated (%) C=16.97, H=1.48, N=1.41; Found: C=17.01, H=1.14, N=1.04. **

3.3.4 Synthesis of PCMOF2½(Pyrazole)

PCMOF2(Pyrazole) (50.0 mg, 0.125 mmol) and $Na_3H_3L2\cdot 2.75H_2O$ (22.7 mg, 0.0623 mmol, 2 to 1 ratio with respect to Na_3L1 and Na_3H_3L2) were individually ground into fine powders using a mortar and pestle. The ground powders were placed in a vial and mechanically shaken. The resulting mixture was placed into a silicon tube, sealed and pressed under a hydrostatic pressure of 10,000 pounds/inch^2 for 2 minutes. The resulting pellet was removed from the silicone tube and placed into a 23 mL Teflon autoclave, along with a vial of water (1.7 mL). The Teflon autoclave was then sealed in a stainless steel jacket and heated to 80 °C over 2 hours, held at 80 °C for 48 hours then cooled back to room temperature over 12 hours. The pellet was then placed in a desiccator for minimum of 12 hours to remove excess moisture, and ground into a fine powder using a mortar and pestle. Pink crystalline powder of PCMOF2½(Pyrazole) was obtained in quantitative yield. *$[Na_3L1]_{1.00}[Na_3H_3L2]_{0.52}[Pyrazole]_{0.35}\cdot 2.42H_2O$*. Elemental analysis for $[Na_3L1]_{1.00}[Na_3H_3L2]_{0.52}[Pyrazole]_{0.35}\cdot 2.42H_2O$. Calculated (%): C=17.46, H=1.78, N=1.39; Found: C=17.06, H=1.38, N=1.79. ^{1}H NMR (400 MHz, D_2O): δ = 8.24 (m,

Na_3H_3L2 aromatic H), δ = 7.76 (s, broad, pyrazole 2H), δ = 6.47 (t, pyrazole 1H); $^{31}P\{^1H\}$ NMR (162 MHz, D_2O, unreferenced): δ = 12.04 (s, Na_3H_3L2). TGA: 21 – 325 °C: gradual mass loss of -15.43% observed, -6.22% calculated for loss of 2.42 waters, -3.38% calculated for loss of 0.35 pyrazole, remaining mass loss may be attributed to the partial decomposition of 0.52 Na_3H_3L2; 325 – 450 °C: -40.26% observed, framework decomposition; 450 – 1000 °C: -23.66% observed, framework decomposition (Figure 3.3).* Postimpedance characterization: Elemental analysis for $[Na_3L1]_{1.00}[Na_3H_3L2]_{0.50}[Pyrazole]_{0.24}\cdot 1.60H_2O$. Calculated (%): C=17.44, H=1.53, N=1.00; Found: C=17.04, H=1.16, N=1.06.** Postimpedance, anhydrous conditions: Elemental analysis for $[Na_3L1]_{1.00}[Na_3H_3L2]_{0.50}[Pyrazole]_{0.46}\cdot 0.70H_2O$ Calculated (%): C=18.66, H=1.39, N=1.93; Found: C=18.33, H=1.39, N=2.31.***

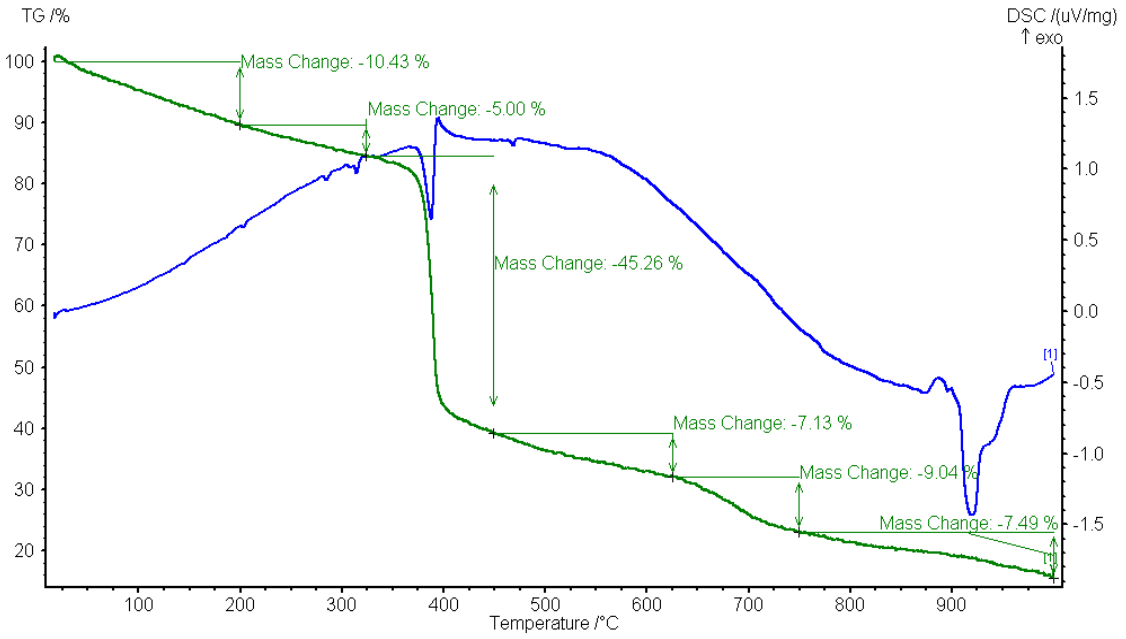

Figure 3.3 Combined TGA (in green)/DSC (in blue) of PCMOF2½(Pyrazole) pre-impedance with the calculated mass losses. Measured at 2K per minute under N_2 atmosphere.

3.3.5 Synthesis of PCMOF2(Triazole)

An aliquot of H_3L1 solution (10 mL, 1.0 gram, 2.7 mmol) was removed and diluted to a concentration of 50 mg/mL with RO water (10 mL). 1*H*-1,2,4-Triazole (0.096 g, 1.4 mmol) was added, and the mixture was stirred for 2 minutes. Sodium carbonate (0.174 g, 1.64 mmol) was added part wise over approximately 30 seconds, and the mixture was stirred until a total of five minutes has elapsed since the start of the sodium carbonate addition. The solution was poured into acetone (200 mL) and was stirred for two minutes. The white precipitate that was formed was collected by vacuum filtration through a 350 mL fine glass frit (4.5 to 5 μm), and then washed with two 100 mL portions of acetone. The product was dried on the frit for several minutes with compressed air also being blown over the top, before being transferred to a pre-weighted 20 mL vial to finish drying in a vacuum oven at room temperature and 10 mbar vacuum. PCMOF2(Triazole) was obtained as a white powder (0.579 g, 78.3% yield). Elemental analysis calculated (%) C=16.73, H=1.62, N=2.90; Found: C=16.62, H=1.28, N=2.98. TGA: 23 – 175 °C: -6.34% observed, -6.33% calculated for loss of 1.68 waters; 261 – 302 °C: -6.85% observed, -7.74% expected for loss of 0.34 1,2,4-Triazole; 369 – 380 °C: -36.73% observed, decomposition. $[Na_3L1]_{1.00}[1,2,4\text{-}Triazole]_{0.34}\cdot 1.68H_2O$. There was no need to further expose PCMOF2(Triazole) sample to conversion conditions since the powder XRD of *as synthesized* PCMOF2(Triazole) matched that of β-PCMOF2 (did not show peaks that corresponded to the low temperature α-PCMOF2 phase). Henceforth, the *as synthesized* sample was used for the impedance measurements and as a starting material for the subsequent PCMOF2½(Triazole) synthesis. $[Na_3L1]_{1.00}[1,2,4\text{-}Triazole]_{0.34}\cdot 1.68H_2O$. Elemental analysis for $[Na_3L1]_{1.00}[1,2,4\text{-Triazole}]_{0.34}\cdot 1.68H_2O$

calculated (%) =16.73, H=1.62, N=2.90; Found: C=16.62, H=1.28, N=2.98. TGA: 23 – 175 °C: -6.34% observed, -6.33% calculated for loss of 1.68 waters; 261 – 302 °C: -6.85% observed, -7.74% expected for loss of 0.34 1,2,4-Triazole; 369 – 380 °C: -36.73% observed, decomposition.* Postimpedance characterization: Elemental analysis for $[Na_3L1]_{1.00}[1,2,4\text{-Triazole}]_{0.24}\cdot 1.21H_2O$ calculated (%) C=16.53, H=1.36, N=2.14; Found: C=16.31, H=1.03, N=2.19. **

3.3.6 Synthesis of PCMOF2½(Triazole)

PCMOF2(Triazole) (50.0 mg, 0.120 mmol) and $Na_3H_3L2\cdot 2.75H_2O$ (21.9 mg, 0.0600 mmol, 2 to 1 ratio with respect to Na_3L1 and Na_3H_3L2) were individually ground into fine powders using a mortar and pestle. The ground powders were placed in a vial and mechanically shaken. The resulting mixture was placed into a silicon tube, sealed and pressed under a hydrostatic pressure of 10,000 pounds/inch^2 for 2 minutes. The resulting pellet was removed from the silicone tube and placed into a 23 mL Teflon autoclave, along with a vial of water (1.7 mL). The Teflon autoclave was then sealed in a stainless steel jacket and heated to 80 °C over 2 hours, held at 80 °C for 48 hours, and then cooled back to room temperature over 12 hours. The pellet was then placed in a desiccator for minimum of 12 hours to remove excess moisture, and ground into a fine powder using a mortar and pestle. Pale orange crystalline powder of PCMOF2½(Triazole) was obtained in quantitative yield. $[Na_3L1]_{1.00}[Na_3H_3L2]_{0.50}[Triazole]_{0.28}\cdot 0.81H_2O$. Postimpedance characterization: Elemental analysis for $[Na_3L1]_{1.00}[Na_3H_3L2]_{0.50}[\text{Triazole}]_{0.28}\cdot 0.81H_2O$ Calculated (%): C=17.44, H=1.30, N=1.79; Found: C=17.29, H=1.58, N=2.18. ^{1}H NMR (400 MHz, D_2O): δ = 8.17 (m, Na_3H_3L2 aromatic H), δ = 8.52 (s, broad, 1,2,4-Triazole 2H); ^{31}P {^{1}H} NMR (162 MHz, D_2O, unreferenced): δ = 12.07 (s, Na_3H_3L2). TGA: 21 –

325 °C: gradual mass loss of -12.76% observed, -2.23% calculated for loss of 0.81 waters, -2.94% calculated for loss of 0.28 1*H*-1,2,4-triazole, remaining mass loss may be attributed to the partial decomposition of 0.50 Na_3H_3L2; 325 – 450 °C: -41.73% observed, framework decomposition; 450 – 1000 °C: -18.85% observed, framework decomposition (Figure 3.4).* Postimpedance characterization: Elemental Analysis for $[Na_3L1]_{1.00}[Na_3H_3L2]_{0.50}[Triazole]_{0.20}\cdot 0.95H_2O$. Calculated (%): C=17.22, H=1.31, N=1.25; Found: C=16.88, H=1.04, N=0.88.**

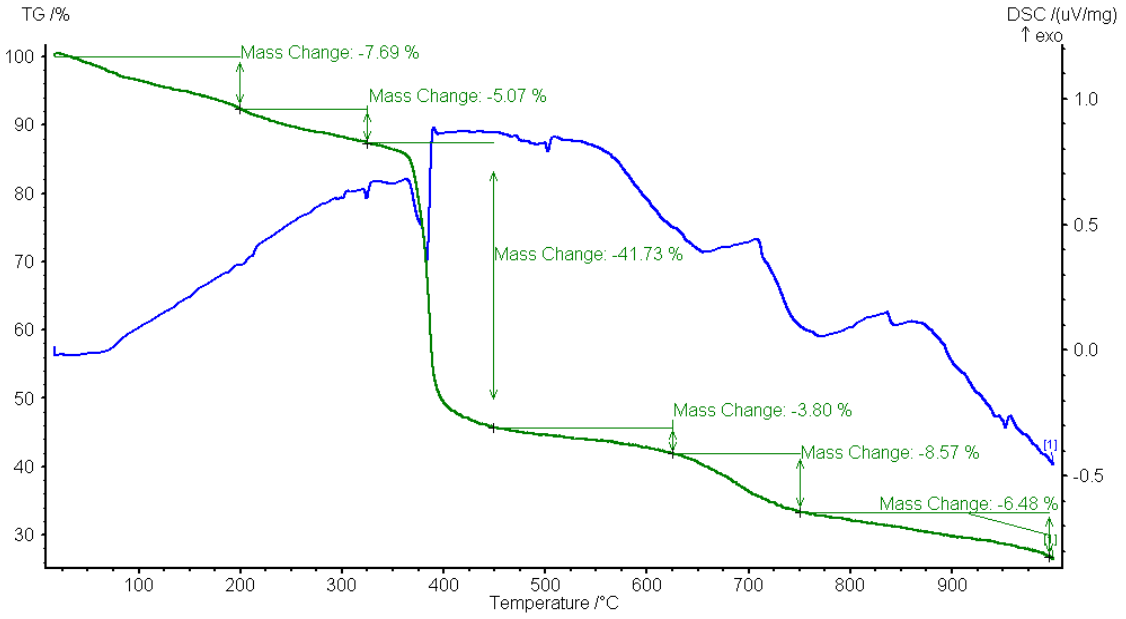

Figure 3.4 Combined TGA (in green)/DSC (in blue) of PCMOF2½(Triazole) pre-impedance with the calculated mass losses. Measured at 2K per minute under N_2 atmosphere.

*3.3.7 Synthesis of PCMOF2½ *Melamine**

With regards to the nomenclature of PCMOF2½ *Melamine*, it is analogous to PCMOF2½ except melamine molecules were used in lieu of Na_3H_3L2 in isomorphously replacing one-third of Na_3L1.

α-PCMOF2 and melamine were individually ground into fine powders using a mortar and pestle. Ground α-PCMOF2·2.75H_2O (50.1 mg, 0.104 mmol) and ground melamine (6.56 mg, 0.0520 mmol, 2 to 1 ratio with respect to Na_3L1 and melamine) were placed in a vial and mechanically shaken to produce a mechanical mixture. The resulting mixture was placed into a silicon tube, sealed and pressed under a hydrostatic pressure of 10,000 pounds/inch^2 for 2 minutes. The resulting pellet was removed from the silicone tube. To achieve the solid state synthesis, the resulting pellet was placed into a 23 mL Teflon autoclave, along with a vial of water (1.7 mL). The Teflon autoclave was then sealed in a stainless steel jacket and heated to 80 °C over 2 hours, held at 80 °C for 48 hours, and then cooled back to room temperature over 12 hours. The pellet was then placed in a desiccator for minimum of 12 hours to remove excess moisture, and ground into a fine powder using a mortar and pestle. Pale pink crystalline powder of PCMOF2½ *Melamine* was obtained in quantitative yield. *$[Na_3L1]_{1.00}[Melamine]_{0.52}\cdot 0.80H_2O$*. Elemental analysis for $[Na_3L1]_{1.00}[Melamine]_{0.52}\cdot 0.80H_2O$ Calculated (%): C=17.73, H=1.52, N=8.53; Found: C=17.66, H=1.39, N=8.68. Postimpedance characterization: Elemental analysis for $[Na_3L1]_{1.00}[Melamine]_{0.48}\cdot 0.67H_2O$ Calculated (%): C=17.70, H=1.44, N=7.98; Found: C=17.88, H=1.72, N=7.94.

3.3.8 Asterisk notes

* With respect to the TGA % mass losses of PCMOF2½(Pyrazole) and PCMOF2½(Triazole), the expected mass losses calculated from the heterocycle loadings and the hydration states (via elemental analysis) were smaller than and the experimental mass losses (as seen in TGA). It is hypothesized that the nature of the multi-component system accelerates the onset of framework decomposition, lowering the framework

decomposition temperature from 369 °C to 175 - 302°C range, thereby contributing to the greater % mass losses between 175 – 302 °C.

** Due to the limited sample availability for the post-impedance analysis, only powder XRD and elemental analyses were performed.

*** With respect to the increase of pyrazole from 0.35 to 0.49 for the pre-impedance to post-impedance composition under anhydrous conditions, multiple PCMOF2½(Pyrazole) samples, with ratios of pyrazole between 0.35 and 0.49, were combined to reach sufficient sample size for the anhydrous conductivity measurements. Approximately 300 mg of powdered PCMOF2½(Pyrazole) sample is necessary for anhydrous conductivity analysis. The original PCMOF2½(Pyrazole) synthesis, which was used for the full characterization and the conductivity measurements under hydrated conditions, yielded only 75 mg.

3.3.9 AC impedance measurements

Powdered samples of PCMOF2½(Pyrazole), PCMOF2½(Triazole), PCMOF2(Pyrazole), PCMOF2(Triazole), PCMOF2½ *Melamine* (3 to 5 mg each) were placed in a glass cell and were compressed between 2 solid titanium electrodes (0.3175 cm diameter). The sample length was measured by the difference between the empty cell and the filled cell, and was typically to 1 to 2 mm in length. The sample cells were placed inside a humidity and temperature controlled chamber (ESPEC BTL-433) and connected to a Princeton Applied Research VersaSTAT 3 impedance analyzer using a 2 probe setup. AC impedance data was collected by cycling between 10^6 and 1 Hz with 10-100 mV of applied potential using VersaStudio software. Samples were equilibrated for between 8 to 12 hours after each step in temperature or 48 to 120 hours for each step in relative

humidity ranging from 25 to 85 °C and 30% to 90% relative humidity. Environmental controls: Exposure of the samples to humid environment was performed for conditions at and below 90% relative humidity using the ESPEC BTL-433 humidity control oven. The temperature and humidity the conditions were within the operating capacities of the oven.

Proton conductivity of all samples was measured under 90% relative humidity condition at various temperatures. The temperature was varied from 25 °C to 85 °C for minimum of two heating and cooling cycles with sufficient time for sample equilibration between each step. Following the heating and cooling cycles, the temperature was held at 25 °C and the humidity was decreased from 90% to the minimum of 30% to measure the humidity dependent proton conductivity of the samples.

3.3.10 The list of additional PCMOFs that were investigated

The following combination of compounds was also synthesized analogous to the above procedures and their initial conductivity measured. The samples did not show conductivity below 10^{-6} S cm^{-1} at 25°C and 90% relative humidity after 7 days of equilibration time in the conductivity apparatus. These samples were not investigated further.

*PCMOF2½ *Melamine* (Pyrazole)*

Pre-Impedance: Elemental analysis for $[Na_3L1]_{1.00}[Melamine]_{0.47}[Pyrazole]_{0.26}\cdot 1.06H_2O$ Calculated (%): C=18.61, H=1.71, N=8.81; Found: C=18.61, H=1.71, N=8.82.

*PCMOF2½ *Melamine* (Triazole)*

Pre-Impedance: Elemental analysis for $[Na_3L1]_{1.00}[Melamine]_{0.60}[Triazole]_{0.33}\cdot 0.20H_2O$ Calculated (%): C=19.02, H=1.51, N=12.03; Found: C=19.27, H=1.89, N=12.37.

*PCMOF2½ *Melamine* (Imidazole)*

Pre-Impedance**:** Elemental analysis for $[Na_3L1]_{1.00}[Melamine]_{0.53}[Imidazole]_{0.15}\cdot 0.43H_2O$ Calculated (%): C=18.77, H=1.52, N=9.98; Found: C=18.96, H=1.57, N=10.33.

PCMOF2½(Imidazole)

Pre-Impedance**:** Elemental analysis for $[Na_3L1]_{1.00}[Na_3H_3L2]_{0.45}[Imidazole]_{0.16}\cdot 1.70H_2O$ Calculated (%): C=17.05, H=1.52, N=0.69; Found: C=16.66, H=1.15, N=1.01.

PCMOF2(Imidazole)

Pre-Impedance: Elemental analysis for $[Na_3L1]_{1.00}[Imidazole]_{0.23}\cdot 1.30H_2O$ Calculated (%): C=17.05, H=1.39, N=1.37; Found: C=16.98, H=1.12, N=1.01.

3.4 Results – subsections

3.4.1 Compositional analysis

With respect to the multi-component PCMOF2½(Pyrazole) and PCMOF2½(Triazole), the presence of H_3L2 and the corresponding heterocycle were confirmed through ^{1}H and ^{31}P NMR analysis in the pre-impedance samples. Elemental analysis and thermogravimetric analysis confirmed $[Na_3L1]1.00[Na_3H_3L2]_{0.52}[Pyrazole]_{0.35}\cdot 2.42H2O$ as the pre-impedance composition of PCMOF2½(Pyrazole). Elemental analysis confirmed $[Na_3L1]1.00[Na_3H_3L2]_{0.50}[Pyrazole]_{0.24}\cdot 1.60H2O$ as the post-impedance composition of PCMOF2½(Pyrazole). Both pre- and post-impedance PCMOF2½(Pyrazole) samples contained 2:1 ratio of L1:L2 as has been initially prepared. The presence of nitrogen in the pre- and post-impedance analysis was critical in confirming the presence of pyrazole. Unfortunately, a significance decrease in the pyrazole loading was observed for the post-impedance PCMOF2½(Pyrazole) compared to that of pre-impedance

PCMOF2½(Pyrazole): x = 0.35 pyrazole to 0.24 pyrazole. Similar loss of heterocycle was observed for the PCMOF2½(Triazole) samples pre- and post-impedance: x = 0.28 to 0.20 triazole. This will be explored further in the discussion.

Detailed compositional analysis on all PCMOFs has been presented under heading 3.3 Experimental.

3.4.2 Powder XRD analysis

Figure 3.5 shows the powder XRDs analysis of the various PCMOFs featured in this work with the focus on PCMOF2½(Pyrazole). We performed powder XRD analysis throughout the synthesis to confirm the preservation of the original β-PCMOF2 structure. In synthesizing PCMOF2½(Pyrazole), finely ground powders of PCMOF2(Pyrazole) and Na_3H_3L2 were mechanically mixed. The powder XRD of the mechanical mixture exhibited a superimposed powder XRD of its two components (Figure 3.5: I, J and K). The resultant mechanical mixture was then pressed into a pellet and placed under high temperature and humidity conditions to achieve isomorphous ligand replacement, a thermodynamically driven solid state reaction. The resultant powder XRD of PCMOF2½(Pyrazole) resembled that of β-PCMOF2 with a slight 2θ shift for the peaks that correspond to the 011 plane (in the plane of the ligand arene rings) and the 001 plane (the plane perpendicular to ligands) with a decrease of ~0.088 and 0.032 Å in the d-spacing, respectively (Figure 3.6 and Table 3.2). As well, two small additional peaks were present at 23.5° and 25.9° 2θ which may correspond to the visible Na_3H_3L2.

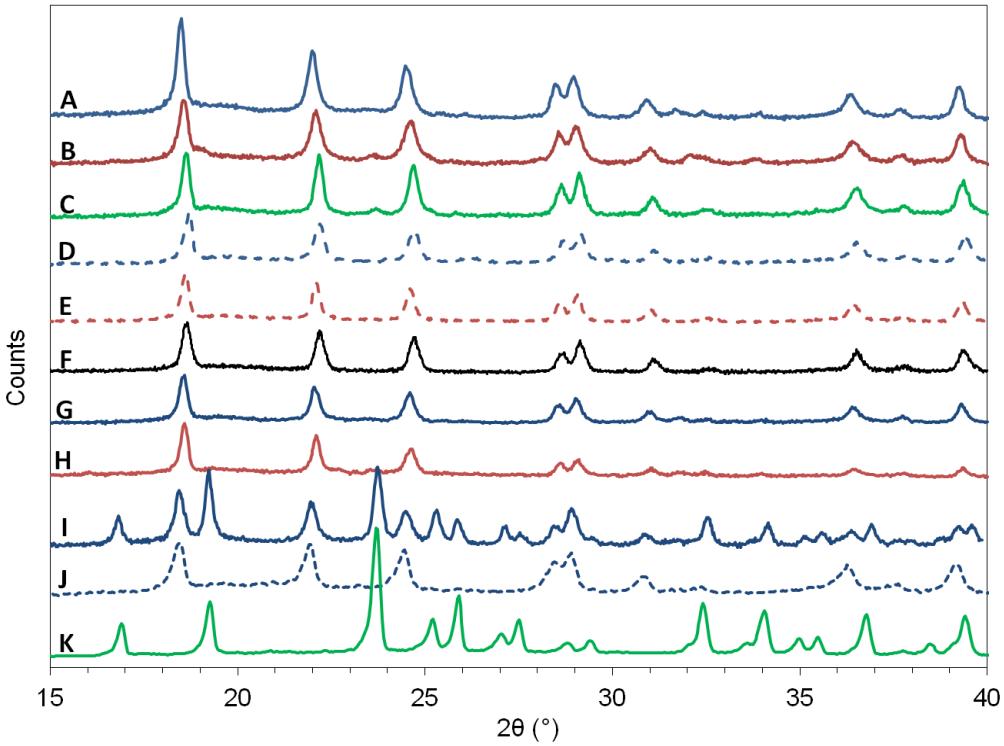

Figure 3.5 Powder XRD patterns of [A] PCMOF2½(Pyrazole), post-impedance; [B] PCMOF2½(Triazole), post-impedance; [C] PCMOF2½, post-impedance; [D] PCMOF2(Pyrazole), post-impedance; [E] PCMOF2(Triazole), post-impedance; [F] β-PCMOF2, post-impedance; [G] PCMOF2½(Pyrazole), pre-impedance; [H] PCMOF2½(Triazole), pre-impedance; [I] Mechanical mixture of PCMOF2(Pyrazole) and Na_3H_3L2 (Resembles J + K); [J] PCMOF2(Pyrazole); [K] Na_3H_3L2.

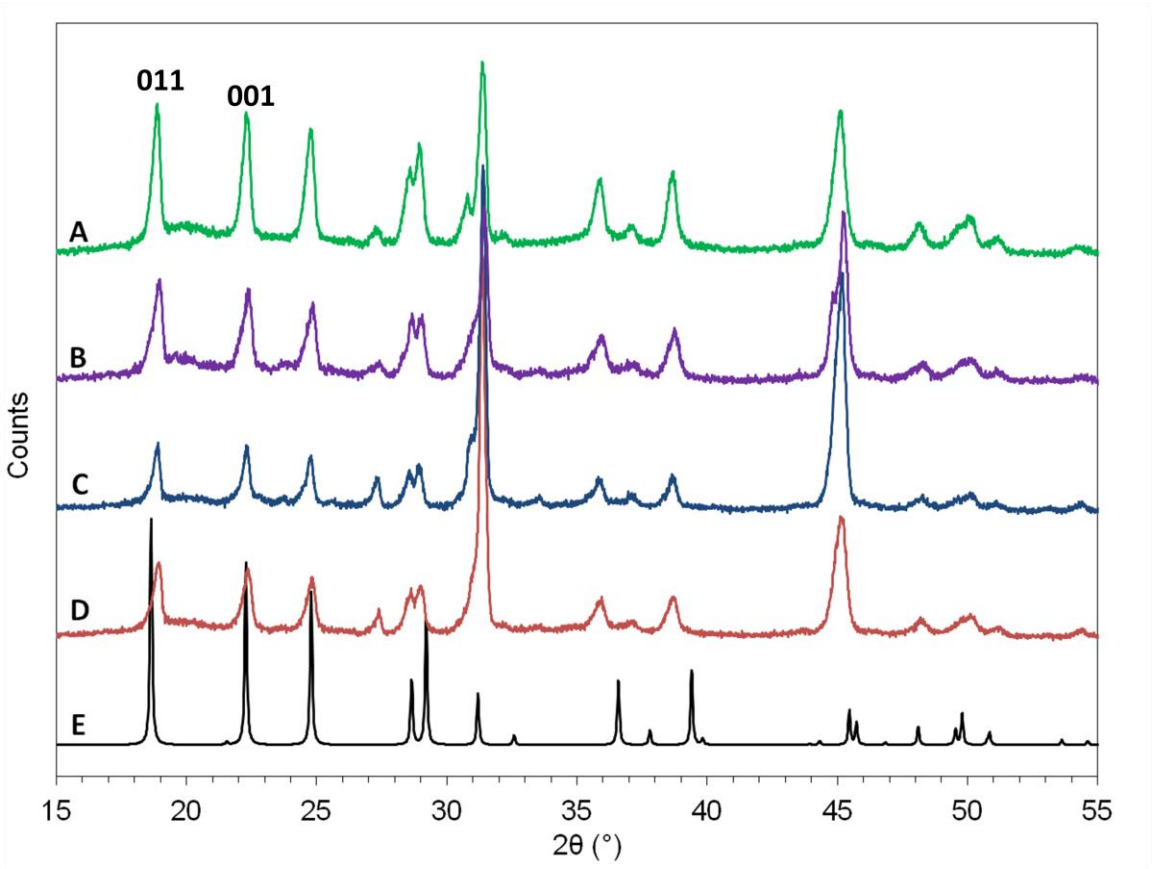

Figure 3.6 Powder XRD patterns of [A] PCMOF2½ *Melamine* with NaCl standard; [B] PCMOF2½(Triazole) with NaCl standard; [C] PCMOF2½(Pyrazole) with NaCl standard; [D] PCMOF2½ with NaCl standard; [E] β-PCMOF2, simulated pattern from the single crystal structure. Peaks at 18.87 and 22.29 2θ are indexed to be 011 and 001 hkl values respectively based on the single crystal structure of β-PCMOF2.

	hkl index	2θ (degrees)	d-spacing (Å)	Δd from β-PCMOF2 (Å)
β-PCMOF2	011	18.56	4.780	0
PCMOF2½	011	18.93	4.688	-0.093
PCMOF2½(Pyrazole)	011	18.91	4.693	-0.088
PCMOF2½(Triazole)	011	18.99	4.673	-0.107
PCMOF2½ *Melamine*	011	18.87	4.703	-0.078
β-PCMOF2	001	22.12	4.019	0
PCMOF2½	001	22.35	3.978	-0.041
PCMOF2½(Pyrazole)	001	22.30	3.986	-0.032
PCMOF2½(Triazole)	001	22.36	3.976	-0.043
PCMOF2½ *Melamine*	001	22.29	3.988	-0.030

Table 3.2 Experimental PXRD d-spacing differences between the PCMOFs featured in this study. The c-axis is perpendicular to the ligand/MOF layers in the β-PCMOF2 structure. NaCl was used as an internal standard with the following reference peaks: 2θ = 27.36, 31.70, 35.44, 53.86 and 56.46 degrees. Powder XRDs used for the d-space calculation were collected with sample width of 0.01° and scan speed of 1°/minute, using Cu K_α X-ray source (λ = 0.15418 nm).

Interestingly, these differences were also present for the powder XRD of PCMOF2½ *Melamine* (Figure 3.7). There was a slight 2θ shift for the peak corresponding to the 011 plane and the 001 plane with a decrease of ~0.078 and 0.030 Å in the d-spacing, respectively (Figure 3.6 and Table 3.2). Additionally, a small peak was present at 26.2° 2θ which corresponds to the largest powder XRD peak of pristine melamine (Figure 3.7).

In general, all PCMOFs investigated showed powder XRDs analogous to that of β-PCMOF2 both before and after impedance measurements, confirming the preservation of the original β-PCMOF2 structure. Exception was the powder XRD of PCMOF2½ *Melamine* (Imidazole) which contained numerous extra peaks (Figure 3.8). It is

hypothesized that the non-conductive nature of PCMOF2½ *Melamine* (Imidazole) is linked to the presence of the impure phases (extra peaks) shown in the powder XRD. This will be further explored in the discussion.

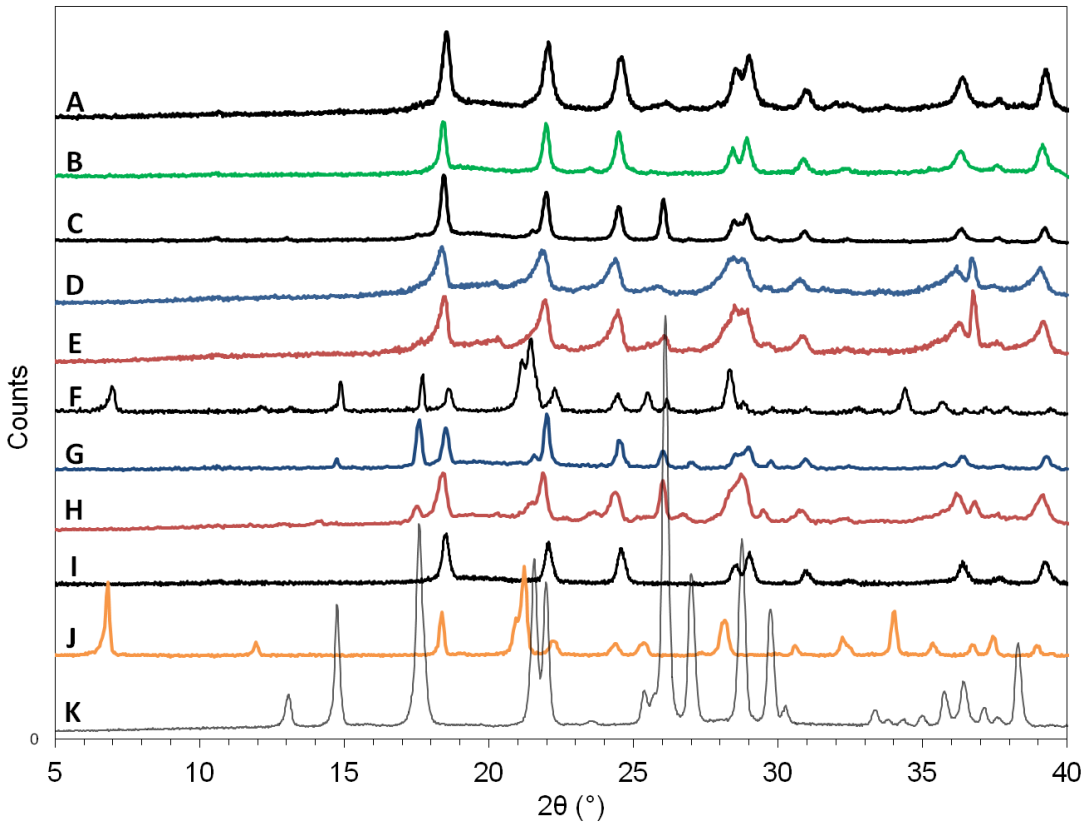

Figure 3.7 Powder XRD pattern of all compounds that contain Melamine: [A] PCMOF2½ *Melamine*, post-impedance; [B] PCMOF2½, post-impedance; [C] PCMOF2½ *Melamine*, pre-impedance; [D] PCMOF2½ *Melamine*(Pyrazole), pre-impedance [has an Aluminum plate peak around 37 degrees]; [E] PCMOF2½ *Melamine*(Triazole), pre-impedance [has an Aluminum plate peak around 37 degrees]; [F] α-PCMOF2 & Melamine, mechanical mixture; [G] PCMOF2(Pyrazole) & Melamine, mechanical mixture; [H] PCMOF2(Triazole) & Melamine, mechanical mixture; [I] = β-PCMOF2; [J] α-PCMOF2; [K] Pristine melamine.

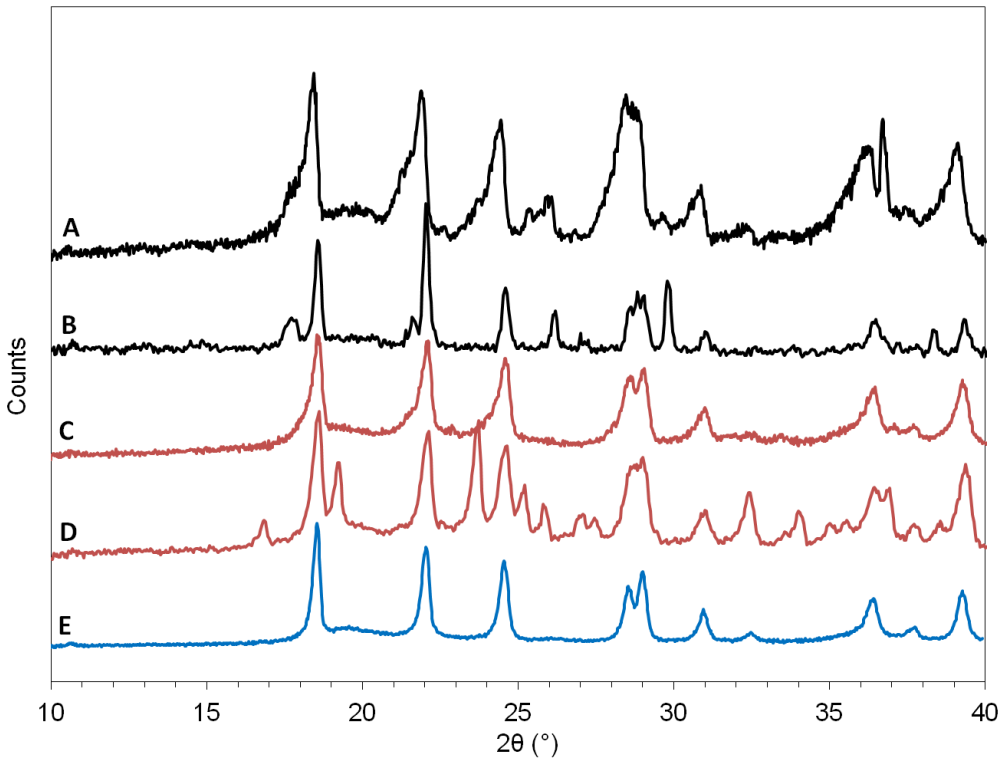

Figure 3.8 Powder XRD patterns of all compounds that contain Imidazole: [A] PCMOF2½ *Melamine* (Imidazole), pre-impedance; [B] PCMOF2(Imidazole) + Melamine, mechanical mixture; [C] PCMOF2½(Imidazole), pre-impedance; [D] PCMOF2(Imidazole) + Na_3H_3L2, mechanical mixture; [E] PCMOF2(Imidazole), pre-impedance.

3.4.3 Proton conductivity and activation energy

Impedance analysis was performed on all PCMOFs that showed conductivity > 10^{-6} S cm^{-1} at 85 °C and 90% relative humidity. PCMOF2½(Pyrazole) exhibited the highest conductivity among all at 85 °C and 90% relative humidity (Figure 3.9 and 3.10). The Nyquist plots obtained from the second heating cycle are shown in Figure 3.9 and it shows that PCMOF2½ exhibited very low resistances, resulting in only the tail end of a semi-circle being observed at high frequencies due to the limitations of the instrument. At lower frequencies, the capacitive tail is also observed, as expected for blocking effects of the mobile charge at the electrode interface. Henceforth, the conductivity was calculated

from the real-axis intercept of the Nyquist plot (Figure 3.9). When the conductivity of PCMOF2½(Pyrazole) was measured at 25 °C and 30% relative humidity, however, the conductivity decreased enough to show a distorted semicircle (Figure 3.9, inset), which is a partial resolution of the two-semicircles resulting from the bulk conductivity and the grain boundary effect. A distorted semicircle provides evidence of ion migration as well as the higher bulk conductivity compared to the conductivity between the individual particles, which is related to the grain boundary effect. For the impedance measurements under hydrated conditions, this was not observable. Under reduced humidity conditions, the increase in the bulk and grain-boundary resistance allowed some partial resolution of the distinction between the bulk and the grain-boundary resistance.

Conductivity of all PCMOFs including the control experiments were measured for at least two heating and cooling cycles from 25 °C to 85 °C at 90% relative humidity. The second cooling cycle is shown in the log conductivity plot as a function of temperature (Figure 3.10). PCMOF2½(Pyrazole) showed higher conductivity (1.1×10^{-1} S cm^{-1}) compared to that of PCMOF2½(Triazole) (5.2×10^{-2} S cm^{-1}) at 85 °C and 90% relative humidity. Similar difference in conductivity was also observed between the two control samples: PCMOF2(Pyrazole) and PCMOF2(Triazole). The conductivity of PCMOF2(Pyrazole) (4.6×10^{-2} S cm^{-1}) was greater than that of PCMOF2(Triazole) (1.9×10^{-2} S cm^{-1}) at 85 °C and 90% relative humidity (Table 3.1).

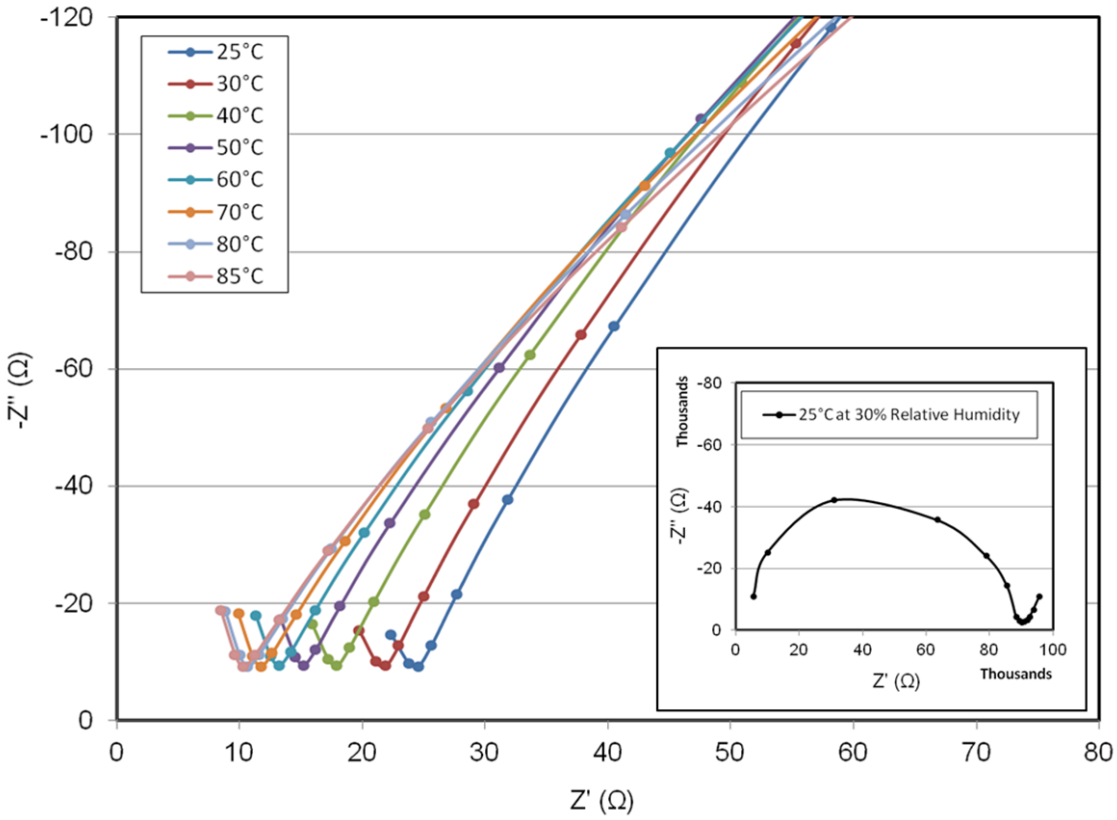

Figure 3.9 Nyquist plot for PCMOF2½(Pyrazole) at 90% relative humidity. The Inset shows the Nyquist plot measured at 30% Relative humidity and 25 °C. The significantly decreased conductivity at this condition enabled observation of a closed (distorted) semicircle. The conductivity was calculated from the real-axis intercept (resistance) using the equation σ = (1/R) × (Length/Area); the length was measured to be 0.0830 cm, and the area was measured to be 0.07917 cm^2.

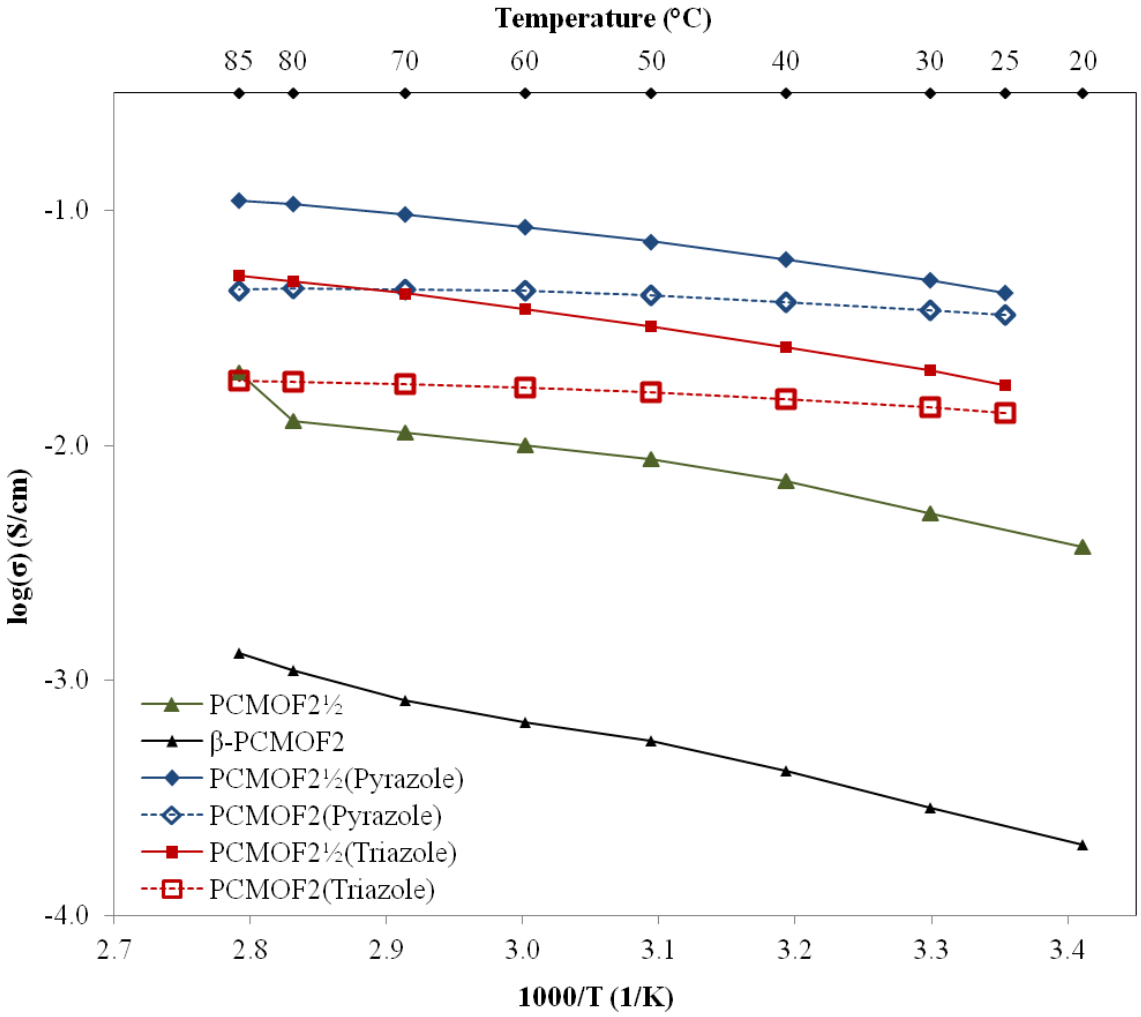

Figure 3.10 Proton conductivity data measured at 90% relative humidity for various PCMOFs.

Since PCMOF2½(Pyrazole) was the first MOF to have proton conducting properties over 10^{-1} S cm^{-1}, we decided to measure its conductivity for four consecutive heating and cooling cycles to investigate the stability and reproducibility. Each cycle was measured at 90% relative humidity and from 25 °C to 85 °C with minimum of 8 hour equilibration time between each temperature change. The third and fourth cooling cycle showed slightly decreased conductivity of 1.07×10^{-1} S cm^{-1} and 1.05×10^{-1} S cm^{-1}

respectively, however, all four cycles showed retraceable and linear conductivity indicating the stability of PCMOF2½(Pyrazole) (Figure 3.11 and 3.12).

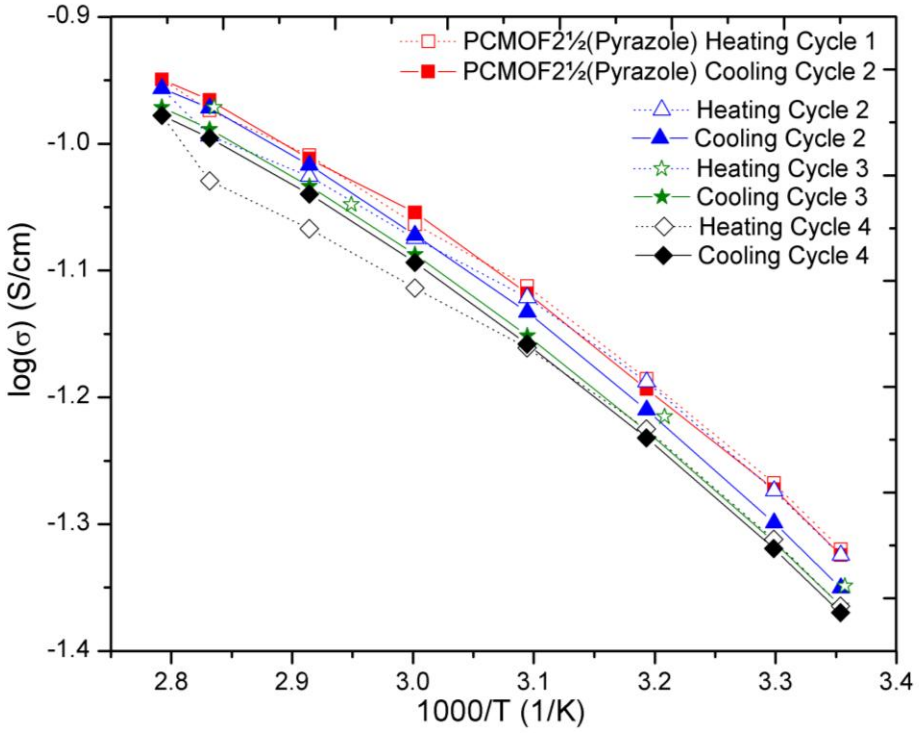

Figure 3.11 Log conductivity versus 1/temperature plot of the multiple heating and cooling cycles of PCMOF2½(Pyrazole).

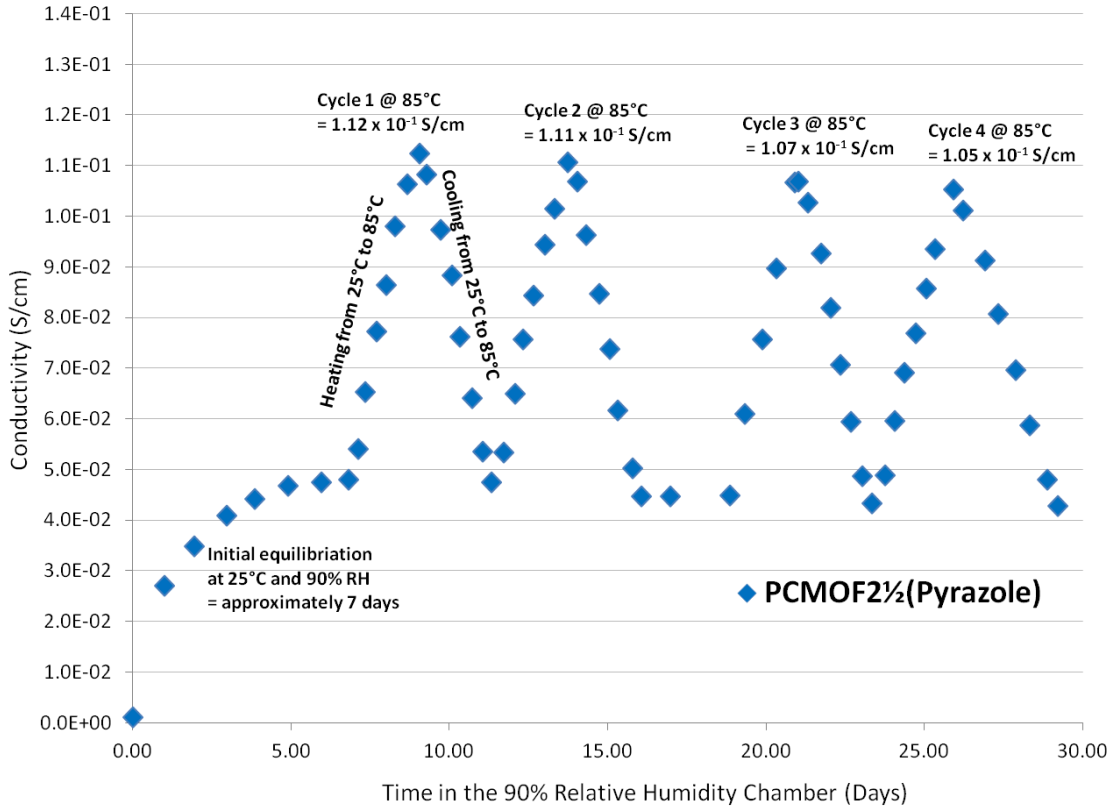

Figure 3.12 Conductivity versus time plot of PCMOF2½(Pyrazole) at various temperatures and under 90% relative humidity.

The conductivity of PCMOF2½(Pyrazole) was then measured under various humidity conditions at 25 °C (Figure 3.13). We believe that both water and heterocycle molecules fill the pores and function as proton carriers. Under variable humidity measurements, the conductivity was found to be highly dependent on the humidity, which suggests that the water playing a critical role in proton conduction. Interestingly, both PCMOF2½(Pyrazole) and PCMOF2½(Triazole) showed rapid decrease in conductivity when the relative humidity was lowered from 90% to 30%, where as the conductivity of PCMOF2(Pyrazole) and PCMOF(Triazole) experienced a much smaller decrease (Table 3.1 and Figure 3.13).

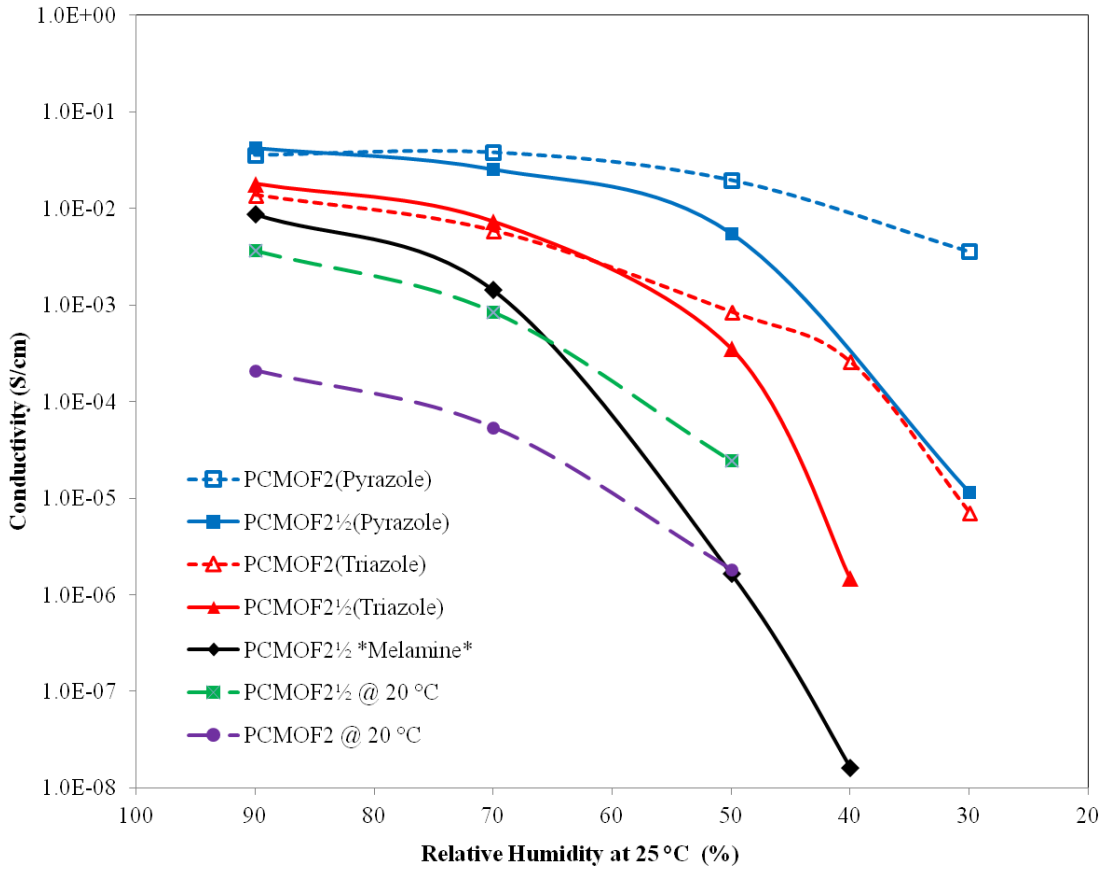

Figure 3.13 Log conductivity of various samples at variable humidity conditions. Note that the conductivity of PCMOF2½ and β-PCMOF2 were measured at 20 °C where as the conductivity of the remaining samples were measured at 25 °C.

The activation energies showed an interesting trend depending on which design strategy was applied. All activation energies were within the range of Grotthuss mechanism (>0.40 eV). Lower activation energy indicates a highly efficient Grotthuss mechanism. High activation energy can potentially correspond to a less organized conduction pathway and/or stronger host-guest interaction experienced by charge carriers resulting in smaller degrees of motional entropy (Equation 1.1: Arrhenius equation).

β-PCMOF2 had the greatest activation energy among all the PCMOFs investigated in this study: 0.28 eV. PCMOF2½ showed activation energy of 0.21 eV,

showing decreased energy barrier for Grotthus proton conduction mechanism potentially due to the increased concentration in the free acidic protons contributing to the facility of proton conduction, in addition to the enhancement of conductivity.

Interestingly, PCMOF2(Triazole) and PCMOF2(Pyrazole) showed very low activation energies (0.08 eV), indicating a much lower energy barrier for proton hopping. PCMOF2½(Pyrazole) and PCMOF2½(Triazole) showed activation energies of 0.16 and 0.19 eV respectively (Table 3.1).

3.5 Discussion

Since this work features a large number of newly synthesized PCMOFs as well as previously reported PCMOFs with their conductivity measured under new conditions (Table 3.1), the discussion will focus on PCMOF2½(Pyrazole), a PCMOF that successfully utilizes both heterocycle loading and isomorphous ligand replacement to exhibit the greatest increase in its proton conductivity.

3.5.1 Synthesis and characterization of PCMOF2½(Pyrazole)

Synthesis of a mixed ligand MOF is inherently challenging because it is difficult to predict how the individual components will react to one another. In synthesizing PCMOF2½(Pyrazole), a three-component mixed ligand MOF, it was critical to employ appropriate synthetic parameters to enable mutual compatibility between the two design strategies. The synthesis of PCMOF2½(Pyrazole) was done in a two-step process where PCMOF2(Pyrazole) was first synthesized, and then mixed with Na_3H_3L2 and placed under solid state reaction conditions to yield PCMOF2½(Pyrazole).

The synthesis of PCMOF2(Pyrazole) was tailored to kinetically capture pyrazole within the β-PCMOF2 framework. To an aqueous solution containing fully dissolved

H_3L1, sodium carbonate and pyrazole, a copious amount of acetone was added to force precipitation of the kinetic product – PCMOF2(Pyrazole). The powder XRD of the *as synthesized* PCMOF2(Pyrazole) was analogous to the β-PCMOF2 with additional peaks at 11.2 and 20.3° 2θ that correspond to the low temperature α-phase of PCMOF2 (Figure 3.14). Therefore, *as synthesized* PCMOF2(Pyrazole) was pelletized and exposed to high temperature and humidity to fully convert the α-PCMOF2 to β-PCMOF2 (Figure 3.14). During this conversion, however, we observed a small loss of pyrazole (x = 0.49 to 0.45) based on the elemental analysis. The resultant PCMOF2(Pyrazole) was then mixed with Na_3H_3L2, pelletized and subsequently exposed to high humidity and high temperature conditions for 48 hours to achieve complete ismorphous ligand replacement. Again, loss of pyrazole was observed (x = 0.45 to 0.35) (Figure 3.15).

Despite the loss of pyrazole under the synthetic conditions, full characterization and conductivity measurements were carried out. Previous study by Hurd *et al.* indicated that small change in loading only brought small change in conductivity, and the heterocycle loading of x = 0.30 was sufficient to impart enhanced conductivity.[2] During the course of conductivity (impedance) analysis, PCMOF2½(Pyrazole) was exposed to 90% relative humidity and four heating and cooling cycles from 25 °C to 85 °C for 30 days (Figure 3.12), followed by exposure to reduced humidity (decrease from 90% to 30% relative humidity) for 10 days at 25 °C (Figure 3.13). Here, similar loss of pyrazole was observed between the pre- and post-impedance samples: x = 0.35 to x = 0.24 respectively (Figure 3.15).

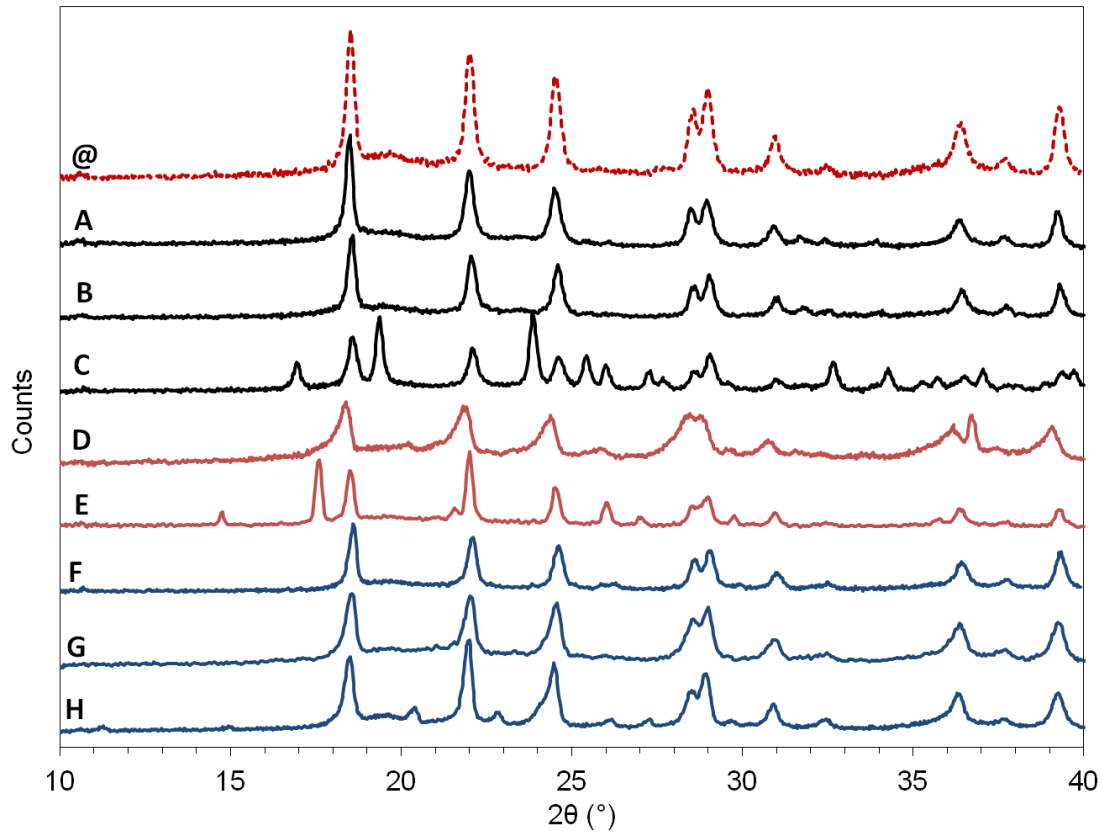

Figure 3.14 Powder XRD patterns of all compounds that contain Pyrazole: [@] PCMOF2½(Pyrazole, post-impedance, anhydrous condition [A] PCMOF2½(Pyrazole), post-impedance, hydrated condition; [B] PCMOF2½(Pyrazole), pre-impedance; [C] PCMOF2(Pyrazole) + Na_3H_3L2, mechanical mixture; [D] PCMOF2½ *Melamine* (Pyrazole), pre-impedance; [E] PCMOF2(Pyrazole) + Melamine, mechanical mixture; [F] PCMOF2(Pyrazole), post-impedance; [G] PCMOF2(Pyrazole), pre-impedance, post-solid state synthesis; [H] PCMOF2(Pyrazole), as synthesized.

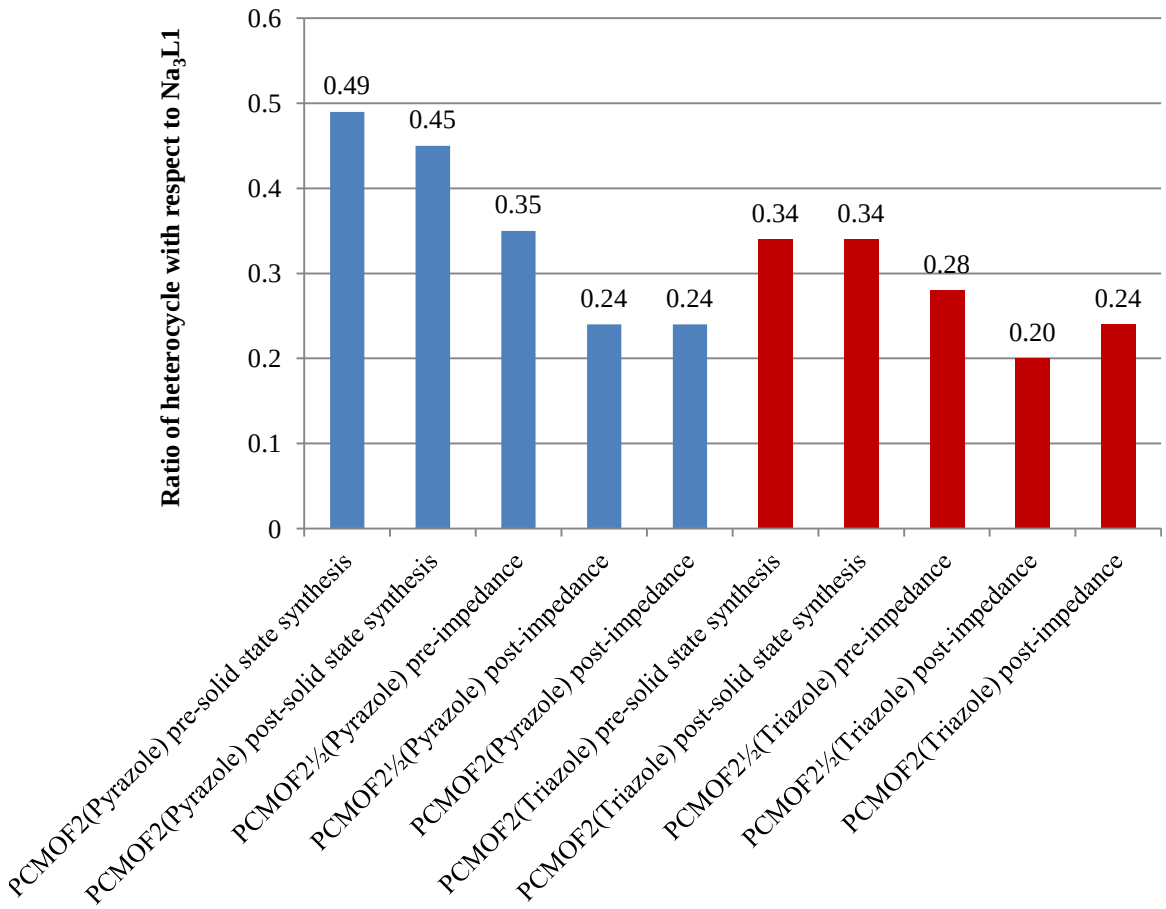

Figure 3.15 Bar graph indicating the ratio of heterocycle with respect to Na_3L1 for samples that contain pyrazole and triazole. Note the decrease in heterocycle content as the duration of exposure to solid state synthesis condition is increased.

PCMOF2½(Pyrazole) was placed under anhydrous conditions and its conductivity measured (Figure 3.16) – no apparent loss of pyrazole was observed which indicates that the heterocycle loss was linked to the presence of humidity.

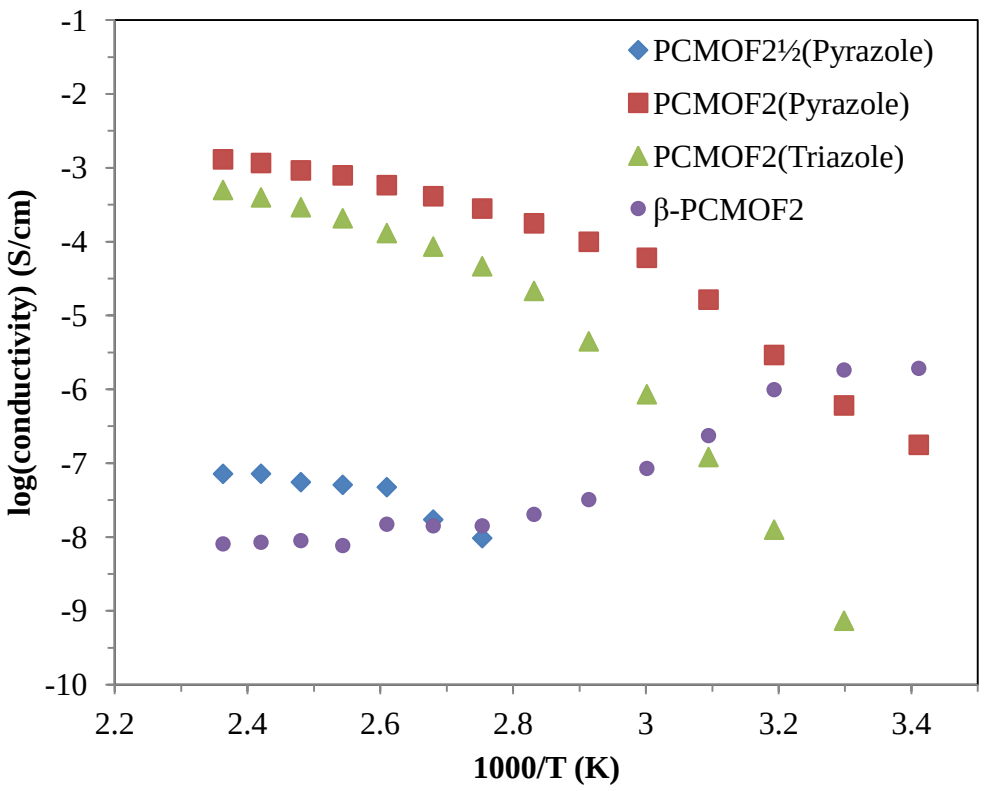

Figure 3.16 Log conductivity versus 1/temperature plot of the second cooling cycle measured under anhydrous conditions. The temperature range was decreased from 150 °C to 20 °C at 10 °C intervals.

In comparing PCMOF2½ to PCMOF2½(Pyrazole), the inclusion of pyrazole increased the conductivity fivefold under hydrated condition (Figure 3.10 and Table 3.1). Furthermore, the resultant conductivity was stable despite losing almost 18% of loaded pyrazole during the course of conductivity measurements. From the first cooling cycle to the fourth cooling cycle, the decrease of maximum conductivity was less than 7% (<0.07 S cm^{-1}). This was determined by comparing the peak conductivities for the four complete heating and cooling cycles (Figure 3.12). Lastly, the post-impedance powder XRD of PCMOF2½ matched that of the pre-impedance pattern, corroborating the preservation of the original crystalline structure (Figure 3.14).

Based on the conductivity analysis, we carefully hypothesized that there may be a point of non-zero stable heterocycle retention, which may be the ultimate thermodynamic state for the mixed ligand system PCMOF2½(Pyrazole). It is possible that the inclusion of H_3L2 allows greater host-guest interaction between L2 and the trapped heterocycles, preventing the complete loss of the heterocycle out of the framework. The increased host-guest interaction is evident from the increase in the activation energy from comparing PCMOF2(Pyrazole) to PCMOF2½(Pyrazole), 0.08 eV and 0.16 eV respectively. Referring back to the Arrhenius equation, the activation energy is directly linked to the facility of proton transport, and stronger host-guest interaction between pyrazole and L2 would increase the activation energy. Under PCMOF2½(Pyrazole) system, the motional entropy and mobility of the heterocycle guests is decreased which induces greater energy barrier for the movement and re-orientation of pyrazole following proton transfer. Furthermore, greater degree of heterocycle loss is observed between pre- and post-impedance samples of PCMOF2(Pyrazole) compared to that of PCMOF2½(Pyrazole), x = 0.45 → 0.24 and x = 0.35 → 0.24 respectively. The heterocycle in PCMOF2(Pyrazole) experiences less host-guest interaction and has greater freedom of movement. This translates to the smaller activation energy (0.08 eV) and greater loss of pyrazole.

3.5.2 Mechanism of isomorphous ligand replacement

When PCMOF2½ was first reported (2013), the exact mechanism of isomorphous lignad replacement remained elusive.[1] Specifically, a simple macroscopic mechanical mixture of Na_3L1 (α-phase) and Na_3H_3L2 converted into the PCMOF2½ phase with a comparable enhancement in conductivity compared to a hydrothermally prepared PCMOF2½ that was designed to mix the two phases in their nanoscale. The mechanical

mixture yielded conductivity of 1.9×10^{-2} S cm^{-1} compared to the hydrothermally prepared PCMOF2½'s conductivity of 2.1×10^{-2} S cm^{-1} at 90% relative humidity and 85 °C.

It was initially attributed that the mechanical mixture's conversion to PCMOF2½ took place in-situ during the conductivity measurements, which consists of continuous exposure to high humidity (90% relative humidity), high temperatures (two temperature cycles from 25 °C to 85 °C), and high pressure (pressed between two electrodes) for an extended period of time (three weeks). The evidence for conversion was that the conductivity only stabilized after the first heating and cooling cycle, as well as a freshly prepared and pelletized mechanical mixture yielded identical PCMOF2½ when it was exposed to the similar high temperature and humidity conditions akin to the conductivity measurements (Figure 2.2, 2.3, 2.7, and 2.8).

Furthermore, it was initially thought that only α-PCMOF2 could undergo isomorphous ligand replacement because α-PCMOF2 possesses the thermodynamic drive to convert to β-PCMOF2. This energetic drive was thought to be instrumental in isomorphously incorporating Na_3H_3L2 within the β-PCMOF2 framework. It was believed that the pelletization and exposure to high temperature and high humidity were essential for the conversion to PCMOF2½.

Herein, we successfully elucidated the exact mechanism of isomorphous ligand replacement. Isomorphous ligand replacement synthesis is a thermodynamically driven solid state reaction. Pelletization accelerates the process because it increases the contact between the multi-phases. Additionally, the high temperature and humidity condition

accelerates the mobility of the molecules and drives the reaction because it increases the positional and vibrational entropy of the solid constituents. Intriguingly, this synthetic approach is conceptually similar to that of *Accelerated Aging* which describes the natural mineral weathering process. The recent work by Friscic *et al*. illustrates how *Accelerated Aging* can be used to efficiently synthesize MOFs to yield products are in their respective thermodynamic states.[4] Friscic *et al*. demonstrated a successful topological transformation of ZnO into the unusual close-packed varieties of zeolitic imidazolate framework in a static reaction mixture by exposing the mechanical mixture to a salt catalyst (<4% mol ammonium sulfate) and humidity. The reaction does not use bulk solvents, high temperatures or milling, but instead provides an alternative synthetic pathway that is energy-efficient. In the case of isomorphous ligand replacement, both solvothermal and mechanical mixture yields PCMOF2½ in sufficient time. However, exposing the pelletized mechanical mixture to high humidity and temperature significantly *accelerates the molecular mobility* to yield PCMOF2½: the thermodynamic product.

SEM-EDX mapping, paired with powder XRD, provided excellent insight into the mechanism. We isolated the intermediate stages of PCMOF2½ conversion (Figure 2.11, 2.12). SEM-EDX mapping of the intermediate stages revealed decreasing particle sizes, starting from a macroscopic grouping of L1 and L2 corresponding to the initial mechanical mixture, to the nanometer scale distributions corresponding to the intermediate and fully converted PCMOF2½s (Figure 2.13). The powder XRDs of the intermediate stages contained step-wise reduction in the peaks from Na_3H_3L2, further corroborating the isomorphous inclusion of Na_3H_3L2 into the β-PCMOF2 framework.

Furthermore, a pellet of pure Na_3L1, pressed onto a pellet of Na_3H_3L2 was made and it was converted fully into PCMOF2½ (Figure 2.16). SEM-EDX mapping showed higher concentration of P atoms (as present in L2) for sites near the interface and lower amounts progressively further away. Reverse trend was observed for S atoms (as present in L1). Lastly, the ratio of L1:L2 was determined by elemental analysis and SEM/EDX measurements. The distance from the L1-L2 interface determined whether sulfur (L1) or phosphorous (L2) was predominant in the site (Figure 2.16 – 2.18).

In conclusion, the isomorphous ligand replacement synthesis is a thermodynamic solid state reaction. Its mechanism is similar to the natural mineral weathering process and *accelerated aging*.[4] Furthermore, the high-temperature β-phase of PCMOF2, instead of the low-temperature α-phase, can also be mixed with Na_3H_3L2 and converted into PCMOF2½.

3.5.3 Systematic differences in the conductivities and the activation energies of PCMOFs

We observed several interesting systematic differences when we compared the conductivities and the activation energies of PCMOF2½(Pyrazole), PCMOF2½(Triazole), PCMOF2(Pyrazole), and PCMOF2(Triazole) under hydrated conditions (90% relative humidity). The results are reproduced in the table below.

Name	Conductivity ($S\ cm^{-1}$)	T (°C)	RH (%)	Ea (eV)
PCMOF2½(Pyrazole)	1.1×10^{-1}	85	90	0.16
PCMOF2½(Triazole)	5.2×10^{-2}	85	90	0.19
PCMOF2(Pyrazole)	4.6×10^{-2}	85	90	0.08
PCMOF2(Triazole)	1.9×10^{-2}	85	90	0.08

Table 3.3 A list of conductivities and activation energies of PCMOFs discussed in this section.

Upon incorporating heterocycles in the framework, β-PCMOF2(Pyrazole) and PCMOF2(Triazole) have their activation energies decreased from 0.28 eV (β -PCMOF2) to 0.08 eV. When these PCMOFs were converted to PCMOF2½(Pyrazole) and PCMOF2½(Triazole) by isomorphous addition of Na_3H_3L2, their activation energies increased to 0.16 & 0.19 eV respectively. In addition, the conductivities of PCMOF2(Pyrazole) and PCMOF2½(Pyrazole) were about 2× higher than the conductivities of PCMOF2(Triazole) and PCMOF2½(Triazole), respectively.

In addressing this, we decided to look back to the Arrhenius equation (Equation 1.1) and link the magnitude of the activation energy to the resultant proton conductivity.

The magnitude of activation energy is directly linked with the facility of proton transport. For PCMOF2(Pyrazole) and PCMOF2(Triazole), their small activation energy (0.08 eV) indicate a facile proton conduction pathway. This, however, does not necessarily result in increased conductivity at higher temperatures because the limiting factor could be the number of freely available acidic protons. Although the energy barrier for proton transfer is lowered, the number of available protons is constant. This observation corroborates the findings from Hurd *et al* where the increase in the number of

heterocycles charge carriers only imparted moderate variation in the resultant conductivity.[2]

The insertion of the more protic Na_3H_3L2 via isomorphous ligand replacement increased the conductivities of PCMOF2(Pyrazole) and PCMOF2(Triazole), but their activation energies were also increased (Table 3.3). It is hypothesized that the increased host-guest interaction between Na_3H_3L2 and the heterocycles contributed to the increase in activation energy. It can be speculated that the freely available acidic protons of H_3L2 interacts strongly with the amphiprotic heterocycles, potentially decreasing the motional enthalpy and entropy of the charge carriers.

This increased host-guest interaction in PCMOF2½(Pyrazole), however, can be overcome at higher temperatures to impart greater increase of conductivity at 85 °C compared to that of PCMOF2(Pyrazole). Perhaps the increase in the number of free proton in the conduction network necessitating greater energy input for movement. Increasing the number of charge carriers impart enhanced conductivity, but the limiting factor is the number of free protons in the conduction network. The proton hopping is extremely facile for PCMOF2(Pyrazole) in part because the number of transportable proton is limited.

Name	pK_a
Benzenesulfonic acid	-0.60 *
Phenlphosphonic acid	1.88 *
Monohydrogen phenylphosphonic acid	12.32 [15]
1H-pyrazol-2-ium	2.5 [16]
1H-1,2,4-triazol-2-ium	2.39 [5]
1H-imidazol-3-ium	6.9 [5]
Hydroxonium	-1.74 [17]

Table 3.4 A list of pK_as of the acidic moieties investigated in this work. The pK_a values with * were calculated using Advanced Chemistry Development (ACD/Labs) software V11.02 (© 1994-2014 ACD/Labs).

The conductivity is also dependent on the pK_a values of the conjugate acid form of the heterocycles. Under hydrated conditions, the hydroxonium ions (with pK_a of -1.74), Na_3H_3L2 (pK_a of 12.32) and the corresponding heterocycles (pK_a of 2.5 for 1*H*-pyrazole and pK_a of 2.39 for 1*H*-1,2,4-triazole) execute proton transfer via a reversible acid-base reaction.[5] According to the free-energy change for the acid-base reaction and Hess's law, smaller the difference in the pK_a between hydroxonium and the conjugate form of the heterocycle, smaller the Gibb's free energy difference between the forward and the reverse reaction, resulting in more facile proton conduction. Although 1*H*-1,2,4-triazol-2-ium has slightly smaller pK_a (2.39) compared to that of 1*H*-pyrazol-2-ium (2.5),[5] PCMOFs impregnated with 1*H*-pyrazole imparted slightly higher conductivity than PCMOFs impregnated with 1*H*-1,2,4-triazole. A potential explanation for the difference in conductivity for pyrazole doped samples compared to triazole doped samples may come from the strength of the host-guest interactions.

In addition to the pK_a values, a potential explanation for the difference in conductivity for pyrazole doped samples compared to triazole doped samples may come from the strength of the host-guest interactions.[6] There are two main factors that affect

proton conductivity of impregnated heterocycles – their size and hydrogen bonding proficiency. Triazole, being a smaller molecule than pyrazole, is speculated to have greater conductivity based on the size alone. It seems that the orientation of nitrogen molecules in pyrazole favors more facile hydrogen bonding network/proton conduction network in the PCMOF2 and PCMOF2½ framework compared to that of triazole.[7] Furthermore, the host-guest interaction is thought to be weaker for pyrazole than that of triazole molecules due to pyrazole molecule having only two nitrogen atoms compared to triazole's three nitrogen atoms. Lastly, the ratio between the number of hydrogen bond doner sites and the hydrogen bond acceptor sites for pyrazole is 1 to 1 where as for that of triazole is 1 to 2. Perhaps this 1 to 1 ratio, coupled with the 1,2 nitrogen orientation in pyrazole, effectively limits the re-orientation and facilities proton conduction with minimal re-orientation of the pyrazole molecule. Unpublished work by Hurd *et al* further supports this hypothesis – the anhydrous conductivity of PCMOF2(Pyrazole) was measured to be 1.30×10^{-3} S cm^{-1} at 150 °C at its second cooling cycle, a greater conductivity compared to that of PCMOF2(Triazole): 2×10^{-4} S cm^{-1} at 150 °C (Figure 3.16).

3.5.4 Challenges in merging design strategies

Isomorphous ligand replacement and heterocycle doping require careful choosing of the molecular candidates to successfully impart enhanced conductivity. Also, adherence to the design parameters becomes imperative when the two strategies are merged. We investigated whether melamine could be isomorphously inserted into the β-PCMOF2 framework.

The PCMOF2½ *Melamine* was synthesized and its conductivity fully measured (Figure 3.17). PCMOF2½ *Melamine* is analogous to PCMOF2½ except that melamine molecules were used in lieu of Na_3H_3L2 in isomorphously replacing one-third of Na_3L1. Melamine was selected to investigate the versatility of isomorphous ligand replacement – whether a neutral ligand that does not share the same counter-cation (sodium) as L1 can still be incorporated into the β-PCMOF2 framework. Melamine (1,3,5-triazine-2,4,6-triamine) is a C_3 symmetric, single-core aromatic, organic base with a pK_a of 5.39.[8] Melamine contains three amines that can act as proton donor/acceptor sites. It was hypothesized that melamine could impart greater number of proton carriers to enhance proton conduction. Based on the powder XRD, it seemed that the isomorphous ligand replacement was incomplete during the initial 48 hour exposure to humidity and 85 °C (Figure 3.7). We speculated that melamine's absence of the counter cation hindered its movement & insertion into the β-PCMOF2 framework.

The Powder XRD of PCMOF2½ *Melamine* was analogous to that of β-PCMOF2, with the characteristic 2θ shifts of isomorphous ligand replacement shown in the powder XRD of PCMOF2½ (Figure 3.6 and Table 3.2). PCMOF2½ *Melamine*'s conductivity was measured under 90% relative humidity conditions for two heating and cooling cycles (Figure 3.18). Only after the second heating and cooling cycle, the conductivity became stable and reproducible (Figure 3.19), suggesting that greater reaction time was needed to complete isomorphous ligand replacement. PCMOF2½ "Melamine" did exhibited enhanced conductivity on par with that of PCMOF2½ with respect to β-PCMOF2: 2.5×10^{-2} S cm^{-1} at 85 °C and 90% relative humidity (Figure 3.17, Table 3.1).

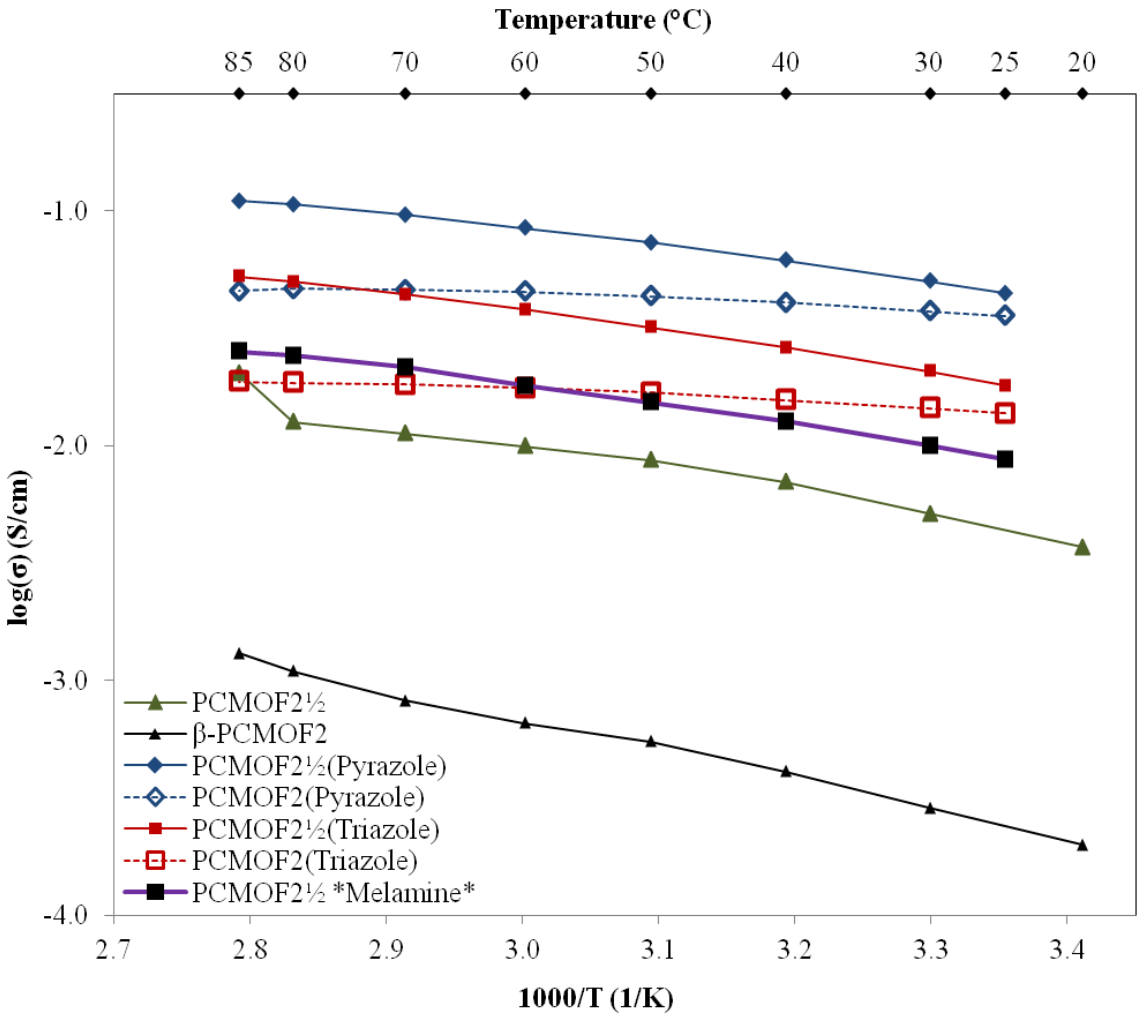

Figure 3.17 Log conductivity versus 1/temperature plot of various PCMOFs at their respective second cooling cycles, measured at 90% relative humidity.

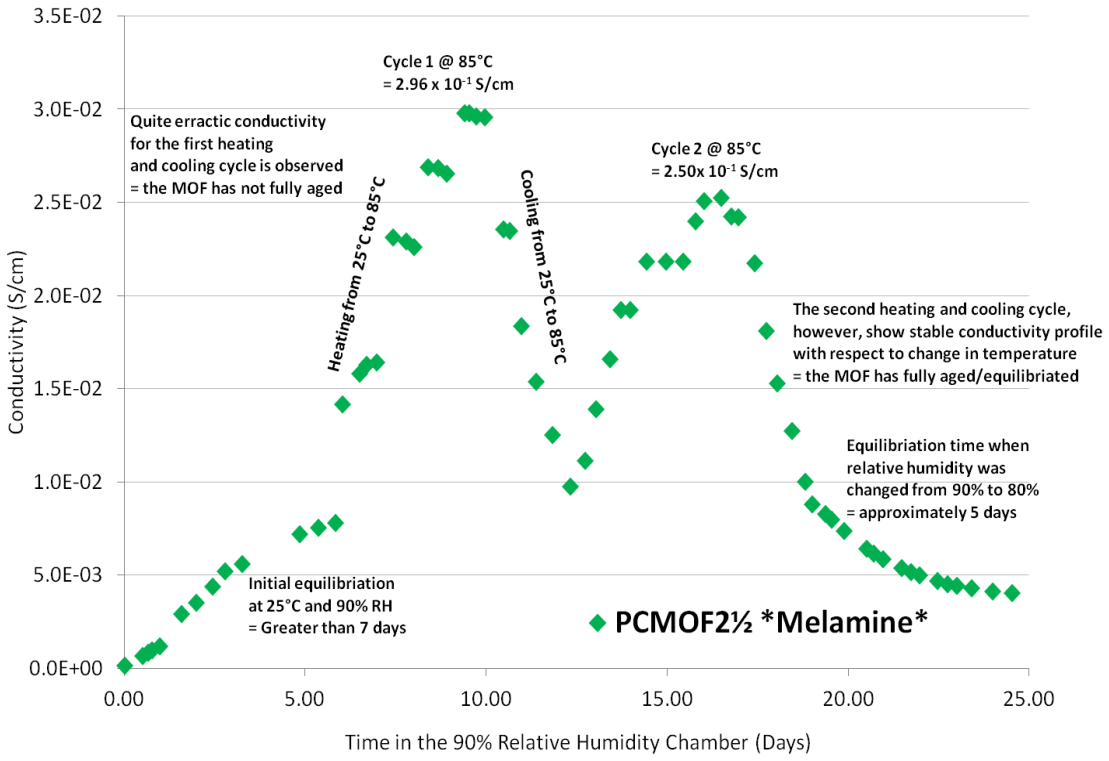

Figure 3.18 Conductivity versus time plot of PCMOF2½ *Melamine* at various temperatures and 90% relative humidity.

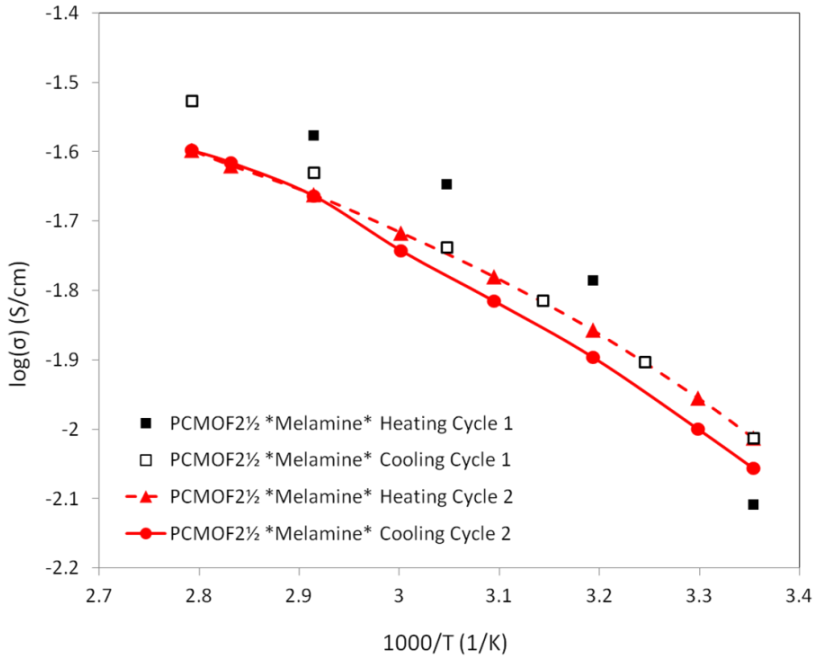

Figure 3.19 Log conductivity versus 1/temperature plot of the multiple heating and cooling cycles required for the equilibration of PCMOF2½ *Melamine*.

The conductivity of PCMOF2½ *Melamine* decreased drastically (below 10^{-8} S cm^{-1}) when the humidity was decreased from 90% to 40%, outpacing all other PCMOFs (Table 3.1 and Figure 3.13). We hypothesized that the presence of water was quintessential in utilizing the basicity of melamine for proton conduction. According to the Arrhenius equation, melamine can be thought of as providing additional proton acceptor sites (organic base) not free acidic protons as Na_3H_3L2. Yet, melamine is just as effective in increasing the overall conductivity of β-PCMOF2 because melamine increases the number of charge carriers. Under reduced humidity conditions, however, there are no sufficient water molecules to provide free acidic protons and melamine's basic sites can be seen as locking the protons in place, resulting in a drastic decrease in conductivity.

We also investigated Imidazole as a potential heterocycle dopant since the pK_a of the conjugate acid form of imidazole, with pK_a of 7.18, is very close to that of water (pK_a of 7).[9] We synthesized PCMOF2(Imidzaole) and PCMOF2½(Imidazole) and measured their respective conductivities. The both samples showed no significant proton conductivity at 85 °C and 90% relative humidity. We hypothesized the absence (or the significant decrease of) conductivity to be caused by the strong host-guest interaction between the imidazole molecule and the β-PCMOF2 framework as well as imidazole and imidazolium's higher pK_a (pK_{a1} = 6.9, pK_{a2} = 14.52) values compared to that of triazole and triazolium cation (pK_{a1} = 2.39, pK_{a2} = 9.97).[9] pK_a values indicates that the triazole-triazolium pair would form a more balanced mix of protonated and unprotonated molecules – it is just as important to provide sufficient unprotonated sites that can act as facile proton acceptors in addition to maximizing the number of proton donors. The

strong host-guest interaction would lock imidazole in place, significantly decreasing the motional entropy and rotational freedom, ultimately resulting in decreased conductivity.[9]

Interestingly, when PCMOF2(Pyrazole), PCMOF2(Triazole) and PCMOF2(Imidazole) were mixed with melamine to investigate melamine's compatibility with heterocycles, the resulting PCMOFs all failed to show proton conductivity greater than 10^{-6} at 25 °C and 90% relative humidity, conductivity 3 orders of magnitude lower than the original β-PCMOF2.

First of all, melamine does not fully satisfy the parameters for isomorphous replacement. Also melamine negates the increase in conductivity imparted via hetercycle doping. It is hypothesized that the basic melamine interacts strongly with the amphiprotic hetercycles, forming an acid-base pair which decreases the rotational freedom and mobility of the heterocycles. Referring back to the Arrhenius equation (Equation 1.1), this interaction would decrease the motional entropy and enthalpy of the proton carriers, adversely affecting the resultant conductivity. Perhaps the acid-base interaction fully deprotonates the heterocycles and fully protonate melamine, affecting the homogenous charge distribution within the conduction network, rendering the PCMOF non-conductive. It is also possible that this strong acid-base interaction, especially between imidazole and melamine, results in the impure phase as present in the powder XRD of PCMOF2½ *Melamine* (Imidazole) (Figure 3.8).

Finally, with regards to PCMOF2½(Pyrazole)'s loss of heterocycle upon exposure to humidity, the focus of this study was to investigate whether the synergistic merging of the different design strategies was feasible, not to make a commercial material for fuel-

cell applications. The loss of heterocycle can be seen as a shortcoming in merging the two design strategies.

3.5.5 Discussion of relevant works from the literature

There are several examples of metal-organic frameworks in literature that utilize rational design strategies to impart/enhance their proton conductivities.

Fedin *et al.*[10] investigated the enhanced conductivity of a MIL-101 framework by successfully impregnated the MOF with strong acids. Toluensulfonic and triflic acids were incorporated into a chrominum (III) terephthalate coordinated framework, resulting in a proton-conducting solid electrolytes hybrid. The strong acids co-exist in the MIL-nanocages as droplets and they impart proton conductivity via Grotthuss mechanism and continuous re-organization of the droplets. MIL-101(Triflic acid) exhibits conductivity of 8×10^{-2} S cm^{-1} at 60 °C and 15% relative humidity. The impregnated acids provide both freely available acidic protons as well function as proton carriers since the host MIL-101 framework does not impart inherent proton conductivity.

Kitagawa *et al.*[11] illustrated the first example of encapsulating a proton carrier molecule in a PCP/MOF (porous coordination polymer) framework to enhance its proton conductivity. They investigated two analogous porous coordination polymers (PCPs) - Im@Al(μ_2-OH)(1,4-naphthalenedicarboxylate) and Im@Al(μ_2-OH)(1,4-benzenedicarboxylate) where imidazole (Im) molecules were loaded into the 1-D channel. The conductivity of Im@Al(μ_2-OH)(1,4-naphthalenedicarboxylate) reached 2.2 $\times 10^{-5}$ S cm^{-1} at 120 °C under anhydrous conditions with the activation energy of 0.6 eV. In contrast, the conductivity of Im@Al(μ_2-OH)(1,4-benzenedicarboxylate) reached 1.0 ×

10^{-7} S cm^{-1} at 120°C with the activation energy of 0.9 eV.. The two PCPs differ in the polarity of pore interiors; the difference in conductivity was attributed to the varying degree of host-guest interaction between the imidazole and the host framework, affecting imidazole's motional entropy.

Horike and Kitagawa *et al.*[12] have investigated a series of porous coordination polymers (PCPs) where they fine-tuned the PCP's flexibility via mixed ligand approach. Two isostructural PCPs composed of $[Zn(5NO_2\text{-ip})(bpy)]_n$ (5-NO_2-ip = 5-nitroisophthalate, bpy = 4,4'-bipyridyl) and $[Zn(5\text{-MeO-ip})(bpy)]_n$ (MeO = 5-methoxyisophthalate) were investigated as well as the hybrids of two where differing ratios of 5-NO_2-ip and 5-MeO-ip were employed. This ratio, in turn, resulted in an incremental increase in the gating pressures - the isostructural mixing of the two ligand derivates imparted control of the PCP's flexibility.

Deng *et al.*[13] investigated a series of multivariate MOFs that are isostructural with MOF-5 but containing various combinations of derivatives. Up to eight distinct functionalities have been incorporated into the isostructural framework. One combination, MTV-MOF-5-EHI, exhibited up to 400% better selectivity for CO_2/CO compared to its single-component MOF-5 counterparts. Whether proton conductivity or gas selectivity, a mixed ligand approach can be a valuable tool to impart and fine-tune desired properties.

Ghosh *et al.*[14] reported a 3-D MOF with acid-base pairs in its coordination space that efficiently conducts protons under both anhydrous and humid conditions. The MOF consists of an anionic framework that is interpenetrated with a cationic supramolecular

net, formed by electrostatic and hydrogen-bonding interactions between sulfate anions and dimethyl ammonium cations. The MOF showed very high water assisted proton conductivity: 4.2×10^{-2} S cm^{-1} at 98% relative humidity as well as high anhydrous conductivity: 1×10^{-4} S cm^{-1} at 150 °C.

3.6 Conclusion

We have successfully applied two design strategies - isomorphous ligand replacement and heterocycle doping - to synergistically enhance the proton conductivity of a proton conducting metal-organic framework: β-PCMOF2. Of ten PCMOFs investigated in this study, one resulting material, PCMOF2½(Pyrazole), has its proton conduction raised 1.9 orders of magnitude compared to the parent material, to 1.1×10^{-1} S cm-1 at 85 °C and 90% relative humidity, while maintaining the parent MOF structure. Moreover, the conductivity of PCMOF2½(Pyrazole) has reached a value comparable to that of Nafion under fuel cell operating conditions, a step closer to utilizing PCMOFs for fuel cell applications.

The exact mechanism of isomorphous replacement synthesis was elucidated to be a thermodynamically driven solid state reaction that utilizes the inherent mobility of the solid state molecules, similar to the natural mineral weathering process and accelerated aging. This solid state synthesis was the only way to achieve isomorphous ligand replacement to yield the following new compounds: PCMOF2½(Pyrazole), PCMOF2½(Triazole) and PCMOF2½ *Melamine*.

Studying metal-organic frameworks can be powerful tool in exploring the molecular design strategies and the material’s structure-property relationships. The

crystalline and modular nature of MOF allows purposeful design of the material in its molecular level. Synergistic merging of design strategies can be a difficult task, when successfully executed however, can result in enhancement of desired properties greater than sum of its parts. It is becoming increasingly apparent that an appropriate choice of molecular candidates is paramount in merging design strategies.

3.7 References

1) Kim, S.; Dawson, K. D.; Gelfand, B. S.; Taylor, J. M.; Shimizu, G. K. H. *J. Am. Chem. Soc.* **2013**, *135*, 963-966.
2) Hurd, J. A.; Vaidhyanathan, R.; Thangadurai, V.; Ratcliffe, C. I.; Moudrakovski, I. L.; Shimizu, G. K. H. *Nat. Chem.* **2009**, *1*, 705−710.
3) Taylor, J. M.; Mah, R. K.; Moudrakovski, I. L.; Ratcliffe, C. I.; Vaidhyanathan, R.; Shimizu, G. K. H. *J. Am. Chem. Soc.* **2010**, *132*, 14055–14057.
4) Cliffe, M. J.; Mottillo, C.; Stein, R. S.; Bucar, D.; Friscic, T. *Chem. Sci.* **2012**, *3*, 2495-2500.
5) Yang, C.; Costamagna, P.; Srinivasan, S.; Benziger, J.; Bocarsly, A. B. *J. Power Sources.* **2001**, *1*, 1-9.
6) (a) Seeliger, D.; Hartnig, C.; Spohr, E. *Electrochim. Acta.* **2005**, *50*, 4234-4240. (b) Choi, P.; Jalani, N. H.; Datta, R. *J. Electrochem. Soc.* **2005**, *152*, E123-E130. (c) Guhathakurta, S.; Min, K. *J. Polym. Sci. Pol. Phys.* **2009**, *47*, 2178-2187. (d) Bureekaew, S.; Horike, S.; Higuchi, M.; Mizuno, M.; Kawamura, T.; Tanaka, D.; Yanai, N.; Kitagawa, S. *Nat. Mater.* **2004**, *43*, 2334-2375.
7) (a) Kreuer, K. D. *Solid. State. Ionics.* **1997**, *94*, 55-62. (b) Kreuer, K. D.; Fuchs, A.; Ise, M.; Spaeth, M.; Maier, J. *Electrochim. Acta.* **1998**, *43*, 1281-1288.

8) Li, Y. Y.; Xu, Z. G.; Feng, Y. Y.; Liu, X. Y.; Chen, T.; Zhang, H. X. *Chromatographia*, **2011**, *74*, 523-530.

9) (a) Guhathakura, s.; Min, K. *Polymer*. **2009**, *59*, 1034-1045. (b) Guhathakurta, S.; Min, K. *Polym. Sci. Pol. Phys.* **2009**, *47*, 2178-2187. (c) Li, S.; Zhou, Z.; Zhang, Y.; Liu, M.; Li, W. *Chem. Mater.* **2005**, *17*, 5884-5886. (d) Zhou, Z.; Liu, r.; Wang, J.; Li, S.; Liu, M.; Bracdas, J. L. *J. Phys. Chem. A.* **2006**, *110,* 2322-2324. (e) Creagh, L. T.; Truitt, P. *J. Org. Chem.* **1968**, *33*, 2956-2957.

10) Dybtsev, D. N.; Ponomareva, V. G.; Aliev, s. B.; Chupakhin, A. P.; Gallyomav, M. R.; Morez, N. K.; Kolesov, B. A.; Kovalenko, K. A.; Shutova, E. S.; Fedin, V. P. *ACS Appl. Mater. Intervaces.* **2014**, *6 (7),* 5161-5167.

11) Bureekaew, S.; Horike, S.; Higuchi, M.; Mizuno, M.; Kawamura, T.; Tanaka, D.; Yanai, N.; Kitagawa, S. *Nat. Material*. **2009**, *8*, 831-836.

12) Horike, S.; Inubushi, Y.; Hori, T.; Fukushima, T.; Kitagawa, S. *Chem. Sci.* **2012**, *3*, 116-120.

13) Deng, H.; Doonan, C. J.; Furukawa, H.; Ferreira, R. B.; Towne, J.; Knobler, C. B.; Wang, B.; Yaghi, O. M. *Science*, **2010**, *327,* 846-850.

14) Nagarkar, S. S.; Unni, S. M.; Sharma, A.; Kurungot, S.; Ghosh, S. K. *Angew. Chem. Int. Ed.* **2014**, *53,* 2638-2642.

15) Salvado, M. A.; Pertierra, P.; Garcia-Granda, S.; Barcina, L. M.; Llavona, R.; Rodriguez, J. *Zeitschrift fur Kristallographie* **2001**, *216*, 326-330

16) Dewick, P. M. *Essentials of Organic Chemistry: For Students of Pharmacy, Medicinal Chemistry and Biological Chemistry*. John Wiley & Sons, **2006**. Print.

17) Taft, R. W.; Wolf, J. F.; Beauchamp, J. L.; Scorrano, G.; Arnett, E. M.; *J. Am. Chem. Soc.* **1978**, *100*, 1240-1249.

Chapter Four: **CONCLUSION**

4.1 Summary of the findings

Two rational design strategies – isomorphous ligand replacement and heterocycle doping - were investigated to enhance proton conductivity of a proton conducting MOF named β-PCMOF2. Also in depth study was done to synergistically merge the two design strategies together. In total, 8 new PCMOFs were synthesized and 3 previously reported PCMOFs' conductivities were measured under new conditions (Table 4.1, Figure 4.1). Chapter 2 focused on PCMOF2½ where an entire C_3-symmetric trisulfonate ligand was substituted with a C_3-symmetric tris(hydrogen phosphonate) ligand to yield PCMOF2½, which had its proton conductivity raised 1.5 orders of magnitude, to 2.1×10^{-2} S cm^{-1} at 85 °C and 90% relative humidity compared to the parent material, while maintaining the parent MOF structure. Chapter 3 focused on PCMOF2½(Pyrazole), a PCMOF that successfully utilizes both heterocycle loading and isomorphous ligand replacement to exhibit the greatest increase in its proton conductivity. With respect to the nomenclature of PCMOF2½(Pyrazole), "2½" indicates the isomorphous insertion of Na_3H_3L2 into the β-PCMOF2 framework to increase the number of freely available acidic protons. "(Pyrazole)" indicates the kinetic trapping of pyrazole within the pores of β-PCMOF2 to increase the number of available charge carriers. Via synergistic merging of these two strategies, PCMOF2½(Pyrazole) had its conductivity the increased by 1.9 orders of magnitude from β-PCMOF2 to reach 1.1×10^{-1} S cm^{-1} at 85 °C and 90% relative humidity, a value greater than that of PCMOF2½ and PCMOF2(Pyrazole) for which each design strategy was applied in solo. Moreover, the conductivity of PCMOF2½(Pyrazole) has reached a value that is industrially applicable – conductivity comparable to that of

Nafion under fuel cell operating conditions. Finally the exact mechanism of isomorphous ligand replacement synthesis was elucidated to be a thermodynamically driven solid state reaction, akin to a natural mineral weathering process called accelerated aging. It was found that isomorphous ligand replacement for PCMOF2½, PCMOF2½(Pyrazole), PCMOF2½(Triazole), and PCMOF2½ *Melamine* were only achievable via this solid state synthesis.

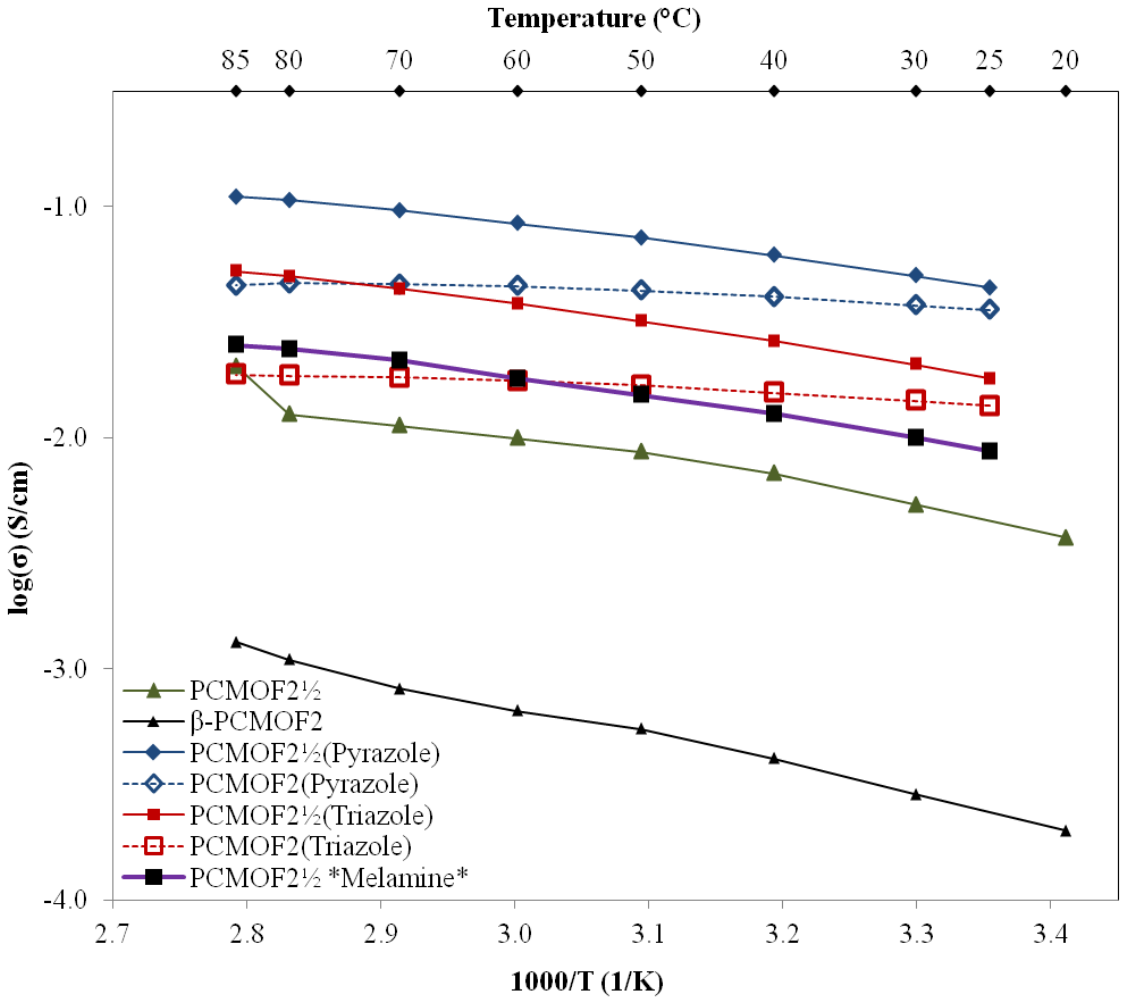

Figure 4.1 Proton conductivity data (90% relative humidity) for all PCMOFs featured in this work.

Name	Conductivity/S cm^{-1}	T /°C	RH/%	Ea[7]/eV
PCMOF2½(Pyrazole)[1]	1.1×10^{-1}	85	90	0.16
PCMOF2½(Pyrazole)[1]	1.2×10^{-5}	25	30	n/a
PCMOF2½(Pyrazole)[1]	7.2×10^{-7}	150	0	0.20[8] 0.98[9]
PCMOF2½(Triazole)[1]	5.2×10^{-2}	85	90	0.19
PCMOF2½(Triazole)[1]	1.5×10^{-6}	25	40	n/a
PCMOF2(Pyrazole)[2]	4.6×10^{-2}	85	90	0.08
PCMOF2(Pyrazole)[2]	3.6×10^{-3}	25	30	n/a
PCMOF2(Pyrazole)[3]	1.3×10^{-3}	150	0	0.42[10]
PCMOF2(Triazole)[4]	1.9×10^{-2}	85	90	0.08
PCMOF2(Triazole)[4]	7.2×10^{-6}	25	30	n/a
PCMOF2(Triazole)[5]	5×10^{-4}	150	0	0.34[11]
PCMOF2½ [6]	2.1×10^{-2}	85	90	0.21
PCMOF2½ [6]	2.4×10^{-5}	20	50	n/a
β-PCMOF2 [4,6]	1.3×10^{-3}	85	90	0.28
β-PCMOF2 [4,6]	1.8×10^{-6}	20	50	n/a
β-PCMOF2 [5]	1×10^{-9}	100	0	n/a
PCMOF2½ *Melamine* [1]	2.5×10^{-2}	85	90	0.19
PCMOF2½ *Melamine* [1]	1.6×10^{-8}	25	40	n/a
PCMOF2½ *Melamine* (Pyrazole)[1]	These PCMOFs exhibited proton conductivity below 10^{-6} S cm^{-1} at 85 °C and 90% relative humidity.			
PCMOF2½ *Melamine* (Triazole)[1]				
PCMOF2½ *Melamine* (Imidazole)[1]				
PCMOF2(Imidazole)[1]				
PCMOF2½(Imidazole)[1]				

1. New compounds and new conductivity data
2. A compound previously synthesized by Hurd *et al* (unpublished); its conductivity was measured under new conditions.
3. A compound and conductivity investigated by Hurd *et al* (unpublished).

4. A compound previously reported by Hurd *et al*; its conductivity was measured under new conditions.
5. Compound and conductivity previously reported by Hurd *et al.*
6. Compounds and conductivity previously reported by Kim *et al* (the author).
7. Activation energy measured between the temperature of 85 °C and 25 °C.
8. Activation energy measured between the temperature of 150 °C and 110 °C.
9. Activation energy measured between the temperature of 110 °C and 90 °C.
10. Activation energy measured between the temperature of 150 °C and 60 °C.
11. Activation energy measured between the temperature of 150 °C and 90 °C.

Table 4.1 List of PCMOFs featured in this thesis and their conductivity profiles.

4.2 References (Chapter 1 and Chapter 4)

1) Kim, S.; Dawson, K. D.; Gelfand, B. S.; Taylor, J. M.; Shimizu, G. K. H. *J. Am. Chem. Soc.* **2013**, *135*, 963-966.
2) Shimizu, G. K. H.; Taylor, J. M.; Kim, S. *Science*. **2013**, *41*, 354-355.
3) (a) Férey, G.; Serre, C.; Devic, T.; Maurin, G.; Jobic, H.; Llewellyn, P. L.; De Weireld, G.; Vimont, A.; Daturi, M.; Chang, J. S. *Chem. Soc. Rev.* **2011**, *40*, 550-562. (b) Suh, M. P.; Park, H. J.; Prasad, T. K.; Lim, D.-W. *Chem. Rev.* **2012**, *112*, 782-835. (c) Li, J. R.; Sculley, J.; Zhou, H. C. *Chem. Rev.* **2012**, *112*, 869–932. (d) Mason, J. A. ; Sumida, K. ; Herm, Z. R. ; Krishna, R.; Long, J. R. *Energy Environ. Sci.*, **2011**, *4*, 3030. (e) Phan, A.; Doonan, C. J.; Uribe-Romo, F. J.; Knobler, C.B.; O'Keeffe, M.; Yaghi, O. M. *Acc. Chem. Res.* **2010**, *43*, 58.
4) Lee, J.; Farha, O. K.; Roberts, J.; Scheidt, K. A.; Nguyen, S. T.; Hupp, J. T. *Chem. Soc. Rev.* **2009**, *38*, 1450-1459.

5) Kreno, L. E.; Leong, K.; Farha, O. K.; Allendorf, M.; Van Duyne, R. P.; Hupp, J. T. *Chem. Rev*. **2012**, *112*, 1105-1125.

6) (a) Ramaswamy, P.; Wong, N. E.; Shimizu, G. K. H. *Chem. Soc Rev*. **2014**, advance online publication, (DOI:10.1039/c4cs00093e). (b) Yoon, M.; Suh, K.; Natarajan, S.; Kim, K. *Angew. Chem. Int. Ed.* **2013**, *52*, 2-15. (c) Horike, S.; Umeyama, D.; Kitagawa, S.; *Acc. Chem. Res.* **2013**, *46*, 2376-2384. (d) Yamada, T.; Otsubo, K.; Makiura, R.; Kitagawa, H. *Chem. Soc. Rev.* **2013**, *42*, 6655-6669.

7) (a) Sadakiyo, M.; Yamada, T.; Kitagawa, H. *J. Am. Chem. Soc*. **2009**, *131*, 9906-9907. (b) Taylor, J. M.; Mah, R. K.; Moudrakovski, I. L.; Ratcliffe, C. I.; Vaidhyanathan, R.; Shimizu, G. K. H. *J. Am. Chem. Soc.* **2010**, *132*, 14055–14057.

8) Hurd, J. A.; Vaidhyanathan, R.; Thangadurai, V.; Ratcliffe, C. I.; Moudrakovski, I. L.; Shimizu, G. K. H. *Nat. Chem.* **2009**, *1*, 705−710.

9) Taylor. J. M.; Dawson, K. D.; Shimizu, G. K. H. *J. Am. Chem. Soc.* **2013**, *135*, 1193-1196.

10) "Metal-organic frameworks advance fuel cell technology." *Canadian Chemical News*| *L'Actualité chimique canadienne*. March/April, **2013,** Accessed April 28th 2014.

APPENDIX – COPYRIGHT RELEASE FORMS

Co-author copyright release form

I, Benjamin S. Gelfand, hereby grant permission to SiRim Kim to reproduce any portion of the published article(s) and prepared manuscript(s) listed below to be included in his Masters of Science thesis titled: *Design Proton Conductivity in a Metal-Organic Framework from a Molecular Scale.* Furthermore, I grant permission for the University of Calgary to submit the completed work to the University of Calgary Thesis Repository - The Vault [http://thesis.ucalgary.ca] and Library and Archives Canada [http://collectionscanada.gc.ca/obj/s4/f2/frm-nl59-2-e.pdf]

Permission granted for the published articles(s) and/or prepared manuscript(s) below

Published Article: Enhancing Proton Conductivity in a Metal-Organic Framework by Isomorphous Ligand Replacement. SiRim Kim, Karl W. Dawson, Benjamin S. Gelfand, Jared M. Taylor, and George K.H. Shimizu* *Journal of the American Chemical Society,* **2013,** *135,* 963-966.

Prepared Manuscript: Synergistic Merging of Two Design Strategies in a Proton Conducting Metal-Organic Framework. SiRim Kim, Jeff A. Hurd, Karl W. Dawson, Benjamin S. Gelfand, Norman E. Wong, and George K.H. Shimizu*

Name (Please print)

BENJAMIN SIDNEY GELFAND

Signature

Date: April 28th 2014

Co-author copyright release form

I, Norman E. Wong, hereby grant permission to SiRim Kim to reproduce any portion of the published article(s) and prepared manuscript(s) listed below to be included in his Masters of Science thesis titled: *Design Proton Conductivity in a Metal-Organic Framework from a Molecular Scale.* Furthermore, I grant permission for the University of Calgary to submit the completed work to the University of Calgary Thesis Repository - The Vault [http://thesis.ucalgary.ca] and Library and Archives Canada [http://collectionscanada.gc.ca/obj/s4/f2/frm-nl59-2-e.pdf]

Permission granted for the published articles(s) and/or prepared manuscript(s) below

Prepared Manuscript: Synergistic Merging of Two Design Strategies in a Proton Conducting Metal-Organic Framework. SiRim Kim, Jeff A. Hurd, Karl W. Dawson, Benjamin S. Gelfand, Norman E. Wong, and George K.H. Shimizu*

Name (Please print)

NORMAN E. WONG

Signature

Date: April 28th 2014

Co-author copyright release form

I, George K.H. Shimizu, hereby grant permission to SiRim Kim to reproduce any portion of the published article(s) and prepared manuscript(s) listed below to be included in his Masters of Science thesis titled: *Design Proton Conductivity in a Metal-Organic Framework from a Molecular Scale.* Furthermore, I grant permission for the University of Calgary to submit the completed work to the University of Calgary Thesis Repository - The Vault [http://thesis.ucalgary.ca] and Library and Archives Canada [http://collectionscanada.gc.ca/obj/s4/f2/frm-nl59-2-e.pdf]

Permission granted for the published articles(s) and/or prepared manuscript(s) below

Published Article: Enhancing Proton Conductivity in a Metal-Organic Framework by Isomorphous Ligand Replacement. SiRim Kim, Karl W. Dawson, Benjamin S. Gelfand, Jared M. Taylor, and George K.H. Shimizu* *Journal of the American Chemical Society,* **2013,** *135,* 963-966.

Prepared Manuscript: Synergistic Merging of Two Design Strategies in a Proton Conducting Metal-Organic Framework. SiRim Kim, Jeff A. Hurd, Karl W. Dawson, Benjamin S. Gelfand, Norman E. Wong, and George K.H. Shimizu*

Name (Please print)

GEORGE SHIMIZU

Signature

Date: April 28th 2014

Co-author copyright release form

I, Jared M. Taylor, hereby grant permission to SiRim Kim to reproduce any portion of the published article(s) and prepared manuscript(s) listed below to be included in his Masters of Science thesis titled: *Design Proton Conductivity in a Metal-Organic Framework from a Molecular Scale.* Furthermore, I grant permission for the University of Calgary to submit the completed work to the University of Calgary Thesis Repository - The Vault [http://thesis.ucalgary.ca] and Library and Archives Canada [http://collectionscanada.gc.ca/obj/s4/f2/frm-nl59-2-e.pdf]

Permission granted for the published articles(s) and/or prepared manuscript(s) below

Published Article: Enhancing Proton Conductivity in a Metal-Organic Framework by Isomorphous Ligand Replacement. SiRim Kim, Karl W. Dawson, Benjamin S. Gelfand, Jared M. Taylor, and George K.H. Shimizu* *Journal of the American Chemical Society,* **2013,** *135,* 963-966.

Name (Please print)

JARED M. TAYLOR

Signature

Date: April 29th 2014

Co-author copyright release form

I, Jeff A. Hurd, hereby grant permission to SiRim Kim to reproduce any portion of the published article(s) and prepared manuscript(s) listed below to be included in his Masters of Science thesis titled: *Design Proton Conductivity in a Metal-Organic Framework from a Molecular Scale.* Furthermore, I grant permission for the University of Calgary to submit the completed work to the University of Calgary Thesis Repository - The Vault [http://thesis.ucalgary.ca] and Library and Archives Canada [http://collectionscanada.gc.ca/obj/s4/f2/frm-nl59-2-e.pdf]

Permission granted for the published articles(s) and/or prepared manuscript(s) below

Prepared Manuscript: Synergistic Merging of Two Design Strategies in a Proton Conducting Metal-Organic Framework. SiRim Kim, Jeff A. Hurd, Karl W. Dawson, Benjamin S. Gelfand, Norman E. Wong, and George K.H. Shimizu*

Name (Please print)

JEFF A. HURD

Signature Date:

Co-author copyright release form

I, Karl W. Dawson, hereby grant permission to SiRim Kim to reproduce any portion of the published article(s) and prepared manuscript(s) listed below to be included in his Masters of Science thesis titled: *Design Proton Conductivity in a Metal-Organic Framework from a Molecular Scale.* Furthermore, I grant permission for the University of Calgary to submit the completed work to the University of Calgary Thesis Repository - The Vault [http://thesis.ucalgary.ca] and Library and Archives Canada [http://collectionscanada.gc.ca/obj/s4/f2/frm-nl59-2-e.pdf]

Permission granted for the published articles(s) and/or prepared manuscript(s) below

Published Article: Enhancing Proton Conductivity in a Metal-Organic Framework by Isomorphous Ligand Replacement. SiRim Kim, Karl W. Dawson, Benjamin S. Gelfand, Jared M. Taylor, and George K.H. Shimizu* *Journal of the American Chemical Society,* **2013,** *135,* 963-966.

Prepared Manuscript: Synergistic Merging of Two Design Strategies in a Proton Conducting Metal-Organic Framework. SiRim Kim, Jeff A. Hurd, Karl W. Dawson, Benjamin S. Gelfand, Norman E. Wong, and George K.H. Shimizu*

Name (Please print)

KARL DAWSON

Signature

Date: May 6th 2014